Essays on Malliavin Calculus in Finance

Makar Pravosud

TESI DOCTORAL UPF/2024

Department
Faculty of Economy and Business

Thesis Supervisors:
Dr. Elisa Alòs and Dr. Eulalia Nualart

upf. Universitat Pompeu Fabra Barcelona

To my parents and to my beloved wife, who is an endless source of care, support and inspiration.

Acknowledgements

I would like to express deep sense of gratitude to my supervisors Eulalia Nualart and Elisa Alòs. Over the last five years they guided me in my development as a researcher and taught me step by step how to transform an idea and lengthy calculations into an excellent academic paper.

Also, I am very thankful to Filippo Ippolito who gave me a chance to become a Master student at BSE back in 2017 and later to continue my studying on a doctorate program. In addition, a big thank you to Christian Brownlees who guided me in my first year of PhD studies.

Apart from academic procedures there is also a lot of administrative regulations to follow. With respect to this, I would like to thank Marta Araque and Laura Agusti who helped to deal with all rules and procedures and made it seamless.

Finally, I am very grateful to my Alma Maters Barcelona School of Economics and Universitat Pompeu Fabra for all the financial support they provided to me all over these years.

Makar Pravosud
Barcelona, March 2024

Abstract

In this thesis we study the asymptotic behaviour of the at-the-money skew and the level of the implied volatility of a European, an Asian, Inverse and Quanto Inverse call options under a general stochastic volatility model. In particular, we consider dynamics of the underlying asset driven by stochastic volatility Black-Scholes and Bachelier type of models. Additionally, we present analytical results regarding the relationship between the skew and the curvature of the implied volatility and the corresponding local volatility in the case of rough volatility models.

Resum

En aquesta tesi s'estudia el comportament asimptòtic de la inclinació *at-the-money* i el nivell de volatilitat implícita d'opcions call Europees, Esiàtiques, Enverses i Quanto inverses sota un model de volatilitat estocàstica general. En particular, considerem la dinàmica de l'actiu subjacent impulsada per la volatilitat estocàstica dels models tipus Black-Scholes i Bachelier. Adicionalment, presentem resultats analítics sobre la relació entre la inclinació i la curvatura de la volatilitat implícita i la corresponent volatilitat local en el cas de models de volatilitat aproximada.

Contents

List of Figures

List of Tables

Introduction

The regular or vanilla option is a financial instrument which gives a buyer the right to buy an underlying asset at a pre-agreed price at a specific date in the future. This financial derivative is one of the most traded financial instrument nowadays. Its popularity relies on many factors including great leveraging power, higher potential returns and trading flexibility. As a result, hedgers, speculators, private investors and others can fully satisfy their investment needs using options.

In order to understand the contribution of this thesis to the realm of quantitative finance we start with a brief overview of the topic. Vanilla options have been traded for a long time. The first trading records are related to the speculation on olive harvest and dated back to the sixth century b.c. However, for a long time the option pricing problem had been remaining unsolved. The first solid try to tackle the problem was conducted by Louis Bachelier in 1900. Unfortunately, his work was not treated seriously and had been unrecognized until Samuelson rediscovered it in 1965. Finally, in 1973 Black, Scholes and Merton found the right way to price vanilla options. Since then the world of quantitative finance has received renowned Black-Scholes pricing formula.

The Black-Scholes formula had worked well until 1987 stock market crash. After the crash the option market started to exhibit what is know today as the implied volatility smile. Meaning that if we plot the implied volatility versus strike price, we will usually observe lower implied volatilities around the at-the-money strike, and higher implied volatilities for out and in-the-money strikes. Consequently, quantitative researchers started to propose new pricing models, accounted for the implied volatility smile. Nowadays, there is no universal model which can be applied to all asset classes and all markets. As a result, each trading desk has its own favorite smile model. The most popular pricing methodologies are based on the Local, Stochastic and Rough volatility models.

It is often convenient to describe the shape of the implied volatility surface in terms of just one number which is called the skew. The skew measures the change in the implied volatility between two different strike prices. Why accounting for the the skew is so important? The price of the option is strongly related with the ability to hedge the risks associated with this derivative. Using the model which is unable to account for the skew will ultimately result in the incorrect hedge ratios which will cause considerable variations in the P&L of the hedged position. Apart from hedging issue the smile causes the distortions into the pricing of exotic derivatives.

One of the most important parts of the implied volatility surface is its at-the-money region, which is usually the most liquid and the most traded slice in the whole surface. The short maturity end of the implied volatility surfaces is the most volatile part as it has high correlation between the implied and spot realised volatilities. This results in the pronounced skew which flattens with the increase of maturity of an option due to the mean reverting nature of volatility. From the modelling perspective, short maturity blow up in the skew is a challenge and not every pricing model is able to capture it. As a result, one of the key characteristics of an option pricing model is the asymptotic behaviour of the implied volatility skew generated by it.

In the case of vanilla options the topic of the asymptotic behaviour of the implied volatility and its skew is deeply studied in the literature, which is reviewed in details in the following chapters. As regards mathematical tools, they vary based on a problem and a chosen pricing model and include solutions to Volterra integral equation, large deviations theory, the Saddlepoint approximation method, etc. The key challenge in using the aforementioned methods is their restrictiveness to a specific model at hand. Alternatively, Malliavin calculus is more versatile tool since it allows to get analytical results for certain classes of models rather than a particular model. And, as one will see in the following chapters, the derived formulas are not expansions, but exact decompositions.

Nevertheless, in the case of vanilla options there are still several outstanding problems which are addressed in this thesis. The first problem is the asymptotic behavior of the local volatility surface generated by a class of rough volatility models. In the case of a regular stochastic volatility model the so called "one over two" rule links the short-end at-the-money skew of the implied volatility to the short-end at-the-money skew of the corresponding local volatility. For a long time such rule

did not exist for rough volatility models. The first successful attempt to establish such rule was conducted recently by Bourgey, De Marco, Friz, and Pigato. The authors mainly relied on large deviations and rough paths techniques to get the result. In this thesis we confirm their findings via Malliavin calculus and extend the result by establishing the rule for short-end curvatures of the implied and local volatilities.

Secondly, the problem which has not been fully studied in the literature is the asymptotic behaviour of the implied volatility and its skew in the case of stochastic volatility Bachelier model. This model has gained a lot of attention from practitioners in the light of negative energy prices observed in April 2020. In this thesis we present the latest findings and highlight analytical results for certain options under stochastic volatility Bachelier model.

By contrast to vanilla options, analytical results regarding the asymptotic behaviour of the implied volatility level and its skew in the case of exotic options are hardly available. The complications arise due to the dependency of an option's payoff on the path of an underlying asset. One of the most vivid examples is an Asian option. The contract, which is widely traded and especially popular on energy markets, does not have a closed form solution even in the simple Black-Scholes scenario. Resultantly, several chapters of the presented thesis are dedicated to the rigorous study of the short-end implied volatility and its skew in the case of exotic options such as an Asian, Inverse and Quanto Inverse options under a general stochastic volatility model including rough volatility.

The thesis is organised as follows. In the first chapter we study the short-time behavior of the at-the-money implied volatility for European and arithmetic Asian call options with a fixed strike price. An asset price is assumed to follow the Bachelier model with a general stochastic volatility process. Using techniques of the Malliavin calculus such as the anticipating Itô's formula we first compute the level of the implied volatility when maturity converges to zero. Then, we find a short maturity asymptotic formula for the skew of the implied volatility that depends on the roughness of a volatility model. We apply our general results to the SABR and fractional Bergomi models, and provide some numerical simulations that confirm the accurateness of the asymptotic formula for the skew.

In the second chapter we study the short-time behavior of the at-the-money implied volatility for arithmetic Asian options with a fixed strike price. An asset price is assumed to follow the Black-Scholes model with a general stochastic volatility process. We provide sufficient conditions on a stochastic volatility in order to compute the level of the implied volatility of an option when maturity converges to zero. Then, we find a short maturity asymptotic formula for the skew slope of the implied volatility that depends on the correlation between the price of an underlying asset and its volatility and the Hurst parameter of the volatility model. We apply our general results to the SABR and fractional Bergomi models, and provide numerical simulations that confirm the accurateness of the asymptotic formulas.

In the third chapter we provide an overview of certain crypto derivatives and present analytical results regarding the short-time behavior of the at-the-money implied volatility for Inverse European and Quanto Inverse European options with a fixed strike price. As in the previous chapter the asset price is assumed to follow the Black-Scholes model with a general stochastic volatility process.

In the fourth chapter we study the relationship between the short-end of the local and the implied volatility surfaces. We recover recent $\frac{1}{H+3/2}$ rule, where H denotes the Hurst parameter of the volatility process, for rough volatilitites. The rule states that the short-time skew slope of the at-the-money implied volatility is $\frac{1}{H+3/2}$ of the corresponding slope of local volatilities. Moreover, we prove that at-the-money short-end curvature of the implied volatility can be written in terms of the short-end skew and curvature of the local volatility and vice versa, and that this relationship depends on H. The contents of this chapter are published in the paper Elisa Alòs, David García-Lorite and Makar Pravosud [4].

Chapter 1

On the implied volatility of European and Asian call options under stochastic volatility Bachelier model

I

1.1 Introduction

The life of quantitative finance and derivatives pricing has started when Louis Bachelier presented an option pricing model in his Ph.D. thesis [14]. However, the suggested model is arithmetic and allows negative asset prices, as a result, the Bachelier model has not gained popularity. Until recently the model has not been widely studied in the literature and applied in practice. Nowadays option pricing models are strongly based on the Black-Scholes model. Local, stochastic and even fractional volatility models (see Alòs and Lorite [5] for an introduction to these topics) are extensions of the Black-Scholes model, where the volatility is allowed to be a function of the price of the stock price (local), a diffusion process (stochastic) or a function of a fractional Brownian motion (fractional). As the Black-Scholes model is a geometric Brownian motion (following a log-normal distribution), all the above models are also exponentials of random variables, and they share the positivity of the stock price. This plausible and intuitive property has been assumed for a long time for the prices of the underlying asset of an option.

From a practical perspective, the Bachelier model has started to gain more attention when negative prices have been registered, for example, on April 20th 2020, when crude oil futures crossed the zero mark and took negative values. As a prompt response to enable markets to continue to function normally, the CME Clearing started to use the Bachelier model to cope with negative underlying prices. The empirical paper by Galeeva and Ehud [29] studies the turbulent period on the oil-futures options markets which was observed in the middle of February 2020. The authors analyzed the observed implied volatilities by applying the Bachelier and Black models to prevail oil-futures option prices.

Apart from the energy market, the Bachelier model is also used in modelling interest rate products, for example, Euro denominated caps. The detailed analysis on the reasons to use a normal model rather than a log-normal one in the case of interest rates is presented in Goodman [37]. The recent paper by Choi et al. [19] is a comprehensive review of various topics related to the Bachelier model for both researchers and practitioners. In particular, they cover topics such as the implied volatility inversion problem, volatility conversion between related models, Greeks and hedging, as well as pricing of exotic options.

Concerning exact analytical results, in the paper by Schachermayer and Teichmann [50], the authors compare the option pricing problem under the Bachelier and Black-Scholes models. They find that prices coincide very well and explain by the means of chaos expansion theory why the Bachelier model yields good short-time approximations of prices and volatilities. In addition to that, the computation of prices and implied volatilities under the Bachelier model model has been presented in, for example, Terkado [52]. However, the existing literature lacks the rigorous analysis of the behaviour of the ATM level and skew of the implied volatility under the Bachelier model with stochastic volatility. By contrast, in the case of a regular Black-Scholes framework, there are numerous papers that study the short end maturity behaviour of the implied volatility under a variety of models such as the Heston, the SABR and fractional Begomi. For example, see Alòs [7], Figueroa-López et al.[23], Fukasawa [27], Fouque et al. [26].

The goal of this chapter is to fill the gap in the existing literature and to analyze the option pricing problem when we allow the volatility of the Bachelier model to be a stochastic process. That is, to study option prices and implied volatilities for local, stochastic and fractional Bachelier models, both for vanilla and for exotic, in particular, Asian options. Specifically, we present analytical results

for the behaviour of the level and the skew of the implied volatility for a general stochastic volatility Bachelier model. Our main tool for proving these results is Malliavin calculus, see Appendix .1 for an introduction to this topic. Additionally, using the findings from the theoretical part of the chapter we do an extensive numerical simulations to investigate the quality of the first order approximations of the implied volatility across different moneyness and maturity scenarios. The presented results are extension of the papers Alòs [3] and Alòs et.al [6].

The chapter is organized as follows. Section 1.2 is devoted to the statement of the problem and main results. Intermediary steps and the proofs of the main results are presented in Sections 1.3 and 1.4. Finally, in Section 1.5 we present and discuss the results of the numerical study.

1.2 Statement of the problem and main results

Let $T > 0$ and consider the following model for asset prices S (without lost of generality, we take the interest rate equal to zero for the sake of simplicity) in a time interval $[0, T]$

$$\begin{aligned} dS_t &= \sigma_t dW_t \\ W_t &= \rho W'_t + \sqrt{(1-\rho^2)} B_t, \end{aligned} \tag{1.1}$$

where $S_0 > 0$ is fixed, W_t, W'_t, and B_t are three standard Brownian motions on $[0, T]$ defined on the same risk-neutral complete probability space $(\Omega, \mathcal{G}, \mathbb{P})$. We assume that W'_t and B_t are independent and $\rho \in (-1, 1)$ is the correlation coefficient between W_t and W'_t, and that σ_t is an a.s. continuous and square integrable process adapted to the filtration generated by W'_t. We denote by $\mathbb{E}_t$ the conditional expectation with respect to the filtration generated by W_t.

Observe that when the volatility σ is constant, equation (1.1) is the classical Bachelier model. Notice that, in this case, asset prices are normally distributed.

We consider the following hypotheses on the volatility of the asset price. These hypotheses have been taken for the sake of simplicity and can be replaced by adequate integrability conditions.

Hypothesis 1.2.1. *There exist positive constants c_1 and c_2 such that for all $t \in [0, T]$,*

$$c_1 \leq \sigma_t \leq c_2.$$

Hypothesis 1.2.2. *For $p \geq 2$, $\sigma \in \mathbb{L}^{2,p}_{W'}$.*

Hypothesis 1.2.3. *There exists $H \in (0, 1)$ and for all $p \geq 1$ there exist constants $c_1, c_2 > 0$ such that for all $0 \leq s \leq r \leq u \leq T \leq 1$*

$$\{\mathbb{E}(|D^{W'}_r \sigma_u|^p)\}^{1/p} \leq c_1 (u - r)^{H - \frac{1}{2}} \tag{1.2}$$

and

$$\{\mathbb{E}(|D^{W'}_s D^{W'}_r \sigma_u|^p)\}^{1/p} \leq c_2 (u - r)^{H - \frac{1}{2}} (u - s)^{H - \frac{1}{2}}. \tag{1.3}$$

We denote by $(V^E_t)_{t \in [0,T]}$ the value of a European call option with fixed strike k. In particular,

$$V^E_0 = \mathbb{E}(S_T - k)_+.$$

In a similar way, we denote by $(V^A_t)_{t \in [0,T]}$ the price of an arithmetic Asian call option with fixed strike k. Then

$$V^A_0 = \mathbb{E}(A_T - k)_+,$$

where $A_T = \frac{1}{T} \int_0^T S_t dt$.

In oder to to deal with Asian options we follow the same approach as in [6], that is, we consider the martingale $M_t = \mathbb{E}_t(A_T)$. Applying the stochastic Fubini's theorem we get that

$$\begin{aligned} A_T = \frac{1}{T} \int_0^T S_t dt &= \frac{1}{T} \int_0^T \left(S_0 + \int_0^t \sigma_u dW_u \right) dt = \\ &= S_0 + \frac{1}{T} \int_0^T \sigma_u \left(\int_u^T dt \right) dW_u. \end{aligned}$$

This implies that

$$dM_t = \frac{\sigma_t(T-t)}{T} dW_t = \phi_t dW_t, \tag{1.4}$$

where

$$\phi_t := \frac{\sigma_t(T-t)}{T}.$$

Notice that, under the classical Bachelier model, A_T is a Gaussian random variable with mean S_0 and variance $\frac{\sigma^2 T}{3}$.

We denote by $B_E(t, S_t, k, \sigma)$ the classical Bachelier price of a European call option with time to maturity $T-t$, current stock price S_t, strike price k and constant volatility σ. That is,

$$B_E(t, S_t, k, \sigma) = (S_t - k)N(d_E(k, \sigma)) + n(d_E(k, \sigma))\sigma\sqrt{T-t},$$

where

$$d_E(k, \sigma) = \frac{S_t - k}{\sigma\sqrt{T-t}}.$$

Here N and n denote the cumulative distribution function and the probability density function of a standard normal random variable, respectively. Additionally, we recall that the Bachelier price satisfies the following PDE

$$\partial_t B_E(t, x, k, \sigma) + \frac{1}{2}\sigma^2 \partial^2_{xx} B_E(t, x, k, \sigma) = 0. \tag{1.5}$$

Similarly, we denote by $B_A(t, S_t, y_t, k, \sigma)$ the Bachelier price of an arithmetic Asian call option with constant volatility σ, where $y_t = \int_0^t S_u du$. A direct computation shows that (see the Appendix .3 for the details)

$$B_A(t, S_t, y_t, k, \sigma) = \left(S_t \frac{T-t}{T} + \frac{y_t}{T} - k\right) N(d_A(k, \sigma)) + \left(\frac{\sigma(T-t)\sqrt{T-t}}{T\sqrt{3}}\right) n(d_A(k, \sigma)),$$

where

$$d_A(k, \sigma) = \frac{S_t \frac{T-t}{T} + \frac{y_t}{T} - k}{\left(\frac{\sigma(T-t)\sqrt{T-t}}{T\sqrt{3}}\right)}.$$

Notice that we have the relation

$$B_A(t, S_t, y_t, k, \sigma) = B_E\left(t, M_t, k, \frac{\sigma(T-t)}{T\sqrt{3}}\right).$$

We next define the implied volatility (IV) of a European call option as the quantity $I_E(t, k)$ such that

$$V_t^E = B_E(t, S_t, k, I_E(t, k)),$$

and we denote by $I_E(t, k_t^*)$, where $k_t^* = S_t$, the corresponding at-the-money implied volatility (ATMIV) which, in the case of zero interest rates, takes the form $B_E^{-1}(t, S_t, S_t, V_t^E)$. Similarly, we define the implied volatility of an Asian call option $I_A(t, k)$ as the quantity such that

$$V_t^A = B_A(t, S_t, y_t, k, I_A(t, k)),$$

and we denote by $I_A(t, k_t^*)$ the corresponding ATMIV which, in the case of zero interest rates, takes the form $B_A^{-1}(t, S_t, y_t, S_t\frac{T-t}{T} + \frac{y_t}{T}, V_t^A)$. We set $k^* = k_0^*$.

The aim of this chapter is to apply the Malliavin calculus techniques developed in Alòs [7] and Muguruza et al. [6] in order to obtain formulas for the ATMIV level and skew as $T \to 0$ under the general stochastic volatility model (1.1).

The main result of this chapter is the following theorem.

Theorem 1.2.4. *Assume Hypotheses 1.2.1-1.2.3. Then,*

$$\lim_{T\to 0} I_E(0, k^*) = \sigma_0 \quad \textit{and} \quad \lim_{T\to 0} I_A(0, k^*) = \sigma_0. \tag{1.6}$$

Moreover,

$$\begin{aligned}&\lim_{T\to 0} T^{\max(\frac{1}{2}-H,0)}\partial_k I_E(0,k^*)\\&= \lim_{T\to 0} T^{\max(\frac{1}{2}-H,0)}\frac{\rho}{\sigma_0 T^2}\int_0^T\int_r^T \mathbb{E}(D_r^{W'}\sigma_u)dudr\end{aligned} \tag{1.7}$$

and

$$\begin{aligned}&\lim_{T\to 0} T^{\max(\frac{1}{2}-H,0)}\partial_k I_A(0,k^*)\\&= \lim_{T\to 0} T^{\max(\frac{1}{2}-H,0)}\frac{9\rho}{\sigma_0 T^5}\int_0^T (T-r)\int_r^T (T-u)^2\mathbb{E}(D_r^{W'}\sigma_u)dudr,\end{aligned} \tag{1.8}$$

Observe that when prices and volatilities are uncorrelated then the short-time skew equals to zero, which coincides with the constant volatility case. Notice also that if the term $\mathbb{E}(D_r^{W'}\sigma_u)$ is of order $(u-r)^{H-\frac{1}{2}}$, the limit of the right hand side of (1.7) will be 0 if $H > 1/2$ and it will converge to a constant when $H = \frac{1}{2}$. When $H < \frac{1}{2}$ we need to multiply by $T^{\frac{1}{2}-H}$ in order to obtain a finite limit.

The results of Theorem 1.2.4 can be used in order to derive approximation formulas for the price of European and Asian call options. Notice that

$$V_0^E = B_E(0,S_0,k,I_E(0,k)) \quad \text{and} \quad V_0^A = B_A(0,S_0,y_0,k,I_A(0,k)).$$

Then, using Taylor's formula we can use the approximations

$$\begin{aligned}I_E(0,k) &\approx I_E(0,k^*) + \partial_k I_E(0,k^*)(k-k^*),\\ I_A(0,k) &\approx I_A(0,k^*) + \partial_k I_A(0,k^*)(k-k^*).\end{aligned} \tag{1.9}$$

The great utility of these relations is that we can use them to approximate the price of European and Asian call options for a wide range of stochastic and fractional volatility models. We numerically investigate the quality of this approximation for the SABR and fractional Bergomi models in Section 1.5.3.

1.3 Preliminary results: decomposition formulas

In this section we provide closed form decomposition formulas for the prices and for the ATM implied volatility skew of European and Asian call options under the stochastic volatility model (1.1) that will be crucial for the proof of the main results.

We start with a preliminary lemma.

Lemma 1.3.1. *Consider the model* (1.1)*. Let* $0 \le t \le s \le T$*,* $\rho \in (-1,1)$ *and* $\mathcal{G}_t := \mathcal{F}_t \vee \mathcal{F}_T^{W'}$*. Then for every* $n \ge 0$*, there exists* $C = C(n,\rho)$ *such that*

$$\begin{aligned}\left|\mathbb{E}\left(\frac{\partial^n}{\partial x^n}\left(\frac{\partial^2}{\partial x^2}B_E(s,M_s,k,v_s)\right)|\mathcal{G}_t\right)\right| &= \left|\mathbb{E}\left(\frac{\partial^n}{\partial x^n}\left(\frac{\partial^2}{\partial x\partial k}B_E(s,M_s,k,v_s)\right)|\mathcal{G}_t\right)\right|\\ &\le C\left(\int_t^T \phi_r^2 dr\right)^{-\frac{n+1}{2}},\end{aligned}$$

where $v_t = \sqrt{\frac{1}{T-t}\int_t^T \phi_r^2 dr}$

Proof. The proof follows the same steps as the proof of Lemma 6.3.1 in [5]. ■

The main result of this section is the following theorem.

Theorem 1.3.2. *Assume Hypotheses 1.2.1-1.2.3. Then, the following relations hold for all* $t \in [0,T]$*,*

$$\begin{aligned}V_t^E &= \mathbb{E}_t\left(B_E(t,S_t,k,v_t')\right) + \mathbb{E}_t\left(\int_t^T H(s,S_s,k,v_s')\sigma_s\left(\int_s^T D_s^W\sigma_r^2 dr\right)ds\right),\\ V_t^A &= \mathbb{E}_t\left(B_E(t,M_t,k,v_t)\right) + \mathbb{E}_t\left(\int_t^T H(s,M_s,k,v_s)\phi_s\left(\int_s^T D_s^W\phi_r^2 dr\right)ds\right),\end{aligned}$$

where $H(s,x,k,\sigma)=\frac{1}{2}\partial^3_{xxx}B_E(s,x,k,\sigma)$, $v'_t=\sqrt{\frac{1}{T-t}\int_t^T\sigma_s^2ds}$, *and* $v_t=\sqrt{\frac{1}{T-t}\int_t^T\phi_s^2ds}$.

Proof. The proof follows similar ideas as the proof of Theorem 25 in [3]. See also Theorem 6.3.2 in [5]. Notice that, as $B_E(T,x,k,\sigma)=(x-k)_+$ for every $\sigma>0$, the prices of our European and Asian call options can be written as

$$V_t^E=\mathbb{E}_t(B_E(T,S_T,k,v'_T))\quad\text{and}\quad V_t^A=\mathbb{E}_t(B_E(T,M_T,k,v_T)).$$

We provide the proof of the decomposition formula for V_t^A. A similar argument applies for V_t^E and we safely skip it. Applying Theorem .1.2 to the function $B_E(t,M_t,k,v_t)$ and $Y_t=\int_t^T\phi_s^2ds$ noticing that $v_t=\sqrt{\frac{Y_t}{T-t}}$, we obtain

$$\begin{aligned}B_E(T,M_T,k,v_T)&=B_E(t,M_t,k,v_t)\\&+\int_t^T\left(\partial_sB_E(s,M_s,k,v_s)+\partial_\sigma B_E(s,M_s,k,v_s)\frac{v_s^2}{2(T-s)v_s}\right)ds\\&+\int_t^T\partial_xB_E(s,M_s,k,v_s)\phi_sdW_s-\int_t^T\partial_\sigma B_E(s,M_s,k,v_s)\frac{\phi_s^2}{2(T-s)v_s}ds\\&+\int_t^T\partial^2_{\sigma x}B_E(s,M_s,k,v_s)\frac{\phi_s}{2(T-s)v_s}\left(\int_s^TD_s^W\phi_r^2dr\right)ds\\&+\frac{1}{2}\int_t^T\partial^2_{xx}B_E(s,M_s,k,v_s)\phi_s^2ds.\end{aligned}$$

Notice that the following relation holds

$$\partial^2_{xx}B_E(s,M_s,k,\sigma)=\frac{\partial_\sigma B_E(s,M_s,k,\sigma))}{\sigma(T-s)}.\tag{1.10}$$

Then we get the following

$$\begin{aligned}B_E(T,M_T,k,v_T)&=B_E(t,M_t,k,v_t)\\&+\int_t^T\left(\partial_sB_E(s,M_s,k,v_s)+\frac{1}{2}v_s^2\partial^2_{xx}B_E(s,M_s,k,v_s)\right)ds\\&+\int_t^T\partial_xB_E(s,M_s,k,v_s)\phi_sdW_s-\frac{1}{2}\int_t^T\partial^2_{xx}B_E(s,M_s,k,v_s)\phi_s^2ds\\&+\frac{1}{2}\int_t^T\partial^3_{xxx}B_E(s,M_s,k,v_s)\phi_s\left(\int_s^TD_s^W\phi_r^2dr\right)ds\\&+\frac{1}{2}\int_t^T\partial^2_{xx}B_E(s,M_s,k,v_s)\phi_s^2ds.\end{aligned}$$

The first integral in the above expression is equal to zero due to equation (1.5). Finally, taking conditional expectations we conclude that

$$\begin{aligned}\mathbb{E}_t\left(B_E(T,M_T,k,v_T)\right)&=\mathbb{E}_t\left(B_E(t,M_t,k,v_t)\right)\\&+\mathbb{E}_t\left(\frac{1}{2}\int_t^T\partial^3_{xxx}B_E(s,M_s,k,v_s)\phi_s\left(\int_s^TD_s^W\phi_r^2dr\right)ds\right).\end{aligned}$$

Observe that by Lemma 1.3.1 and Hypotheses 1.2.1 and 1.2.3, the last conditional expectation is finite. This completes the desired proof. ■

Based on the result of Theorem 1.3.2, we derive an expression for the ATMIV skew of European and Asian call options under the stochastic volatility model (1.1).

Proposition 1.3.3. *Assume Hypotheses 1.2.1-1.2.3. Then, for every $t \in [0,T]$ the following holds*

$$\partial_k I_E(t,k_t^*) = \frac{\mathbb{E}_t\left(\int_t^T \partial_k H(s,S_s,k_t^*,v_s')\Lambda_s' ds\right)}{\partial_\sigma B_E(t,S_t,k_t^*,I_E(t,k_t^*))},$$
$$\partial_k I_A(t,k_t^*) = \frac{\mathbb{E}_t\left(\int_t^T \partial_k H(s,M_s,k_t^*,v_s)\Lambda_s ds\right)}{\partial_\sigma B_A(t,S_t,y_t,k_t^*,I_A(t,k_t^*))},$$

where $\Lambda_s' = \sigma_s \int_s^T D_s^W \sigma_r^2 dr$ and $\Lambda_s = \phi_s \int_s^T D_s^W \phi_r^2 dr$.

Proof. We provide the proof for the second part of the theorem. The first part follows by similar arguments. Since $V_t^A = B_A(t,S_t,y_t,k,I_A(t,k))$, differentiating we obtain that

$$\partial_k V_t^A = \partial_k B_A(t,S_t,y_t,k,I_A(t,k)) + \partial_\sigma B_A(t,S_t,y_t,k,I_A(t,k))\partial_k I_A(t,k).$$

On the other hand, using Theorem 1.3.2, we get that

$$\partial_k V_t^A = \partial_k \mathbb{E}_t\left(B_E(t,M_t,k,v_t)\right) + \mathbb{E}_t\left(\int_t^T \partial_k H(s,M_s,k,v_s)\Lambda_s ds\right).$$

Combining both equations, we obtain that the volatility skew $\partial_k I_A(t,k)$ is equal to

$$\frac{\mathbb{E}_t\left(\int_t^T \partial_k H(s,M_s,k,v_s)\Lambda_s ds\right) + \mathbb{E}_t\left(\partial_k B_E(t,M_t,k,v_t)\right) - \partial_k B_A(t,S_t,y_t,k,I_A(t,k))}{\partial_\sigma B_A(t,S_t,y_t,k,I_A(t,k))}.$$

Finally, using the fact that

$$\partial_k B_E(t,M_t,k_t^*,\sigma) = \partial_k B_A(t,S_t,y_t,k_t^*,\sigma) = -\frac{1}{2}$$

we complete the desired proof. ■

In order to compute the limit of ATMIV skew, we need to identify the leading order terms in the numerator of the formulas obtained in Proposition 1.3.3, for which the next result will be crucial.

Proposition 1.3.4. *Assume Hypotheses 1.2.1-1.2.3. Then, for all $t \le T$,*

$$\begin{aligned}
\mathbb{E}_t\left(\int_t^T G(s,S_s,k,v_s')\Lambda_s' ds\right) &= \mathbb{E}_t\left(G(t,S_t,k,v_t')J_t'\right) \\
&\quad + \mathbb{E}_t\left(\frac{1}{2}\int_t^T \partial_{xxx}^3 G(s,S_s,k,v_s')J_s'\Lambda_s' ds\right) \\
&\quad + \mathbb{E}_t\left(\int_t^T \partial_x G(s,S_s,k,v_s')\sigma_s D^- J_s' ds\right), \\
\mathbb{E}_t\left(\int_t^T G(s,M_s,k,v_s)\Lambda_s ds\right) &= \mathbb{E}_t\left(G(t,M_t,k,v_t)J_t\right) \\
&\quad + \mathbb{E}_t\left(\frac{1}{2}\int_t^T \partial_{xxx}^3 G(s,M_s,k,v_s)J_s\Lambda_s ds\right) \\
&\quad + \mathbb{E}_t\left(\int_t^T \partial_x G(s,M_s,k,v_s)\phi_s D^- J_s ds\right),
\end{aligned}$$

where $G(t,x,k,\sigma) = \partial_k H(t,x,k,\sigma)$, $J_t = \int_t^T \Lambda_s ds$, $J_t' = \int_t^T \Lambda_s' ds$, $D^- J_s' = \int_s^T D_s^W \Lambda_r' dr$ and $D^- J_s = \int_s^T D_s^W \Lambda_r dr$.

Proof. We only prove the second part of the theorem since the first part follows by similar arguments. Applying Theorem .1.2 to the function $\partial_k H(t, M_t, k, v_t) \int_t^T \Lambda_s ds$, we obtain that

$$\begin{aligned}
\int_t^T G(s, M_s, k, v_s)\Lambda_s ds &= G(t, M_t, k, v_t)J_t \\
&+ \int_t^T \left(\partial_s G(s, M_s, k, v_s) + \frac{v_s^2}{2(T-s)v_s} \partial_v G(s, M_s, k, v_s) \right) J_s ds \\
&+ \int_t^T \partial_x G(s, M_s, k, v_s) J_s \phi_s dW_s \\
&- \int_t^T \partial_v G(s, M_s, k, v_s) J_s \frac{\phi_s^2}{2(T-s)v_s} ds + \int_t^T \partial_{vx}^2 G(s, M_s, k, v_s) J_s \Lambda_s \frac{1}{2(T-s)v_s} ds \\
&+ \int_t^T \partial_x G(s, M_s, k, v_s) \phi_s D^- J_s ds + \frac{1}{2} \int_t^T \phi_s^2 \partial_{xx}^2 G(s, M_s, k, v_s) J_s ds.
\end{aligned}$$

Next, equations (1.5) and (1.10) imply that

$$\begin{aligned}
\partial_s G(s, M_s, k, v_s) + \frac{1}{2} v_s^2 \partial_{xx}^2 G(s, M_s, k, v_s) &= 0, \\
\partial_{xx}^2 G(s, M_s, k, v_s) &= \frac{\partial_v G(s, M_s, k, v_s)}{v_s (T-s)}.
\end{aligned}$$

Using the above equations we get that

$$\begin{aligned}
\int_t^T G(s, M_s, k, v_s)\Lambda_s ds &= G(t, M_t, k, v_t)J_t + \int_t^T \partial_x G(s, M_s, k, v_s) J_s \phi_s dW_s \\
&+ \frac{1}{2} \int_t^T \partial_{xxx}^3 G(s, M_s, k, v_s) J_s \Lambda_s ds + \int_t^T \partial_x G(s, M_s, k, v_s) \phi_s D^- J_s ds.
\end{aligned}$$

Finally, taking conditional expectations and noticing that by Lemma 1.3.1 and Hypotheses 1.2.1 and 1.2.3, all conditional expectations are finite, we complete the desired proof. ■

1.4 Proof of Theorem 1.2.4

1.4.1 Proof of (1.6) in Theorem 1.2.4: ATM implied volatility level

This section is devoted to the proof of (1.6) in Theorem 1.2.4. We only show the result for $I_A(0, k^*)$ since the proof for $I_E(0, k^*)$ follows along the same lines. We start proving the result for the implied volatility in the uncorrelated case ($\rho = 0$) that we denote by $I_A^0(t, k)$.

1.4.1.1 The uncorrelated case

We aim to apply the decomposition for the option price obtained in Theorem 1.3.2. Observe that

$$D_s^W \phi_r^2 dr = \frac{(T-r)^2}{T^2} D_s^W \sigma_r^2 = \frac{(T-r)^2}{T^2} 2\sigma_r D_s^W \sigma_r = \frac{(T-r)^2}{T^2} 2\sigma_r \rho D_s^{W'} \sigma_r.$$

Thus, if $\rho = 0$, the decomposition formula give us that $V_0^A = \mathbb{E}(B_E(0, M_0, k, v_0))$. Then the ATMIV satisfies that

$$\begin{aligned}
I_A^0(0, k^*) &= (B_A)^{-1}(0, S_0, y_0, k^*, V_0^A) = \mathbb{E}\left(B_A^{-1}(0, S_0, y_0, k^*, \mathbb{E}B_E(0, M_0, k^*, v_0))\right) \\
&= \mathbb{E}\left(B_A^{-1}(0, S_0, y_0, k^*, \mathbb{E}B_E(0, M_0, k^*, v_0)) \pm B_A^{-1}(0, S_0, y_0, k^*, B_E(0, M_0, k^*, v_0))\right) \\
&= \mathbb{E}\left(B_A^{-1}(0, S_0, y_0, k^*, \Phi_0) - B_A^{-1}(0, S_0, y_0, k^*, \Phi_T)\right) + \sqrt{3}\mathbb{E}(v_0) \\
&= \sqrt{3}\mathbb{E}\left(B_E^{-1}(0, M_0, k^*, \Phi_0) - B_E^{-1}(0, M_0, k^*, \Phi_T)\right) + \sqrt{3}\mathbb{E}(v_0),
\end{aligned}$$

where $\Phi_r := \mathbb{E}_r\left(B_E\left(0, M_0, k^*, v_0\right)\right)$. The last two lines follow from the observation that $B_A^{-1}(t, S_t, y_t, k_t^*, B_E(t, M_t, k_t^*, \sigma)) = \frac{T\sqrt{3}}{T-t}\sigma$.

Observe that as $\rho = 0$, the Brownian motions W and W' are independent. Thus, $\Phi_r = \mathbb{E}\left(B_E\left(0, M_0, k^*, v_0\right)|\mathcal{F}_r^{W'}\right)$ and $(\Phi_r)_{r\geq 0}$ is a martingale wrt to the filtration $(\mathcal{F}_r^{W'})_{r\geq 0}$. By the martingale representation theorem, there exists a square integrable and $\mathcal{F}^{W'}$-adapted process $(U_r)_{r\geq 0}$ such that

$$\Phi_r = \Phi_0 + \int_0^r U_s dW'_s.$$

A direct application of the classical Itô's formula gives

$$\begin{aligned}
&\mathbb{E}\left(B_E^{-1}(0, M_0, k^*, \Phi_0) - B_E^{-1}(0, M_0, k^*, \Phi_T)\right) \\
&= -\mathbb{E}\left(\int_0^T (B_E^{-1})'(0, M_0, k^*, \Phi_s) U_s dW'_s + \frac{1}{2}\int_0^T (B_E^{-1})''(0, M_0, k^*, \Phi_s) U_s^2 ds\right),
\end{aligned}$$

where $(B_E^{-1})'$ and $(B_E^{-1})''$ denote, respectively, the first and second derivative of B_E^{-1} with respect to σ. A direct computation gives

$$B_E^{-1}(0, M_0, k^*, \Phi_s) = \frac{\Phi_s\sqrt{2\pi}}{\sqrt{T}} \quad \text{and} \quad ((B_E)^{-1})''(0, M_0, k^*, \Phi_s) = 0,$$

which leads to

$$I_A^0(0, k^*) = \sqrt{3}\mathbb{E}(v_0).$$

By continuity, we conclude that

$$\lim_{T\to 0} I_A^0(0, k^*) = \sigma_0, \tag{1.11}$$

which proves (1.6) in the uncorrelated case.

1.4.1.2 The correlated case

Using similar ideas as in the uncorrelated case we get that

$$\begin{aligned}
I_A(0, k^*) &= (B_A)^{-1}(0, S_0, y_0, k^*, V_0^A) \\
&= \mathbb{E}\left((B_A)^{-1}(0, S_0, y_0, k^*, \Gamma_T) \pm (B_A)^{-1}(0, S_0, y_0, k^*, \Gamma_0)\right) \\
&= \mathbb{E}\left((B_A)^{-1}(0, S_0, y_0, k^*, \Gamma_T) - (B_A)^{-1}(0, S_0, y_0, k^*, \Gamma_0)\right) + I_A^0(0, k^*) \\
&= \sqrt{3}\mathbb{E}\left(B_E^{-1}(0, M_0, k^*, \Gamma_T) - B_E^{-1}(0, M_0, k^*, \Gamma_0)\right) + I_A^0(0, k^*),
\end{aligned}$$

where $\Gamma_s := \mathbb{E}[B_E(0, M_0, k^*, v_0)] + \frac{\rho}{2}\mathbb{E}\left(\int_0^s H(r, M_r, k_t^*, v_r)\Lambda_r dr\right)$.

A direct application of Itô's formula gives

$$\begin{aligned}
I_A(0, k^*) &= I_A^0(0, k^*) + \mathbb{E}\left(\int_0^T (B_E^{-1})'(0, M_0, k^*, \Gamma_s) H(s, M_s, k_t^*, v_s)\Lambda_s ds\right) \\
&= I_A^0(0, k^*) + \frac{\sqrt{2\pi}}{\sqrt{T}}\mathbb{E}\left(\int_0^T H(s, M_s, k_t^*, v_s)\Lambda_s ds\right).
\end{aligned}$$

Next, Hypotheses 1.2.1 and 1.2.3 together with Lemma 1.3.1 imply that

$$\begin{aligned}
\left|\mathbb{E}\left(\int_0^T H(s, M_s, k^*, v_s)\Lambda_s ds\right)\right| &\leq C\mathbb{E}\left(\left(\int_0^T \phi_r^2 dr\right)^{-1}\left(\int_0^T |\Lambda_s| ds\right)\right) \\
&\leq C\left(\int_0^T \frac{(T-r)^2}{T^2} dr\right)^{-1}\int_0^T \frac{(T-s)^3}{T^3}\int_s^T \mathbb{E}(|D_s^{W'}\sigma_r|) dr ds \\
&\leq C\frac{1}{T^4}\int_0^T (T-s)^3\int_s^T (r-s)^{H-\frac{1}{2}} dr ds \\
&= CT^{H+\frac{1}{2}}.
\end{aligned}$$

Thus, we conclude that $\frac{1}{\sqrt{T}}\mathbb{E}\left(\int_0^T H(s,M_s,k_t^*,v_s)\Lambda_s ds\right)\to 0$ as $T\to 0$. Finally, using (1.11), we get that

$$I_A(0,k^*)\to\sigma_0$$

as $T\to 0$, which concludes the proof of (1.6).

1.4.2 Proof of (1.7) in Theorem 1.2.4: ATMIV skew

We provide the proof for the Asian call option case. The result for the European call follows by the same argument.

Appealing to Propositions 1.3.3 and 1.3.4 we have that

$$\begin{aligned}\partial_k I_A(0,k^*) = \frac{1}{\partial_\sigma B_A(0,S_0,y_0,k^*,I_A(0,k^*))}\Big\{&\mathbb{E}\left(G(0,M_0,k^*,v_0)J_0\right)\\ &+\mathbb{E}\left(\frac{1}{2}\int_0^T \partial^3_{xxx}G(s,M_s,k^*,v_s)J_s\Lambda_s ds\right)\\ &+\mathbb{E}\left(\int_0^T \partial_x G(s,M_s,k^*,v_s)\phi_s D^- J_s ds\right)\Big\}.\end{aligned}\tag{1.12}$$

We start bounding the second term in (1.12). Using Hypotheses 1.2.1 and 1.2.3 together with Cauchy-Schwarz inequality we get that

$$\begin{aligned}&\mathbb{E}(|J_s\Lambda_s|)\\ &\le C\frac{(T-s)}{T^6}\mathbb{E}\left(\left(\int_s^T (T-r)^2|D_s^{W'}\sigma_r|dr\right)\left(\int_s^T (T-u)^3\int_u^T |D_u^{W'}\sigma_r|drdu\right)\right)\\ &\le C\frac{(T-s)}{T^6}\sqrt{\mathbb{E}\left(\left(\int_s^T (T-r)^2|D_s^{W'}\sigma_r|dr\right)^2\right)\mathbb{E}\left(\left(\int_s^T (T-u)^3\int_u^T |D_u^{W'}\sigma_r|drdu\right)^2\right)}\\ &\le C\frac{(T-s)}{T^6}\sqrt{(T-s)^5\int_s^T \mathbb{E}\left(|D_s^{W'}\sigma_r|^2\right)dr(T-s)^8\int_s^T\int_u^T \mathbb{E}\left(|D_u^{W'}\sigma_r|^2\right)drdu}\\ &\le C\frac{(T-s)^{2H+8}}{T^6}.\end{aligned}$$

Then, using Lemma 1.3.1 we conclude that

$$\begin{aligned}&\left|\mathbb{E}\left(\frac{1}{2}\int_0^T \partial^3_{xxx}G(s,M_s,k,v_s)J_s\Lambda_s ds\right)\right|\\ &\qquad\le C\frac{1}{T^3}\int_0^T\frac{(T-s)^{2H+8}}{T^6}dt = CT^{2H}.\end{aligned}$$

We next bound the third term in (1.12). We have that

$$\begin{aligned}\int_s^T D_s^W\Lambda_r dr &= \int_s^T D_s^W\left(\phi_r\int_r^T D_r^W\phi_u^2 du\right)dr\\ &= \int_s^T\left(\left(D_s^W\phi_r\right)\int_r^T D_r^W\phi_u^2 du+\phi_r\int_r^T D_s^W D_r^W\phi_u^2 du\right)dr,\end{aligned}$$

where

$$D_s^W D_r^W\phi_u^2 = 2(D_s^W\phi_u D_r^W\phi_u+\phi_u D_s^W D_r^W\phi_u).$$

Hypothesis 1.2.1 implies that

$$|D_s^W D_r^W\phi_u^2|\le C\frac{(T-u)^2}{T^2}\left(|D_s^{W'}\sigma_u|\,|D_r^{W'}\sigma_u|+|D_s^{W'}D_r^{W'}\sigma_u|\right).$$

Then, appealing to Hypothesis 1.2.3, we get that

$$\begin{aligned}\mathbb{E}\left(\left|\phi_r\int_r^T D_s^W D_r^W \phi_u^2 du\right|\right) &\leq C\frac{(T-r)^3}{T^3}\int_r^T (u-r)^{H-\frac{1}{2}}(u-s)^{H-\frac{1}{2}}du\\ &\leq C\frac{(T-r)^3}{T^3}(T-s)^{2H}\end{aligned}$$

and

$$\begin{aligned}\mathbb{E}\left(\left|D_s^W\phi_r\int_r^T D_r^W\phi_u^2 du\right|\right) &\leq C\frac{(T-r)^3}{T^3}\mathbb{E}\left(|D_s^{W'}\sigma_r|\int_r^T |D_r^{W'}\sigma_u|du\right)\\ &\leq C\frac{(T-r)^3}{T^3}(r-s)^{H-\frac{1}{2}}(T-r)^{H+\frac{1}{2}}.\end{aligned}$$

Therefore, we conclude that

$$\begin{aligned}\mathbb{E}\left(\left|\int_s^T D_s^W\Lambda_r dr\right|\right) &\leq C\int_s^T \frac{(T-r)^3}{T^3}\left((r-s)^{H-\frac{1}{2}}(T-s)^{H+\frac{1}{2}}+(T-s)^{2H}\right)dr\\ &\leq C\frac{(T-s)^{2H+4}}{T^3}.\end{aligned}$$

Finally, using Lemma 1.3.1 we obtain that the third term in (1.12) satisfies that

$$\begin{aligned}\left|\mathbb{E}\left(\int_0^T \partial_x G(s,M_s,k,v_s)\phi_s D^- J_s ds\right)\right| &\leq C\frac{1}{T^2}\int_0^T\frac{(T-s)^{5+2H}}{T^4}ds\\ &= CT^{2H}.\end{aligned}$$

Taking into account the relation $\partial_\sigma B_A(0,S_0,y_0,k^*,\sigma)=\frac{1}{\sqrt{3}}\partial_\sigma B_E(0,S_0,k^*,\sigma)$ we get that

$$\partial_\sigma B_A(0,S_0,y_0,k^*,\sigma)=\frac{\sqrt{T}}{\sqrt{6\pi}}.$$

Thus, as

$$\lim_{T\to 0} T^{\max(\frac{1}{2}-H,0)}\frac{1}{\sqrt{T}}T^{2H}=0,$$

the second and third terms in (1.12) will contribute as 0 in the limit (1.8).

We finally study the first term in (1.12). Direct differentiation give us that

$$G(0,M_0,k^*,v_0)=\frac{1}{2\sqrt{2\pi}v_0^3T^{3/2}}.$$

Thus, by (1.12), we get that

$$\begin{aligned}&\lim_{T\to 0} T^{\max(\frac{1}{2}-H,0)}\partial_k I_A(0,k^*)\\ &=\sqrt{3}\rho\lim_{T\to 0}T^{\max(\frac{1}{2}-H,0)}\frac{1}{T^5}\mathbb{E}\left(v_0^{-3}\int_0^T\sigma_r(T-r)\int_r^T\sigma_u(T-u)^2D_r^{W'}\sigma_u dudr\right).\end{aligned}$$

By continuity, it holds that v_0^{-3} converges towards $\sigma_0^{-3}\sqrt{3}^3$ a.s. as $T\to 0$. On the other hand, by Hypotheses 1.2.1 and (1.2), we have that

$$\begin{aligned}&\left|\mathbb{E}\left(\int_0^T\sigma_r(T-r)\int_r^T\sigma_u(T-u)^2D_r^{W'}\sigma_u dudr\right)\right|\\ &\leq C\int_0^T(T-r)^3\int_r^T(u-r)^{H-\frac{1}{2}}dudr\\ &\leq CT^{4+H+\frac{1}{2}}.\end{aligned}$$

Thus, by dominated convergence, we conclude the proof of (1.8).

1.5 Numerical analysis

In this section we apply the theoretical results presented earlier to some examples of stochastic volatility models. We justify our findings with numerical simulations.

1.5.1 The SABR model

We consider the SABR stochastic volatility model with the skewness parameter equal 1, which is the most common case from a practical point of view. This corresponds to equation (1.1), where S_t denotes the forward price of the underlying asset and

$$d\sigma_t = \alpha\sigma_t dW'_t, \qquad \sigma_t = \sigma_0 e^{\alpha W'_t - \frac{\alpha^2}{2}t}.$$

where $\alpha > 0$ is the volatility of volatility.

Notice that this model does not satisfy Hypothesis 1.2.1, so a truncation argument is needed in order to check that Theorem 1.2.4 is true for this model. We skip it here for the sake of simplicity since it is identical to the one presented in Section 2.5.2.

For $r \leq t$, we have that $D_r^{W'}\sigma_t = \alpha\sigma_t$ and $\mathbb{E}\left(D_r^{W'}\sigma_t\right) = \alpha\sigma_0$. Therefore, applying Theorem 1.2.4 we conclude that

$$\lim_{T\to 0} \partial_k I_A(0,k^*) = \frac{3}{5}\rho\alpha,$$
$$\lim_{T\to 0} \partial_k I_E(0,k^*) = \frac{1}{2}\rho\alpha.$$

We next proceed with some numerical simulations using the following parameters

$$S_0 = 10,\ T = \frac{1}{252},\ dt = \frac{T}{50},\ \alpha = 0.5,\ \rho = -0.3,\ \sigma_0 = (0.1, 0.2, \ldots, 1.4).$$

In order to get estimates of an Asian call option we use antithetic variates. The estimator of the price is defined as follows

$$\hat{V}_{sabr} = \frac{\frac{1}{N}\sum_{i=1}^N V_T^i + \frac{1}{N}\sum_{i=1}^N V_T^{i,A}}{2}, \tag{1.13}$$

where $N = 2000000$ and the sub-index A denotes the value of an Asian call option computed on the antithetic trajectory of a Monte Carlo path.

In order to retrieve the implied volatility we use method presented in Jaeckel [40]. For the estimation of the skew, we use the following expression which allows us to avoid a finite difference method

$$\begin{aligned}
\partial_k \hat{I}^A(0,k^*) &= \frac{-\partial_k B_A(0,X_0,y_0,k^*,I_A(0,k^*)) - \mathbb{E}\left(1_{A_T\geq k^*}\right)}{\partial_\sigma B_A(0,X_0,y_0,k^*,I_A(0,k^*))} = \frac{\frac{1}{2} - \mathbb{E}\left(1_{A_T\geq k^*}\right)}{\sqrt{\frac{T}{6\pi}}}, \\
\partial_k \hat{I}^E(0,k^*) &= \frac{-\partial_k B_E(0,S_0,k^*,I_E(0,k^*)) - \mathbb{E}\left(1_{S_T\geq k^*}\right)}{\partial_\sigma B_E(0,S_0,k^*,I_E(0,k^*))} = \frac{\frac{1}{2} - \mathbb{E}\left(1_{S_T\geq k^*}\right)}{\sqrt{\frac{T}{2\pi}}}.
\end{aligned} \tag{1.14}$$

We use equation (1.14) in order to get estimates of the skew. In Figure 1.1 we present the results of a Monte Carlo simulation which aims to evaluate numerically the level and the skew of the at-the-money implied volatility of an Asian call option under the SABR model. And in Figure 1.2 we do the same, but for the European call option. We observe that all the numerical results fit the theoretical ones.

1.5.2 The fractional Bergomi model

The fractional Bergomi stochastic volatility model assumes equation (1.1) with

$$\sigma_t^2 = \sigma_0^2 e^{v\sqrt{2H}Z_t - \frac{1}{2}v^2 t^{2H}},$$
$$Z_t = \int_0^t (t-s)^{H-\frac{1}{2}} dW'_s,$$

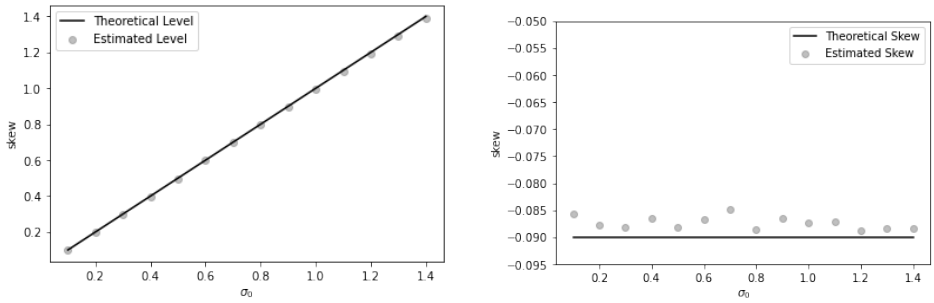

Figure 1.1: At-the-money level and the skew of the Implied Volatility of an Asian call under the SABR model.

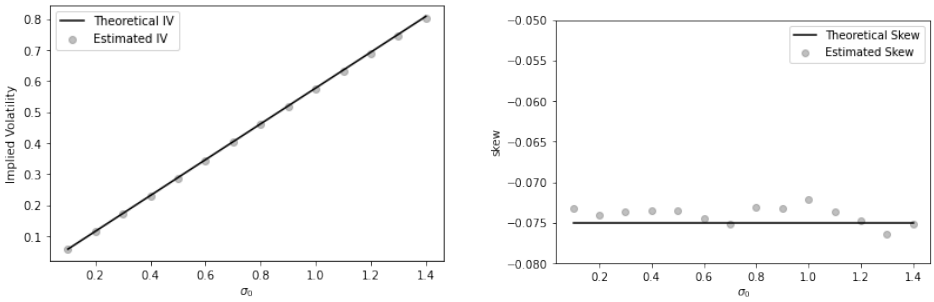

Figure 1.2: At-the-money level and the skew of the Implied Volatility of the European call option under the SABR model.

where $H \in (0,1)$ and $v > 0$.

As for the SABR model, a truncation argument as in Section 2.5.3 is needed in order to apply the results in the previous sections, as Hypothesis 1.2.1 is not satisfied. Moreover, for $r \leq u$, we have

$$D_r^{W'}\sigma_u = \frac{1}{2}\sigma_u v\sqrt{2H}(u-r)^{H-\frac{1}{2}},$$
$$\mathbb{E}(D_r^{W'}\sigma_u) = e^{-\frac{1}{8}v^2u^{2H}}\frac{1}{2}\sigma_0 v\sqrt{2H}(u-r)^{H-\frac{1}{2}},$$

which gives

$$\begin{aligned}\lim_{T\to 0}\partial_k I_A(0,k^*) &= \begin{cases}0 & \text{if} \quad H > \frac{1}{2}\\ \frac{3\rho v}{10} & \text{if} \quad H = \frac{1}{2},\end{cases},\\ \lim_{T\to 0}\partial_k I_E(0,k^*) &= \begin{cases}0 & \text{if} \quad H > \frac{1}{2}\\ \frac{\rho v}{4} & \text{if} \quad H = \frac{1}{2}.\end{cases}\end{aligned} \tag{1.15}$$

and for $H < \frac{1}{2}$

$$\begin{aligned}\lim_{T\to 0} T^{\frac{1}{2}-H}\partial_k I_A(0,k^*) &= \frac{288\rho v\sqrt{2H}}{(2H+9)\left(8H^3+36H^2+46H+15\right)},\\ \lim_{T\to 0} T^{\frac{1}{2}-H}\partial_k I_E(0,k^*) &= \frac{2\rho v\sqrt{2H}}{(3+4H(2+H))}.\end{aligned} \tag{1.16}$$

The parameters used for the Monte Carlo simulation are the following

$$S_0 = 100,\ T = 0.001,\ dt = \frac{T}{50},\ H = (0.4, 0.7),\ v = 0.5,\ \rho = -0.3,\ \sigma_0 = (0.1, 0.2, \ldots, 1.4).$$

In order to get estimates of the price of an Asian call option under the fractional Bergomi model we use antithetic variates presented in equation (1.13). Then, the level of at-the-money implied

volatility of an Asian and European call options are presented on Figures 1.3 and 1.4, respectively. One can see that the result is independent of H.

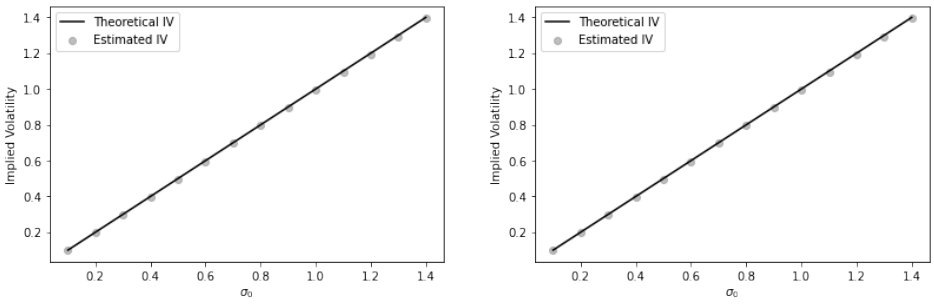

(a) H=0.4 (b) H=0.7

Figure 1.3: At-the-money level of the IV of an Asian call under fractional Bergomi model.

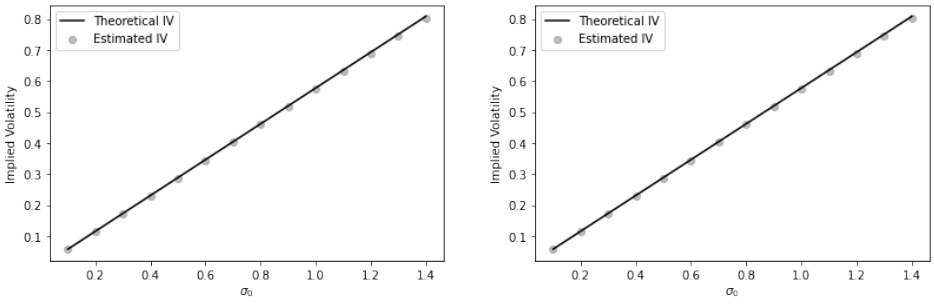

(a) H=0.4 (b) H=0.7

Figure 1.4: At-the-money level of the IV of the European call under fractional Bergomi model.

On Figures 1.5 and 1.6 we present the ATM implied volatility skew as a function of maturity of an Asian and European call options, respectively, for two different values of H, where we observe the blow up to $-\infty$ for the case $H = 0.4$. Equation (1.15) suggests that the theoretical values of the slope of the at-the-money skew (as a function αT^{β}) in the cases of Asian and European call options with $H < \frac{1}{2}$ are -0.0497 and -0.0336, respectively. We conclude that theoretical results are in line with the observed numbers. Due to the blow up of the at-the-money implied

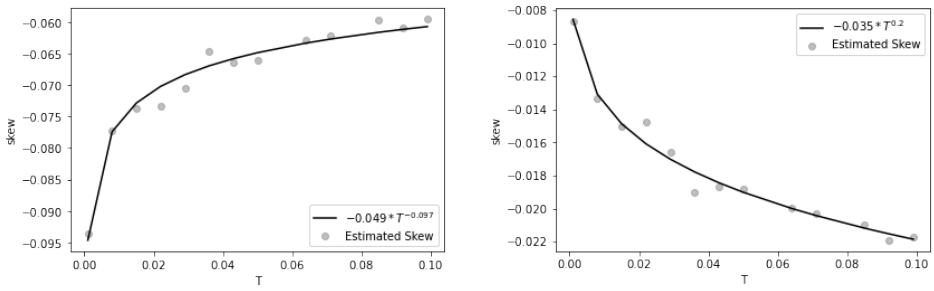

(a) H=0.4, $\sigma_0 = 0.3$ (b) H=0.7, $\sigma_0 = 0.3$

Figure 1.5: At-the-money IV skew of an Asian call as a function of T under fractional Bergomi model.

volatility skew of an Asian and European call options when $H < \frac{1}{2}$ we also plot (as a function of σ_0) the quantities $T^{\frac{1}{2}-H}\partial_k \hat{I}^A(0, k^*)$ and $T^{\frac{1}{2}-H}\partial_k \hat{I}^E(0, k^*)$ for $H = 0.4$ as well as $\partial_k \hat{I}^A(0, k^*)$ and $\partial_k \hat{I}^E(0, k^*)$ for $H = 0.7$ for fixed value of $T = 0.001$. The result is presented at Figures 1.7 and 1.8. We see that numerical estimates agree with the presented theoretical findings.

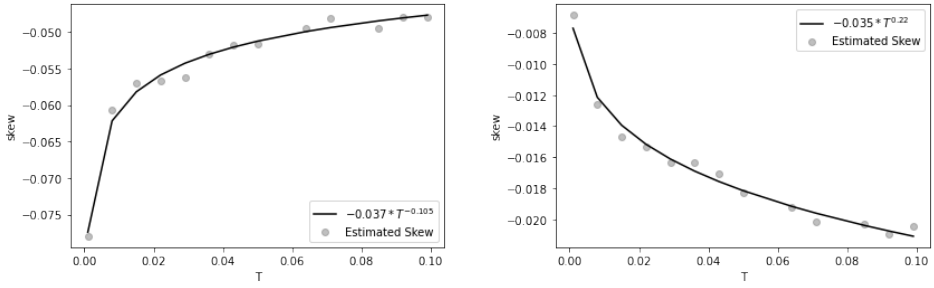

(a) H=0.4, $\sigma_0 = 0.3$ (b) H=0.7, $\sigma_0 = 0.3$

Figure 1.6: At-the-money IV skew of the European call as a function of T under fractional Bergomi model.

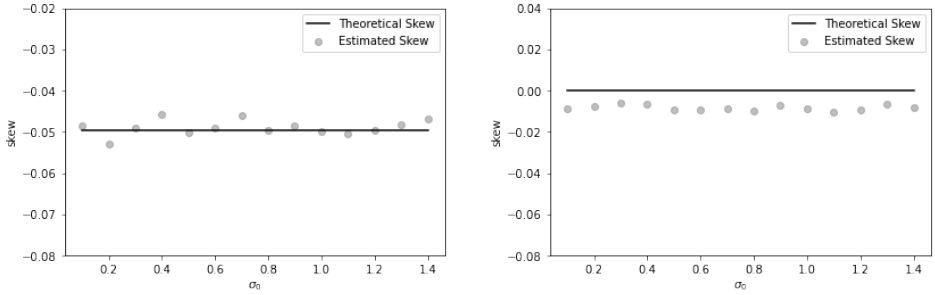

(a) H=0.4 (b) H=0.7

Figure 1.7: At-the-money IV skew of an Asian call as a function of σ_0 under fractional Bergomi model

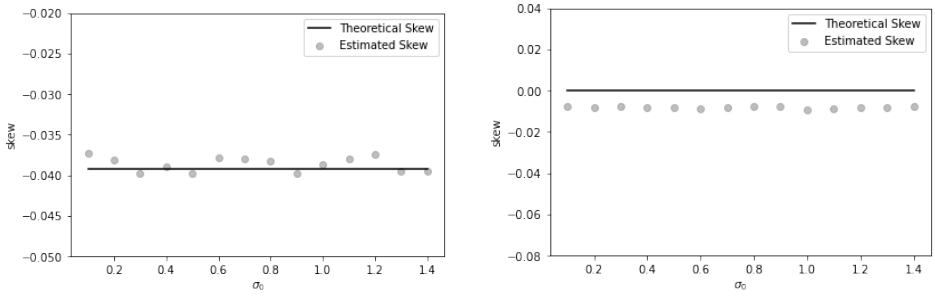

(a) H=0.4 (b) H=0.7

Figure 1.8: At-the-money IV skew of the European call as a function of σ_0 under fractional Bergomi model

1.5.2.1 Local volatility model

We consider the local volatility model

$$dS_t = \sigma(S_t)dW_t,$$

where $\sigma \in C_b^2$ (bounded with bounded first and second derivatives) and $\sigma(x) \geq c > 0$, for all x. We apply Theorem 1.2.4 when S_t follows this model with $\rho = 0$ and $\sigma_t = \sigma(S_t)$. Under the above assumptions it is easy to see that all the hypotheses are satisfied with $H = \frac{1}{2}$. Thus, for the ATMIV level, we directly see that the limit is equal to $\sigma(S_0)$. For the ATMIV skew, we need to compute $D_r\sigma(S_t)$. We have for $r \leq u$,

$$D_r^W \sigma(S_u) = \sigma'(S_u) D_r^W S_u = \sigma'(S_u) \left(\sigma(S_r) + \int_r^u D_r^W \sigma(S_s) dW_s \right).$$

In particular,

$$\mathbb{E}\left(D_r\sigma(S_u)\right) = \mathbb{E}\left(\sigma'(S_u)\sigma(S_r)\right).$$

This can be written as

$$\begin{aligned}\mathbb{E}\left(D_r\sigma(S_u)\right) = \sigma'(S_0)\sigma(S_0) + \mathbb{E}\left((\sigma'(S_u) - \sigma'(S_0))\sigma(S_r)\right) \\ + \sigma'(S_0)\mathbb{E}\left((\sigma(S_r) - \sigma(S_0))\right).\end{aligned}$$

Then, using the mean value theorem and the fact that S_t has Hölder continuous sample paths of any order $\gamma < \frac{1}{2}$, we see that the last two terms of the last display will not contribute in the limit (1.7) and (1.8). Thus, we get

$$\begin{aligned}\lim_{T\to 0} \partial_k I_A(0,k^*) &= \frac{3}{5}\sigma'(S_0), \\ \lim_{T\to 0} \partial_k I_E(0,k^*) &= \frac{1}{2}\sigma'(S_0).\end{aligned}$$

1.5.3 Approximations of implied volatility

In this last section we study numerically the adequacy of the linear approximation of the implied volatility of an Asian and European call options given by equation (1.9) in the case of the SABR and fractional Bergomi models.

1.5.3.1 Asian call option

We start our analysis by presenting the results for the case of an Asian call option.

The SABR Model We proceed with the following numerical experiment. We randomly sample the parameters as $\sigma_0 \sim U(0.2, 0.8)$, $\alpha \sim U(0.3, 1.5)$ and $\rho \sim U(-0.9, 0.9)$, where U stands for the uniform distribution. We fix $S_0 = 10$ and consider the following strikes

$$K = (9.97, 9.9743, 9.9786, 9.9829, 9.9872, 9.9915, 9.9958, 10.0001)$$

and maturities $T = (0.01, 0.1, 0.5, 1, 2)$. We consider the narrow OTM range around ATM region because due to the law of large numbers deep OTM quickly loose the value and prices become indistinguishable from 0. An Asian call option is priced using Monte Carlo with 100000 paths and discretization step 0.01 and the IV is estimated using the same approach as discussed in Section 1.5.1. The approximation accuracy of the Monte Carlo for the IV is computed using the pointwise relative error with respect to the 95% Monte Carlo confidence interval and is presented in Table 1.1.

Maturity/Strike	9.9700	9.9743	9.9786	9.9829	9.9872	9.9915	9.9958	10.0
0.01	0.94	0.92	0.91	0.91	0.91	0.92	0.93	0.94
0.1	0.94	0.94	0.94	0.95	0.95	0.95	0.95	0.95
0.50	1.02	1.02	1.02	1.02	1.02	1.0	1.0	
1.0	1.1	1.1	1.10	1.1	1.1	1.1	1.1	1.0
2.0	1.3	1.3	1.3	1.3	1.3	1.3	1.3	1.3

Table 1.1: Median percentage error wrt the 95% Monte Carlo confidence interval for an Asian call IV under the SABR model.

We then compare the estimated IV with the approximation formula (1.9). We compute in Table 1.2 the median relative percentage error, the 90% quantile and the maximum of the relative percentage error of the Monte Carlo prices computed across 2000 random parameter combinations. We consider the 90% quantile in order to take into account the fact that we might generate 'bad' parameter combinations that may require more Monte Carlo samples to converge. In order to help the visualization of these quantities we also plot the heat map in Figure 1.9.

Overall, we can see that the suggested implied volatility approximation performs well in the ATM region for short dated options. We achieve implied volatility approximation accuracy comparable

Maturity/Strike	9.9700	9.9743	9.9786	9.9829	9.9872	9.9915	9.9958	10.0001
0.01	0.24	0.23	0.22	0.23	0.23	0.24	0.24	0.72
0.10	0.26	0.25	0.25	0.25	0.24	0.24	0.24	0.29
0.50	0.89	0.89	0.87	0.87	0.87	0.87	0.86	0.81
1.00	1.95	1.93	1.92	1.91	1.90	1.89	1.89	1.84
2.00	4.04	4.04	4.03	4.01	4.02	4.05	4.02	4.00

(a) Median % error

Maturity/Strike	9.9700	9.9743	9.9786	9.9829	9.9872	9.9915	9.9958	10.0001
0.01	0.57	0.54	0.51	0.51	0.51	0.53	0.53	1.18
0.10	0.71	0.69	0.66	0.64	0.63	0.62	0.61	0.63
0.50	3.53	3.50	3.47	3.45	3.44	3.41	3.41	3.36
1.00	6.94	6.92	6.91	6.90	6.90	6.86	6.82	6.79
2.00	12.76	12.75	12.71	12.67	12.67	12.58	12.55	12.54

(b) 90th quantile % Error

Maturity/Strike	9.9700	9.9743	9.9786	9.9829	9.9872	9.9915	9.9958	10.0001
0.01	5.17	1.87	1.19	0.95	1.07	1.13	1.20	1.93
0.10	2.26	2.04	1.84	1.67	1.53	1.42	1.36	1.35
0.50	6.17	5.94	5.80	5.68	5.64	5.62	5.61	5.56
1.00	10.78	10.66	10.63	10.61	10.60	10.59	10.58	10.55
2.00	18.65	18.58	18.52	18.46	18.40	18.36	18.31	18.25

(c) Maximum % error

Table 1.2: Approximation error of Asian call IV under the SABR model.

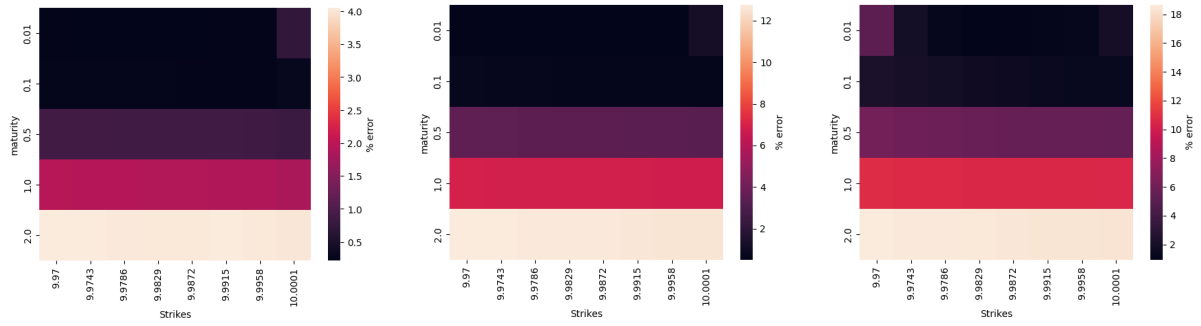

(a) Median (b) 90% Quantile (c) Maximum

Figure 1.9: Accuracy of the approximation (1.9) for an Asian call under the SABR model.

to the original Monte Carlo simulation. However, the quality of it impairs as soon as we move in the maturity ($T > 0.5$) and moneyness dimension.

In order to explain why the approximation impairs with the maturity of an option, we show a "typical" implied volatility surface in the simulated data set at Figure 1.10. One can see that ATM level of the implied volatility $I_A(0, k^*)$ changes considerably with the increase of maturity leading to the decrease in the quality of the linear approximation.

fractional Bergomi Model In the case of the fractional Bergomi model we randomly sample the parameters of the model as $\sigma_0 \sim U(0.2, 0.8)$, $v \sim U(0.3, 1.5)$ and $\rho \sim U(-0.9, 0.9)$. We keep the values of S_0, K and T identical to the one in the SABR case. In order to investigate the influence of fractionalness of the volatility process we consider two values of $H = \{0.2, 0.7\}$. We price the Asian call option using Monte Carlo with 100000 paths and discretization step 0.01.

We start with the case $H = 0.2$. The implied volatility approximation accuracy using Monte Carlo is computed using the corresponding pointwise median relative error with respect to the

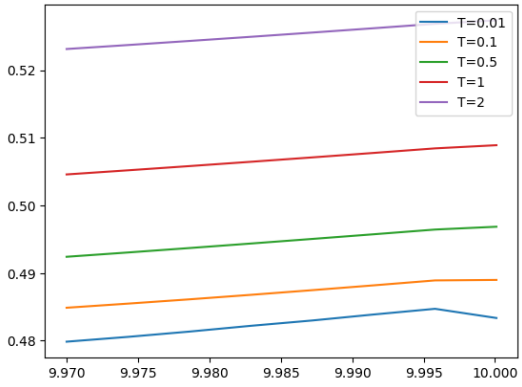

Figure 1.10: Implied volatility surface of an Asian call under the SABR model.

95% Monte Carlo confidence interval. The result is presented at Table 1.3. Next, we look at the

Maturity/Strike	9.9700	9.9743	9.9786	9.9829	9.9872	9.9915	9.9958	10.0001
0.01	1.07	1.01	0.97	0.94	0.93	0.93	0.94	0.95
0.10	0.96	0.96	0.95	0.95	0.95	0.95	0.95	0.95
0.50	0.98	0.98	0.98	0.98	0.98	0.98	0.97	0.97
1.00	1.00	1.00	0.99	0.99	0.99	0.99	0.99	0.99
2.00	1.30	1.29	1.29	1.29	1.28	1.28	1.28	1.28

Table 1.3: Median percentage error wrt the 95% Monte Carlo confidence interval for an Asian call IV under the fractional Bergomi (H=0.2) model.

behaviour of the linear approximation of the implied volatility. The methodology is the same as in the case of the SABR. The results are presented in Table 1.4 and Figure 1.11. Overall, the conclusion is the same as in the case of the SABR model. However, the approximation performs very well at short maturity ($T \leq 0.1$) around ATM region and gets worse with the increase of maturity. This impairment of the approximation is not drastic, but the error is bigger than in Monte Carlo simulation. One can see that the median error is bounded by 3.5 percent over the whole surface under consideration. This behaviour becomes clear by looking at Figure 1.12

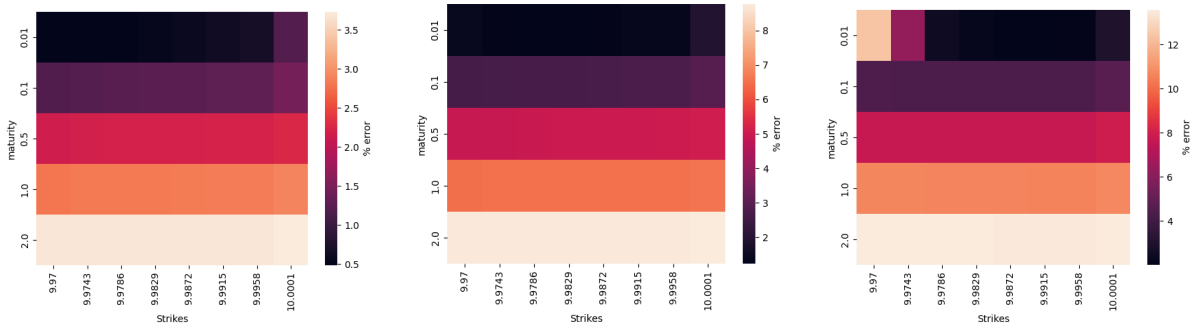

(a) Median (b) 90% Quantile (c) Maximum

Figure 1.11: Accuracy of the approximation (1.9) for an Asian call IV under fractional Bergomi with $H = 0.2$.

Finally, we repeat our analysis in the case of the fractional Bergomi model with $H = 0.7$. The results are presented in Tables 1.5 and 1.6, Figures 1.13 and 1.14. One can see that the "typical" implied volatility surface in the sample is very close to the flat one. The level changes quite slowly as we move in the direction of moneyness and maturity. The curvature seems to be minimal if any. As a result, the linear approximation given by equation (1.9) works quite well in this case

Maturity/Strike	9.9700	9.9743	9.9786	9.9829	9.9872	9.9915	9.9958	10.0001
0.01	0.49	0.50	0.50	0.54	0.59	0.64	0.67	1.19
0.10	1.17	1.21	1.23	1.25	1.26	1.28	1.29	1.46
0.50	2.16	2.18	2.19	2.19	2.19	2.20	2.20	2.26
1.00	2.80	2.82	2.83	2.83	2.84	2.85	2.85	2.90
2.00	3.68	3.68	3.69	3.69	3.69	3.69	3.69	3.73

(a) Median % error

Maturity/Strike	9.9700	9.9743	9.9786	9.9829	9.9872	9.9915	9.9958	10.0001
0.01	1.41	1.28	1.25	1.24	1.29	1.33	1.34	1.93
0.10	2.61	2.64	2.68	2.67	2.69	2.72	2.72	2.93
0.50	4.92	4.93	4.96	4.98	5.00	5.00	5.02	5.07
1.00	6.50	6.51	6.52	6.52	6.52	6.52	6.51	6.57
2.00	8.72	8.74	8.74	8.74	8.74	8.74	8.74	8.77

(b) 90th quantile % Error

Maturity/Strike	9.9700	9.9743	9.9786	9.9829	9.9872	9.9915	9.9958	10.0001
0.01	12.39	6.28	2.45	2.19	2.02	2.06	2.11	2.95
0.10	4.37	4.36	4.35	4.34	4.34	4.34	4.34	4.68
0.50	7.68	7.67	7.67	7.66	7.66	7.67	7.68	7.86
1.00	10.67	10.65	10.63	10.62	10.61	10.59	10.57	10.69
2.00	13.55	13.55	13.54	13.53	13.52	13.51	13.51	13.57

(c) Maximum % error

Table 1.4: Approximation error of an Asian call IV under the fractional Bergomi (H=0.2) model.

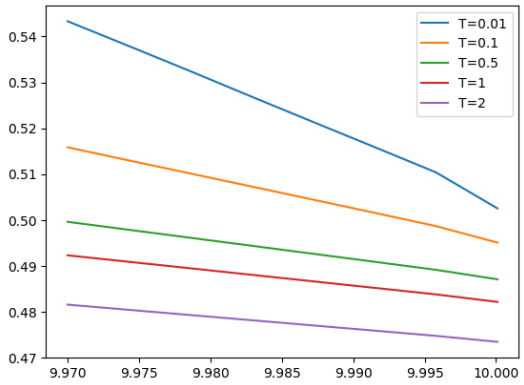

Figure 1.12: Implied volatility surface of an Asian call under the fractional Bergomi (H=0.2) model.

across different moneyness with maturity $T \leq 1$. This is quite different from the behaviour that we observed in the case of the SABR and fractional Bergomi with $H = 0.2$.

Maturity/Strike	9.9700	9.9743	9.9786	9.9829	9.9872	9.9915	9.9958	10.0001
0.01	0.91	0.90	0.90	0.90	0.91	0.92	0.93	0.94
0.10	0.92	0.92	0.92	0.93	0.93	0.93	0.94	0.94
0.50	0.94	0.94	0.94	0.94	0.94	0.94	0.94	0.94
1.00	0.95	0.95	0.95	0.95	0.95	0.95	0.95	0.95
2.00	0.99	0.99	0.99	0.99	0.99	0.99	0.99	0.99

Table 1.5: Median percentage error wrt the 95% Monte Carlo confidence interval for an Asian call IV under the fractional Bergomi (H=0.7) model.

Maturity/Strike	9.9700	9.9743	9.9786	9.9829	9.9872	9.9915	9.9958	10.0001
0.01	0.32	0.30	0.28	0.27	0.27	0.26	0.27	0.74
0.10	0.39	0.36	0.33	0.31	0.31	0.31	0.30	0.46
0.50	0.61	0.62	0.64	0.65	0.68	0.72	0.74	0.82
1.00	1.34	1.36	1.37	1.42	1.42	1.42	1.45	1.50
2.00	3.28	3.27	3.25	3.25	3.25	3.27	3.32	3.38

(a) Median % error

Maturity/Strike	9.9700	9.9743	9.9786	9.9829	9.9872	9.9915	9.9958	10.0001
0.01	0.84	0.77	0.70	0.65	0.62	0.59	0.56	1.19
0.10	1.08	0.97	0.88	0.81	0.74	0.68	0.63	0.79
0.50	2.06	1.93	1.79	1.68	1.55	1.45	1.47	1.54
1.00	3.56	3.44	3.32	3.26	3.22	3.17	3.15	3.16
2.00	7.59	7.60	7.56	7.65	7.64	7.63	7.62	7.51

(b) 90th quantile % Error

Maturity/Strike	9.9700	9.9743	9.9786	9.9829	9.9872	9.9915	9.9958	10.0001
0.01	2.10	1.69	1.32	1.20	1.04	0.99	0.94	1.85
0.10	3.77	3.37	2.97	2.56	2.15	1.75	1.35	1.35
0.50	6.16	5.58	5.01	4.45	3.89	3.34	2.79	2.54
1.00	9.04	8.37	7.72	7.07	6.43	5.80	5.17	5.08
2.00	17.74	16.94	16.15	15.37	14.60	13.84	13.08	12.42

(c) Maximum % error

Table 1.6: Approximation error of an Asian call IV under the fractional Bergomi (H=0.7) model.

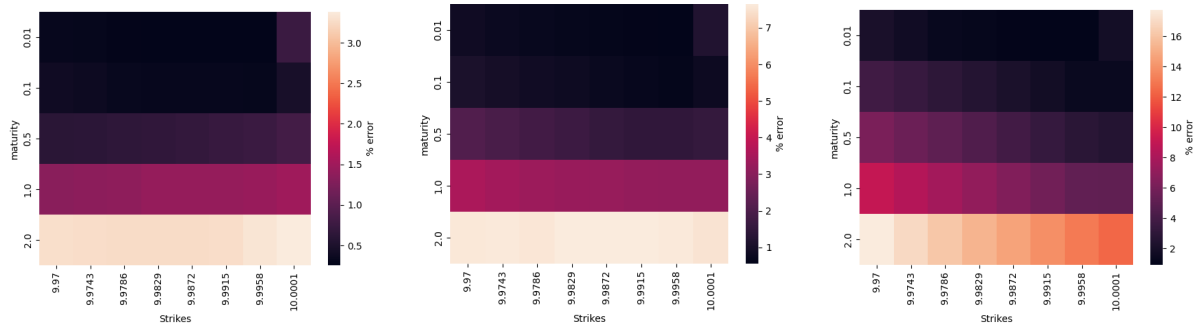

(a) Median (b) 90% Quantile (c) Maximum

Figure 1.13: Accuracy of the approximation (1.9) for an Asian call IV under fractional Bergomi with $H = 0.7$.

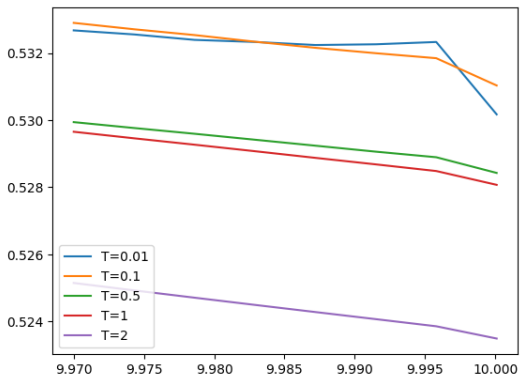

Figure 1.14: Implied volatility surface of an Asian call under the fractional Bergomi (H=0.7) model.

1.5.3.2 European call option

We continue our analysis by repeating the calculations from the previous section in the case of the European call option. By contrast to the Asian case, now we are using Monte Carlo with 200000 paths and discretization step 0.02, $K = (9., 9.1, 9.2, \dots, 10)$. All the other parameters and set up in general are preserved.

The SABR Model We start by looking at the European call option under the Bachelier model with the SABR volatility. The implied volatility approximation accuracy using Monte Carlo is presented in Table 1.7. Next, we look at the behaviour of the implied volatility approximation. The

Maturity/Strike	9.0	9.1	9.2	9.3	9.4	9.5	9.6	9.7	9.8	9.9	10.0
0.01	5.01	5.02	5.11	5.13	5.33	5.39	5.51	5.83	6.10	1.26	0.66
0.10	7.13	7.47	7.59	7.70	7.32	6.10	4.13	2.06	1.02	0.71	0.68
0.50	4.93	4.22	3.57	2.78	2.12	1.63	1.28	1.05	0.89	0.81	0.78
1.00	2.73	2.37	2.09	1.80	1.58	1.39	1.23	1.10	1.01	0.94	0.91
2.00	2.16	2.03	1.92	1.80	1.68	1.56	1.47	1.40	1.33	1.28	1.24

Table 1.7: Median percentage error wrt the 95% Monte Carlo confidence interval for the European call IV under the SABR model.

detailed results of the behaviour of different error types are presented in Table 1.8 and Figure 1.15. Overall, the approximation performs very well around ATM region and gets slightly worse with the increase of maturity. However, the approximation becomes very poor at the short end as we move away from the ATM region. This happens due to considerable curvature of the implied volatility in this region. This behaviour can be clearly seen at Figure 1.16, where we present "typical" surface for our simulated data set. As maturity increases, the curvature considerably decreases leading to the improvement of the approximation (1.9). Notice, that, by contrast to an Asian call option, ATM level of the implied volatility is much more stable making the approximation to work quite well as we increase the maturity of the option.

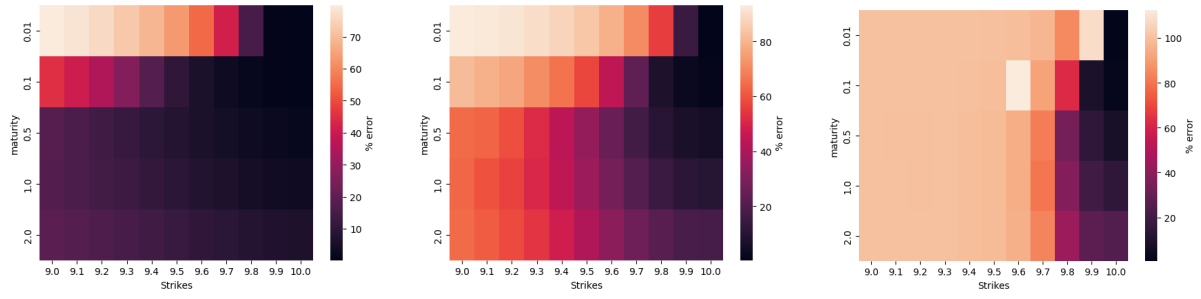

(a) Median (b) 90% Quantile (c) Maximum

Figure 1.15: Accuracy of the approximation (1.9) for the European call under the SABR model.

fractional Bergomi Model We continue our analysis of the behaviour of the implied volatility approximation of the European call under the fractional Bergomi model. We start with the case of $H = 0.2$ and present the accuracy of the Monte Carlo pricing at Table 1.9. Next, we move to the analysis of the behaviour of the implied volatility approximation (1.9). The detailed results regarding different error types are presented in Table 1.10 and Figure 1.18. To sum up, the behaviour of the implied volatility approximation is close to the SABR model. Similarly, the curvature of the implied volatility decreases considerably as options maturity increases. The stability of the ATM implied volatility level gives the improvement (except $T \leq 0.1$) in the quality of the linear approximation for a wide variety of options across all strikes and maturities. This behaviour can be clearly seen at Figure 1.17, where we present "typical" surface in our data set.

We conclude this section by looking at the approximation of the European call implied volatility under the fractional Bergomi model with $H = 0.7$. We present the accuracy of the Monte Carlo

Maturity/Strike	9.0	9.1	9.2	9.3	9.4	9.5	9.6	9.7	9.8	9.9	10.0
0.01	79.81	78.02	75.87	72.65	68.73	63.17	54.73	41.38	15.11	0.50	0.12
0.10	45.08	40.44	34.55	26.61	17.64	10.22	5.74	3.15	1.56	0.68	0.36
0.50	18.00	15.85	13.73	11.79	9.59	7.63	5.95	4.34	2.98	2.01	1.64
1.00	17.40	15.76	14.42	12.59	10.99	9.32	7.54	6.04	4.56	3.62	3.27
2.00	18.97	17.86	16.57	15.07	13.58	11.97	10.36	8.97	7.64	6.76	6.31

(a) Median % error

Maturity/Strike	9.0	9.1	9.2	9.3	9.4	9.5	9.6	9.7	9.8	9.9	10.0
0.01	93.11	92.30	91.62	89.5	87.3	84.13	79.02	70.72	55.43	14.58	0.30
0.10	81.61	79.17	76.51	71.2	65.8	57.31	44.07	23.27	7.53	2.52	1.18
0.50	64.29	62.99	58.69	51.7	43.1	34.75	25.43	16.92	10.34	6.54	5.44
1.00	63.31	59.60	56.81	50.3	44.7	36.31	28.17	20.67	14.55	11.11	10.05
2.00	64.19	61.34	58.16	53.6	47.7	40.42	33.17	26.61	21.58	18.42	17.45

(b) 90th quantile % Error

Maturity/Strike	9.0	9.1	9.2	9.3	9.4	9.5	9.6	9.7	9.8	9.9	10.0
0.01	99.9	99.9	99.9	99.9	99.8	99.6	99.1	96.6	84.89	108.34	0.60
0.10	99.8	99.8	99.8	99.8	99.4	98.8	112.3	91.5	62.06	8.82	2.10
0.50	99.79	99.6	99.6	99.7	98.9	98.2	94.5	81.98	34.07	14.22	8.1
1.00	99.75	99.7	99.6	99.7	99.1	97.9	94.8	80.43	38.08	19.46	14.27
2.00	99.76	99.7	99.7	99.8	99.19	98.1	95.0	83.84	44.11	27.61	24.3

(c) Maximum % error

Table 1.8: Approximation error of the European call IV under the SABR model.

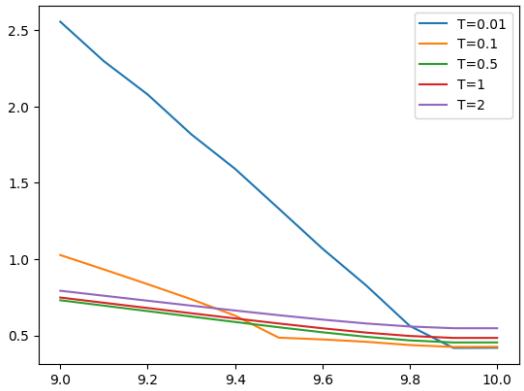

Figure 1.16: Implied volatility surface of the European call under the SABR model.

Maturity/Strike	9.0	9.1	9.2	9.3	9.4	9.5	9.6	9.7	9.8	9.9	10.0
0.01	5.70	5.81	5.86	5.99	6.05	6.24	6.46	6.71	7.15	2.00	0.67
0.10	7.10	7.49	7.74	7.72	7.87	6.76	4.68	2.37	1.13	0.74	0.68
0.50	6.16	5.36	4.18	3.19	2.28	1.58	1.21	0.95	0.80	0.73	0.70
1.00	3.31	2.71	2.15	1.69	1.42	1.17	0.97	0.85	0.78	0.74	0.72
2.00	1.87	1.64	1.43	1.26	1.10	0.97	0.88	0.83	0.78	0.76	0.74

Table 1.9: Median percentage error wrt the 95% Monte Carlo confidence interval for the European call IV under the fractional Bergomi (H=0.2) model.

at Table 1.11. The detailed results regarding different error types are presented in Table 1.12 and Figure 1.20. Due to the equation (1.15) the implied volatility approximation in this case is a horizontal plane leveled at σ_0. Visual justification of the flat skew can be clearly seen at Figure

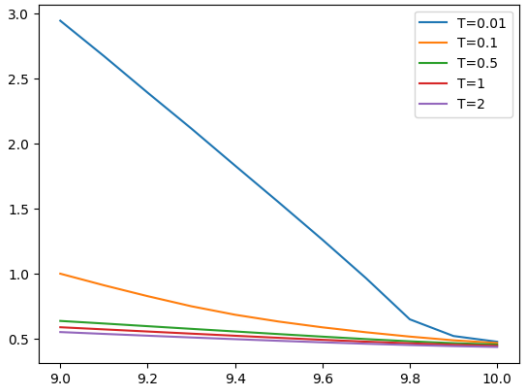

Figure 1.17: Implied volatility surface of the European call under the fractional Bergomi (H=0.2) model.

Maturity/Strike	9.0	9.1	9.2	9.3	9.4	9.5	9.6	9.7	9.8	9.9	10.0
0.01	76.52	74.74	72.48	70.59	67.12	61.92	54.90	42.06	17.64	1.09	0.64
0.10	44.01	39.03	33.18	25.90	16.32	9.26	4.73	1.97	0.98	1.06	1.53
0.50	9.72	7.38	5.62	4.08	2.77	2.04	1.76	1.78	2.17	2.75	2.99
1.00	5.39	4.22	3.30	2.64	2.24	2.19	2.35	2.74	3.15	3.80	3.96
2.00	3.37	2.90	2.86	2.83	2.95	3.28	3.64	3.98	4.82	5.15	5.25

(a) Median % error

Maturity/Strike	9.0	9.1	9.2	9.3	9.4	9.5	9.6	9.7	9.8	9.9	10.0
0.01	94.49	93.43	92.8	91.17	90.03	87.50	83.44	76.84	61.84	17.52	1.5
0.1	81.38	78.6	75.2	71.6	66.11	57.02	43.55	21.90	5.21	3.30	3.8
0.5	57.95	51.8	42.5	34.3	23.15	13.6	8.73	6.95	6.28	7.02	7.3
1.00	39.11	30.8	22.8	15.8	12.06	9.58	8.80	8.09	8.60	9.4	9.6
2.00	20.47	16.7	14.4	12.9	11.63	10.87	10.67	11.20	11.98	12.57	12.9

(b) 90th quantile % Error

Maturity/Strike	9.0	9.1	9.2	9.3	9.4	9.5	9.6	9.7	9.8	9.9	10.0
0.01	99.9	99.9	99.95	99.86	99.97	99.97	99.81	99.73	98.30	77.47	2.8
0.10	99.8	99.8	113.99	99.81	99.74	97.15	97.02	96.83	63.78	6.46	5.8
0.50	99.8	98.8	95.42	96.90	92.12	98.48	79.16	48.12	11.34	11.06	11.4
1.00	94.7	99.2	96.14	95.76	95.07	72.91	32.94	15.38	14.98	14.8	14.7
2.00	97.4	99.4	88.06	88.41	67.31	38.39	19.24	19.54	19.58	19.50	19.3

(c) Maximum % error

Table 1.10: Approximation error of the European call IV under the fractional Bergomi (H=0.2) model.

Maturity/Strike	9.0	9.1	9.2	9.3	9.4	9.5	9.6	9.7	9.8	9.9	10.0
0.01	4.26	4.35	4.27	4.24	4.89	4.39	4.87	4.92	3.79	0.86	0.66
0.10	5.88	5.99	6.68	6.41	5.67	4.25	2.30	1.03	0.71	0.64	0.66
0.50	4.93	3.95	2.91	2.10	1.45	1.07	0.86	0.74	0.68	0.67	0.67
1.00	2.76	2.23	1.74	1.37	1.14	0.95	0.83	0.75	0.72	0.70	0.70
2.00	1.86	1.62	1.41	1.22	1.07	0.96	0.89	0.84	0.80	0.78	0.77

Table 1.11: Median percentage error wrt the 95% Monte Carlo confidence interval for the European call IV under the fractional Bergomi (H=0.7) model.

1.19, where we present "typical" surface observed in our data set.

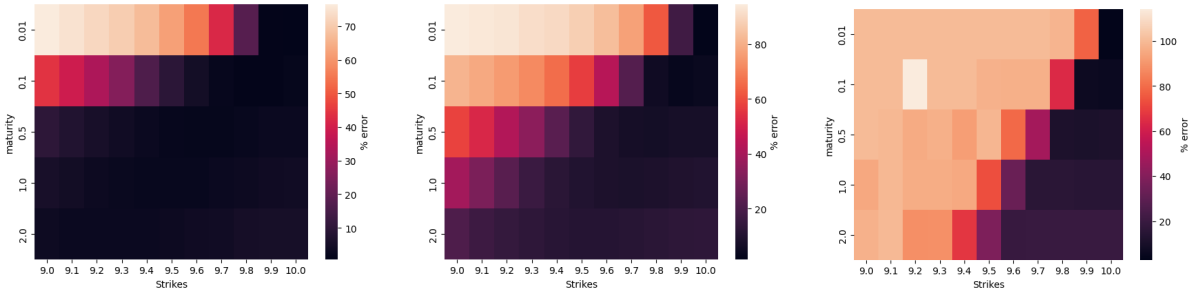

(a) Median (b) 90% Quantile (c) Maximum

Figure 1.18: Accuracy of the approximation (1.9) for the European call under fractional Bergomi (H=0.2) model.

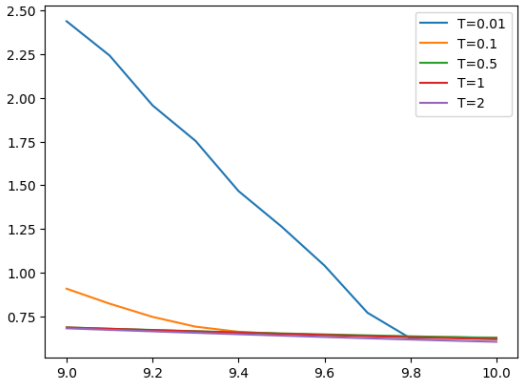

Figure 1.19: Implied volatility surface of the European call under the fractional Bergomi (H=0.7) model.

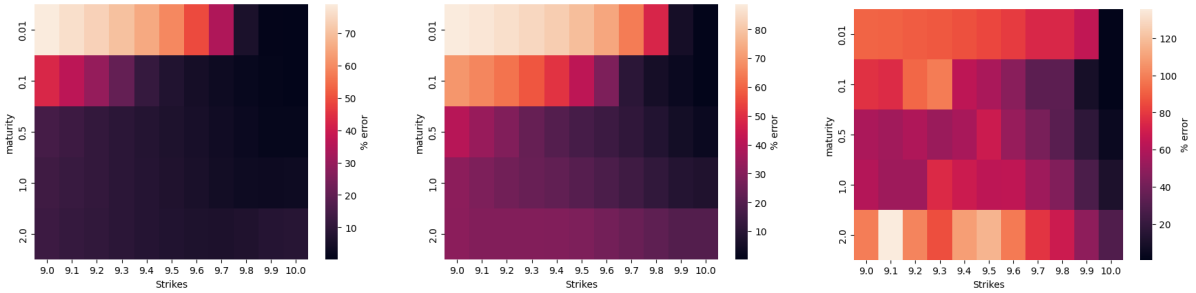

(a) Median (b) 90% Quantile (c) Maximum

Figure 1.20: Accuracy of the approximation (1.9) for the European call under fractional Bergomi (H=0.7) model.

Maturity/Strike	9.0	9.1	9.2	9.3	9.4	9.5	9.6	9.7	9.8	9.9	10.0
0.01	78.96	76.27	73.63	70.05	65.67	59.42	49.13	34.11	5.86	0.69	0.11
0.10	42.65	36.66	29.48	20.49	11.22	6.98	4.47	3.02	1.95	0.98	0.16
0.50	14.28	12.76	10.69	9.22	7.60	6.29	5.17	3.80	2.47	1.27	1.21
1.00	13.16	11.85	10.62	9.17	8.05	6.64	5.35	3.88	2.94	2.69	3.13
2.00	12.59	11.37	10.41	9.18	7.85	6.89	6.35	6.23	6.70	7.92	8.26

(a) Median % error

Maturity/Strike	9.0	9.1	9.2	9.3	9.4	9.5	9.6	9.7	9.8	9.9	10.0
0.01	88.6	87.53	85.8	83.93	81.58	78.05	73.05	64.31	47.62	5.37	0.2
0.10	69.5	66.35	62.5	57.49	50.85	41.63	28.34	10.56	5.41	2.83	0.4
0.50	40.1	34.09	28.9	23.43	19.74	16.83	14.13	11.52	8.27	5.03	2.9
1.00	31.4	28.42	26.1	24.08	22.49	20.28	17.70	15.02	11.88	8.7	7.6
2.00	31.2	29.55	29.4	29.37	29.09	28.46	26.44	24.34	21.68	19.55	19.5

(b) 90th quantile % Error

Maturity/Strike	9.0	9.1	9.2	9.3	9.4	9.5	9.6	9.7	9.8	9.9	10.0
0.01	91.6	90.9	89.5	88.3	86.4	83.8	80.4	73.6	73.50	64.55	0.62
0.10	77.4	75.1	92.8	98.2	63.7	57.3	47.0	33.02	33.19	8.9	0.83
0.50	57.6	54.9	58.8	52.6	56.8	68.4	51.4	42.07	31.86	17.3	4.40
1.00	60.3	53.4	53.4	74.7	68.6	63.6	64.1	53.6	44.64	27.1	11.12
2.00	98.7	135.5	100.9	85.9	109.2	116.8	98.0	78.1	68.54	48.6	28.58

(c) Maximum % error

Table 1.12: Approximation error of the European call IV under the fractional Bergomi (H=0.7) model.

Chapter 2

On the implied volatility of Asian options under stochastic volatility models

2.1 Introduction

This chapter is devoted to the study of Asian call options with payoff of the form

$$\left(\frac{1}{T}\int_0^T S_u du - K\right)_+,$$

where T denotes the maturity, S the price of the underlying, and K the strike of the contract. Asian options of this type are extremely important in energy markets for different reasons. From one hand, typical energy transactions use to take place via multiple deliveries. Then, these transactions are priced on average and not only on a terminal price. Secondly, the payoff is less sensitive to extreme market fluctuations, which becomes interesting in non-liquid markets. Finally, these options tend to be cheaper than the corresponding European vanillas.

The aim of this chapter is to study the short-time maturity behavior of the at-the-money implied volatility (ATMIV) of arithmetic Asian options. The study of implied volatility is useful in many ways. Firstly, it can be used to obtain volatilities for pricing OTC options (and other derivatives) with strikes and maturities that are different from the ones offered by option exchanges. Secondly, the shape of the implied volatility surface can be used to assess the adequacy of an option pricing model. If the option pricing model is adequate, then it should capture the main properties of the empirical implied volatility surface. In particular, one of the key characteristics of the implied volatility is its skew at the short end and one can easily filter the class of suitable models if the theoretical value of the skew is available for the models of interest. Finally, as one will see further in the chapter, one can use implied volatility and its skew to efficiently approximate the option price. Last, but not least, due to the smile effect the hedge ratio has to be adjusted to take into account the market skew. As a result, availability of analytical values of the skew can improve the performance of hedging.

The behavior of the implied volatility for vanilla options has been the object of many works (see for example Lee [42] for a basic introduction to this topic). However, the case of exotic options and more specifically Asian options is less studied and the number of exact analytic results is more limited.

Yang and Ewald [53] compute the implied volatility for OTC traded Asian options under Black-Scholes with constant volatility by combining Monte-Carlo techniques with the Newton method in order to solve nonlinear equations. Approximation methods for pricing Asian options under stochastic volatility models are studied by Forde and Jacquier [24]. Chatterjee et al. [18] develop a Markov chain-based approximation method to price arithmetic Asian options for short maturities under the case of geometric Brownian motion. Fouque and Han [25] generalize the dimension reduction technique of Vecer for pricing arithmetic Asian options. They use the fast mean-reverting stochastic volatility asymptotic analysis to derive an approximation to the option price which takes into account the skew of the implied volatility surface. This approximation is obtained by solving a pair of one-dimensional partial differential equations. The methodology requires the key parameters needed in the PDEs to be estimated from the historical stock prices and the implied volatility surface.

Asymptotics of arithmetic Asian implied volatilities have been studied by Pirjol and Zhu [48] in the case of local volatility. In this paper, the authors make use of large deviations techniques to get accurate approximation formulas for the implied volatility, which are shown to be accurate when compared with the Monte-Carlo simulations. Arithmetic Asian options under the CEV (constant

elasticity of variance) model are studied in Pirjol and Zhu [47]. The leading order short maturity limit of the Asian option prices under the CEV model is obtained in closed form. Authors propose an analytic approximation for the Asian options prices which reproduced the exact short maturity asymptotics. Alòs and León [8] compute the short-time level and the skew of the implied volatility of floating strike arithmetic Asian options under the Black-Scholes model with constant volatility by the means of Malliavin calculus.

In this chapter, we contribute to the existing literature in several ways. We extend the application of the Malliavin calculus developed in Alòs, García-Lorite and Muguruza [6] by giving general sufficient conditions on a general stochastic volatility model in order to obtain formulas for the short-time limit of the at-the-money level and skew of the implied volatility for Asian options. Moreover, we show how studying Asian option under stochastic volatility reduces to the study of European type options where the underlying is respresented by a certain stochastic volatility model, with a modified volatility process which depends on T. This methodology developed in [6] allows to adapt the results on vanilla options to options on a non lognormal-type distribution and it can also be applied to other European-type exotic options. See for example [6] for an application of this technique to the analysis of the VIX skew. This method is very classical in mathematical finance, for instance, when working with stochastic rates.

To sum up, we study the short-end behavior of the ATMIV of Asian options for local, stochastic, and fractional volatilities. In particular, we show that

- The short-end limit of the ATMIV is equal to $\frac{\sigma_0}{\sqrt{3}}$, where σ_0 denotes the short-end limit of the spot volatility. See equation (2.10) in Theorem 2.2.9.
- We compute the the short-end skew of the ATMIV, which depends on the correlation between prices and stochastic volatility and on the Malliavin derivative of the volatility process, which in the case of fractional volatility models will depend on the Hurst parameter $H \in (0,1)$. See equation (2.11) in Theorem 2.2.9. If prices and volatilities are uncorrelated, the short-end skew is equal to $\frac{\sqrt{3}\sigma_0}{30}$. In the case of rough volatilities, that is $H < \frac{1}{2}$, we observe in equations (2.30) and (2.31) a blow-up that is of the same order as the one we observe in vanilla options (see Alòs et al. [7]).
- We apply the preceding results to the constant volatility case, the SABR model, the fractional Bergomi model, and the local volatility, and perform numerical simulations that confirm the accurateness of the asymptotic formulas. See Section 2.5. In the case of local volatilities, we verify that our results fit the asymptotic analysis of Pirjol and Zhu [48] and [47].
- Using the short-end limit of the ATMIV and the skew we obtain an analytic approximation of the price of an arithmetic Asian option that we study numerically for the SABR and fractional Bergomi models (see Section 2.5.5). This is particularly useful for the practitioners since it allows to substitute expensive Monte Carlo simulation and speed up pricing significantly without loss of precision.

The chapter is organized as follows: in Section 2.2 we introduce the main problem, results and notations. In Section 2.3 we introduce some preliminary results needed for the proof of the main theorem. In Section 2.4 we give the proof the main results of the chapter. Finally, Section 2.5 is devoted to the application of the main results to the constant volatility case, the SABR model, the fractional Bergomi model, and the local volatility model, together with some numerical simulations to confirm the accurateness of the asymptotic formulas. We finally use the asymptotic formulas to obtain an analytic approximation of the price of an arithmetic Asian call and we apply it to the SABR and the fractional Bergomi models and compare it with the classical Monte Carlo. The Appendix .2 contains some Malliavin derivatives computations needed through the chapter.

2.2 Statement of the problem and main results

We denote by $(V_t)_{t\in[0,T]}$ the value of a fixed strike arithmetic Asian call option where T is the maturity. Then, the payoff can be written as

$$V_T = (A_T - K)_+, \qquad A_T = \frac{1}{T}\int_0^T S_t dt,$$

where $(S_t)_{t\in[0,T]}$ is the price of the underlying asset and K is the fixed strike price.

We assume without lost of generality that the interest rate is equal to zero and we consider the following general stochastic volatility model for the underlying asset price

$$\begin{aligned} dS_t &= \sigma_t S_t dW_t \\ W_t &= \rho W'_t + \sqrt{(1-\rho^2)} B_t, \end{aligned} \tag{2.1}$$

where $S_0 > 0$ is fixed, W_t, W'_t, and B_t are three standard Brownian motions on $[0,T]$ defined on the same complete probability space $(\Omega, \mathcal{G}, \mathbb{P})$. We assume that W'_t and B_t are independent and $\rho \in (-1,1)$ is the correlation coefficient between W_t and W'_t.

We consider the following assumption on the stochastic volatility of the asset price.

Hypothesis 2.2.1. *The process $\sigma = (\sigma_t)_{t\in[0,T]}$ is adapted to the filtration generated by W', a.s. positive and continuous, and satisfies that for all $t \in [0,T]$,*

$$c_1 \leq \sigma_t \leq c_2,$$

for some positive constants c_1 and c_2.

Remark 2.2.2. *Hypothesis 2.2.1 may seem too restrictive since it is not satisfied by the stochastic volatility models considered in Section 2.5. However, we will show that using a truncation argument, Theorem 2.2.9 is still true in all our examples.*

We define the forward price as the martingale $M_t = \mathbb{E}_t(A_T)$, where $\mathbb{E}_t$ denotes the conditional expectation wrt to the filtration $\mathcal{F}_t$ generated by W_t. Applying the stochastic Fubini's theorem we get that

$$\begin{aligned} A_T = \frac{1}{T}\int_0^T S_t dt &= \frac{1}{T}\int_0^T \left(S_0 + \int_0^t \sigma_u S_u dW_u \right) dt = \\ &= S_0 + \frac{1}{T}\int_0^T \sigma_u S_u \left(\int_u^T dt \right) dW_u = \\ &= S_0 + \frac{1}{T}\int_0^T (T-u)\sigma_u S_u dW_u, \end{aligned}$$

which implies that

$$dM_t = \frac{\sigma_t S_t (T-t)}{T} dW_t = \phi_t M_t dW_t, \tag{2.2}$$

where

$$\phi_t := \frac{\sigma_t S_t (T-t)}{T M_t}.$$

Furthermore, the log-forward price $X_t = \log(M_t)$ satisfies

$$dX_t = \phi_t dW_t - \frac{1}{2}\phi_t^2 dt. \tag{2.3}$$

Remark 2.2.3. *One can easily check that Hypothesis 2.2.1 implies that ϕ_t is positive a.s. and belongs to $L^p([0,T]\times\Omega)$, for all $p \geq 2$. In fact, Hypothesis 2.2.1 implies that for all $p \geq 2$, S_t belongs to $L^p([0,T]\times\Omega)$, A_T belongs to $L^p(\Omega)$, and M_t^{-1} belongs to $L^p([0,T]\times\Omega)$.*

Remark 2.2.4. *Notice that $\phi_0 = \sigma_0$. Moreover,*

$$M_t = \frac{1}{T}\left(\int_0^t S_u du + S_t(T-t) \right). \tag{2.4}$$

Then, $TM_t \geq S_t(T-t)$, and this implies that $\phi_t \leq \sigma_t$ almost surely.

The goal of this paper is to study the implied volatility of the Asian call option V_t which is defined as follows. We denote by $BS(t,x,k,\sigma)$ the classical Black-Scholes price of a European call with time to maturity $T-t$, log-stock price x, log-strike price k and volatility σ. That is,

$$\begin{aligned} BS(t,x,k,\sigma) &= e^x N(d_+(k,\sigma)) - e^k N(d_-(k,\sigma)), \\ d_\pm(k,\sigma) &= \frac{x-k}{\sigma\sqrt{T-t}} \pm \frac{\sigma}{2}\sqrt{T-t}, \end{aligned}$$

where N is the cumulative distribution function of the standard normal random variable.

Next, we observe that, as $BS(T,x,k,\sigma) = (e^x - e^k)_+$ for every $\sigma > 0$, the price of our Asian call option $V_t = \mathbb{E}_t(e^{X_T} - e^k)_+$ can be written as

$$V_t = \mathbb{E}_t(BS(T, X_T, k, v_T)), \qquad v_t = \sqrt{\frac{1}{T-t}\int_t^T \phi_s^2 ds}. \tag{2.5}$$

In particular, $V_T = BS(T, X_T, k, v_T)$. Then, we define the implied volatility of the option as $I(t,k) = BS^{-1}(t, X_t, k, V_t)$, and we denote by $I(t,k^*)$ the corresponding ATMIV which, in the case of zero interest rates, takes the form $BS^{-1}(t, X_t, X_t, V_t)$.

We apply the Malliavin calculus techniques developed in Alòs, García-Lorite and Muguruza [6] in order to obtain formulas for

$$\lim_{T\to 0} I(0,k^*) \quad \text{and} \quad \lim_{T\to 0} \partial_k I(0,k^*)$$

under the general stochastic volatility model (2.1).

In our setting, since we have three Brownian motions W, W' and B, if h is a a random variable in $L^2([0,T])$, then we have in view of relation (2.1) that

$$W(h) = \rho W'(h) + \sqrt{(1-\rho^2)}B(h).$$

Then, a random variable in $\mathbb{D}^{1,2}_{W'} \cap \mathbb{D}^{1,2}_B$ is also in $\mathbb{D}^{1,2}_W$. In fact, it is easy to see that if X is a random variable in $\mathcal{S}^W$, then

$$D^W X = \rho D^{W'} X + \sqrt{1-\rho^2} D^B X. \tag{2.6}$$

Thus, we deduce that for all $X \in \mathbb{D}^{1,2}_{W'} \cap \mathbb{D}^{1,2}_B$,

$$D^W X = \rho D^{W'} X + \sqrt{1-\rho^2} D^B X. \tag{2.7}$$

We will need the following additional assumption on the Malliavin differentiability of the stochastic volatility process.

Hypothesis 2.2.5. *For $p \geq 2$, $\sigma \in \mathbb{L}^{2,p}_{W'}$.*

Remark 2.2.6. *Hypotheses 1 and 2 imply that ϕ_t belongs to $\mathbb{L}^{2,p}_W$ and A_T belong to $\mathbb{D}^{2,p}_W$ for all $p \geq 2$. This hypothesis on A_T corresponds to* **(H1)** *in Alòs, García-Lorite and Muguruza* [6].

In order to give the asymptotic skew of the implied volatility as a function of the roughness of the stochastic volatility process we consider the following assumption.

Hypothesis 2.2.7. *There exists $H \in (0,1)$ such that for all $0 \leq s \leq r \leq t \leq T$*

$$|D^{W'}_r \sigma_t| \leq M_{r,t}(t-r)^{H-\frac{1}{2}} \tag{2.8}$$

and

$$|D^{W'}_s D^{W'}_r \sigma_t| \leq N_{s,r,t}(t-r)^{H-\frac{1}{2}}(t-s)^{H-\frac{1}{2}}, \tag{2.9}$$

where $M_{r,t}$ and $N_{s,r,t}$ are positive random variables satisfying for all $p \geq 1$,

$$\mathbb{E}(\sup_{0\leq r\leq t\leq T\leq 1} M^p_{r,t}) \leq c_1,$$

and

$$\mathbb{E}(\sup_{0\leq s\leq r\leq t\leq T\leq 1} N^p_{s,r,t}) \leq c_2,$$

for some positive constants c_1 and c_2.

Finally, we will need the following additional assumption on the continuity of the paths of the volatility process.

Hypothesis 2.2.8. *There exists $\gamma \in (0, H)$ such that for all $0 \leq s \leq r \leq T \leq 1$*

$$|\sigma_r - \sigma_s| \leq K_{r,s}(r-s)^{\gamma},$$

where $K_{r,s}$ is a positive random variable satisfying for all $p \geq 1$,

$$\mathbb{E}(\sup_{0\leq r\leq t\leq T\leq 1} K_{r,s}^{p}) \leq c$$

where $c > 0$ and H is the Hurst parameter form Hypothesis 3.

We next provide the the main result of this paper, which is the short-time ATMIV level and skew of an Asian call option under the general volatility model (2.1).

Theorem 2.2.9. *Assume Hypotheses 1, 2,* (2.8)*, and 4. Then,*

$$\lim_{T\to 0} I(0,k^*) = \frac{\sigma_0}{\sqrt{3}}. \tag{2.10}$$

If we further assume (2.9)*, then*

$$\begin{aligned}
&\lim_{T\to 0} T^{\max(\frac{1}{2}-H,0)}\partial_k I(0,k^*) \\
&= \lim_{T\to 0} T^{\max(\frac{1}{2}-H,0)}\frac{3\sqrt{3}\rho}{\sigma_0 T^5}\int_0^T \left((T-r)\int_r^T (T-u)^2 \mathbb{E}(D_r^{W'}\sigma_u)du\right)dr \\
&\qquad + \lim_{T\to 0} T^{\max(\frac{1}{2}-H,0)}\frac{\sqrt{3}\sigma_0}{30},
\end{aligned} \tag{2.11}$$

and the limit on the right hand side of (2.11) *is finite.*

We observe that the level (2.10) is independent of the correlation ρ and the Hurst parameter H, and coincides with the constant volatility case, see Pirjol and Zhu [48] and Alòs and León [8]. Observe also that it coincides with the a.s. limit of v_0. In fact, by Hypothesis 1 and since $S_0 = M_0$ we have that a.s.

$$\lim_{T\to 0} v_0 = \lim_{T\to 0}\sqrt{\frac{1}{T^3}\int_0^T \frac{\sigma_s^2 S_s^2 (T-s)^2}{M_s^2}ds} = \frac{\sigma_0}{\sqrt{3}}. \tag{2.12}$$

The skew (2.11) depends on the correlation parameter ρ and on the Hurst parameter H. When prices and volatilities are uncorrelated then the short-time skew equals $\frac{\sqrt{3}\sigma_0}{30}$, which again coincides with the constant volatility case, see Pirjol and Zhu [48] and Alòs and León [8]. Observe also that if the term $\mathbb{E}(D_r^{W'}\sigma_u)$ is of order $(u-r)^{H-\frac{1}{2}}$ (see Hypothesis 2.2.5), then the limit of the right hand side of (2.11) will be 0 if $H > 1/2$ and it will converge to a constant when $H = \frac{1}{2}$. When $H < \frac{1}{2}$ we need to multiply by $T^{\frac{1}{2}-H}$ in order to obtain a finite limit. This is because when $H > 1/2$, the fractional Brownian motion is smoother than standard Brownian motion and the effect of the stochastic volatility on the short-time implied volatility will be the same as it was constant, while when $H < 1/2$, the fractional Brownian motion is rougher than standard Brownian motion and we obtain the same effect as in the case of vanilla options, see Alòs et al. [7].

The results of Theorem 2.2.9 can be used in order to derive an approximation formula for the price of an Asian call option. By definition, the price of the Asian call option writes as

$$V_0 = BS(0, X_0, k, I(0,k))$$

Then, using Taylor's formula we can use the approximation

$$I(0,k) \approx I(0,k^*) + \partial_k I(0,k^*)(k-k^*). \tag{2.13}$$

The great utility of this relation is that we can use it to approximate the price of an Asian call option for a wide range of stochastic and fractional volatility models. We numerically investigate the quality of this approximation for the SABR and fractional Bergomi models in Section 2.5.5.

2.3 Preliminary results

We start quoting the two main results obtained in Alòs et al. [6] that will be crucial for the proof of our main Theorem and use the general framework detailed in Section 2.2. The first result is Theorem 6 in Alòs et al. [6] which shows that the short-time limit of the ATMIV equals the short-time limit of the future average of the volatility of the log forward price.

Theorem 2.3.1. *Assume that for all $p > 1$, $A_T \in \mathbb{D}_W^{2,p}$, $M_t^{-1} \in L^p([0,T] \times \Omega)$, and*

$$\lim_{T\to 0} \mathbb{E}\left(\int_0^T \frac{\Lambda_s}{v_s^2(T-s)} ds\right) = 0, \tag{2.14}$$

$$\lim_{T\to 0} \frac{1}{T^2}\mathbb{E}\left(\frac{1}{v_0}\int_0^T \left(\int_s^T D_s^W \phi_r^2 dr\right)^2 ds\right) = 0, \tag{2.15}$$

where $\Lambda_s = \phi_s \int_s^T D_s^W \phi_r^2 dr$. Then,

$$\lim_{T\to 0} I(0,k^*) = \lim_{T\to 0} \mathbb{E}(v_0).$$

The second result is Theorem 8 of Alòs et al. [6] which gives an approximation formula for the short-time limit of the ATMIV skew.

Theorem 2.3.2. *Assume that for all $p > 1$, $A_T \in \mathbb{D}_W^{3,p}$, $M_t^{-1} \in L^p([0,T] \times \Omega)$, hypotheses* (2.14) *and* (2.15) *are satisfied,*

$$\lim_{T\to 0} \frac{T^{\max(\frac{1}{2}-H,0)}}{\sqrt{T}}\mathbb{E}\left(\int_0^T (v_s^2(T-s))^{-3}\Lambda_s\left(\int_s^T \Lambda_r dr\right) ds\right) = 0, \tag{2.16}$$

$$\lim_{T\to 0} \frac{T^{\max(\frac{1}{2}-H,0)}}{\sqrt{T}}\mathbb{E}\left(\int_0^T (v_s^2(T-s))^{-2}\phi_s\left(\int_s^T D_s^W \Lambda_r dr\right) ds\right) = 0, \tag{2.17}$$

and

$$\lim_{T\to 0} \frac{T^{\max(\frac{1}{2}-H,0)}}{T^2}\mathbb{E}\left(\frac{1}{v_0^3}\int_0^T \Lambda_s ds\right) < \infty. \tag{2.18}$$

Then,

$$\lim_{T\to 0} T^{\max(\frac{1}{2}-H,0)}\partial_k I(0,k^*) = \frac{1}{2}\lim_{T\to 0} \frac{T^{\max(\frac{1}{2}-H,0)}}{T^2}\mathbb{E}\left(\frac{1}{v_0^3}\int_0^T \Lambda_s ds\right).$$

Remark 2.3.3. *Observe that there are two typo in Theorem 8 of Alòs et al. [6]. First a factor $T^{-\gamma}$ missing in their hypothesis* **(H5)**. *Here we are taking $\gamma = \min(H - \frac{1}{2}, 0) \in (-\frac{1}{2}, 0]$. Moreover there is a square missing in the $u_s(T-s)$ and it should be $u_s^2(T-s)$, see for example Lemma 6.3.1 in [5].*

We next present some technical lemmas that will be needed in order to check that the hypotheses of the preceding theorems are satisfied.

Lemma 2.3.4. *Assume Hypothesis 2.2.1. Then, for every $p \geq 1$, there exists a constant $c_p > 0$ such that for all $0 \leq t < T \leq 1$,*

$$\left(\mathbb{E}\left[v_t^{-2p}\right]\right)^{1/p} \leq c_p \frac{T^2}{(T-t)^2}.$$

Proof. We follow a similar idea used in Lemma 3 of [8]. We observe that by the definition of ϕ_t and equation (2.4), we get that

$$\int_t^T \phi_r^2 dr = \int_t^T \left(\frac{\sigma_r S_r(T-r)}{\int_0^r S_u du + S_r(T-r)}\right)^2.$$

Then, using Hypothesis 2.2.1 we get that

$$\int_t^T \phi_r^2 dr \geq c_1^2 \exp\left(-4 \sup_{t\in[0,T]}\left|\int_0^t \sigma_s dW_s - \frac{1}{2}\int_0^t \sigma_s^2 ds\right|\right)\frac{(T-t)^3}{3T^2}.$$

Thus, using again Hypothesis 2.2.1,

$$\left(\int_t^T \phi_r^2 dr\right)^{-p} \leq c_1^{-2p} e^{2pTc_2^2} \exp\left(4p \sup_{t\in[0,T]} \left|\int_0^t \sigma_s dW_s\right|\right) \frac{3^p T^{2p}}{(T-t)^{3p}}. \tag{2.19}$$

By Burkholder-Davis-Gundy inequality and Hypothesis 2.2.1, for any integer $n \geq 1$,

$$\mathbb{E}\left(\sup_{t\in[0,T]} \left|\int_0^t \sigma_s dW_s\right|^n\right) \leq C n^{n/2} (cT)^{n/2},$$

for some positive constants c, C. Therefore, for $T \leq 1$,

$$\mathbb{E}\exp\left(4p \sup_{t\in[0,T]} \left|\int_0^t \sigma_s dW_s\right|\right) \leq C \sum_{n=1}^{\infty} \frac{(cn)^{n/2}}{n!}, \tag{2.20}$$

which is a convergent series. This completes the proof. ■

Lemma 2.3.5. *Assume Hypothesis 2.2.1. Then, for any $p \geq 1$ there exists a constant $c_p > 0$ such that for all $0 \leq t \leq T \leq 1$,*

$$\mathbb{E}(M_t^{-p}) \leq c_p.$$

Proof. Using (2.4) and a similar argument as in the proof of Lemma 2.3.4, we get that

$$\mathbb{E}(M_t^{-p}) \leq e^{pTc_2^2} \mathbb{E}\exp\left(p \sup_{t\in[0,T]} \left|\int_0^t \sigma_s dW_s\right|\right),$$

and the result follows from (2.20). ■

Next, we obtain approximation formulas for ϕ and its Malliavin derivative.

Lemma 2.3.6. *Under Hypotheses 2.2.1, 2.2.5, 2.2.8 and* (2.8)*, the following holds for all $0 \leq s \leq r \leq T$,*

$$\phi_r = \frac{\sigma_0(T-r)}{T} + X_r^1, \tag{2.21}$$

$$\phi_r^2 = \frac{\sigma_0^2(T-r)^2}{T^2} + X_r^2, \tag{2.22}$$

$$D_s^W \phi_r = \frac{\rho(T-r)D_s^{W'}\sigma_r}{T} + \frac{(T-r)\sigma_0^2}{T} - \frac{(T-r)(T-s)\sigma_0^2}{T^2} + X_{T,r,s}^3, \tag{2.23}$$

$$D_s^W \phi_r^2 = \frac{2\sigma_0\rho(T-r)^2 D_s^{W'}\sigma_r}{T^2} + \frac{2(T-r)^2\sigma_0^3}{T^2} - \frac{2(T-r)^2(T-s)\sigma_0^3}{T^3} + X_{r,s}^4, \tag{2.24}$$

where X^i are random variables satisfying for all $0 \leq s \leq r \leq T \leq 1$,

$$|X_r^1| \leq Y_r^1 \frac{(T-r)r^\gamma}{T},$$
$$|X_r^2| \leq Y_r^2 \frac{(T-r)^2 r^\gamma}{T^2},$$
$$|X_{r,s}^3| \leq Y_{r,s}^3 \frac{(T-r)(r-s)^H}{T},$$
$$|X_{r,s}^4| \leq Y_{r,s}^4 \frac{(T-r)^2 r^\gamma (r-s)^H}{T^2},$$

and Y^i are positive random variables satisfying for all $p \geq 1$

$$\mathbb{E}(\sup_{0\leq s\leq r\leq T\leq 1} |Y_{r,s}^i|^p) \leq c_i$$

for some positive constants c_i only dependent on p and $\gamma > 0$ is from Hypothesis 2.2.8.

Proof. We start proving the decomposition for ϕ_r. We consider the function

$$F(S_s, M_s) := \frac{\sigma_0 S_s (T-r)}{T M_s}, \quad 0 \le s \le r.$$

Observe that

$$\phi_r = F(S_r, M_r) + (\sigma_r - \sigma_0)\frac{S_r(T-r)}{TM_r}.$$

Then, using Itô's lemma, we get that we get

$$F(S_r, M_r) = \frac{\sigma_0(T-r)}{T} + \frac{(T-r)}{T}\Big\{ \int_0^r \frac{\sigma_0}{M_s} dS_s \\ - \int_0^r \frac{\sigma_0 S_s}{M_s^2} dM_s + \int_0^r \frac{\sigma_0 \sigma_s^2 S_s^3}{M_s^3}\frac{(T-s)^2}{T^2} ds \Big\}.$$

Then, using Hypotheses 2.2.1 and 2.2.8 and Lemma 2.3.5, we conclude (2.21). Similarly, we can write

$$\phi_r^2 = F^2(S_r, M_r) + (\sigma_r^2 - \sigma_0^2)\frac{S_r^2 (T-r)^2}{T^2 M_r^2}.$$

and applying Itô's formula to the function $F^2(S_s, M_s)$ to obtain (2.22).

We next prove (2.23). Using expression (46) of the Malliavin derivatives computed in the Appendix, we see that the leading terms are equal to

$$\begin{aligned} &\frac{\rho(T-r)S_r D_s^{W'}\sigma_r}{TM_r} + \frac{\rho^2(T-r)\sigma_r S_r \sigma_s}{TM_r} - \frac{\rho^2(T-r)S_r\sigma_r\sigma_s S_s (T-s)}{T^2 M_r^2} \\ &\quad + \frac{(1-\rho^2)(T-r)\sigma_r S_r \sigma_s}{TM_r} - \frac{(1-\rho^2)(T-r)S_r\sigma_r\sigma_s S_s(T-s)}{T^2M_r^2} \\ =&\frac{\rho(T-r)S_r D_s^{W'}\sigma_r}{TM_r} + \frac{(T-r)\sigma_r S_r\sigma_s}{TM_r} - \frac{(T-r)S_r\sigma_r\sigma_s S_s(T-s)}{T^2M_r^2}. \end{aligned}$$

Then, applying Itô's formula to the functions $F(S_s, M_s) = \frac{S_s}{M_s}$ and $F(S_s, M_s) = \frac{S_s^2}{M_s^2}$ as above, we obtain (2.23).

Finally, in order to check (2.24) it suffice to use the formula $D_s^W \phi_r^2 = 2\phi_r D_s^W \phi_r$ together with (2.21) and (2.23). This concludes the proof. ■

2.4 Proof of Theorem 2.2.9

2.4.1 Proof of (2.10) in Theorem 2.2.9: ATM implied volatility level

Proof. By (2.12), it suffices to check that the Hypotheses of Theorem 2.3.1 hold true. It is easy to check that Hypotheses 2.2.1 and 2.2.5 imply the first two hypotheses of Theorem 2.3.1 (see Remarks 2.2.3 and 2.2.6).

We next check (2.14). Using equation (2.19) and Cauchy-Schwarz inequality we get that

$$\begin{aligned} \mathbb{E}\int_0^T \frac{\Lambda_s}{v_s^2(T-s)} ds &\le \int_0^T \frac{T^2}{(T-s)^3}\mathbb{E}(X_T|\Lambda_s|) ds \\ &\le \int_0^T \frac{T^2}{(T-s)^3}\left(\mathbb{E}(X_T^2)\right)^{1/2}\left(\mathbb{E}(\Lambda_s^2)\right)^{1/2} ds, \end{aligned}$$

where $X_T = 3c_1^{-2}e^{2Tc_2^2}\exp\left(4\sup_{t\in[0,T]}\left|\int_0^t \sigma_s dW_s\right|\right)$.

Next, due to equation (2.20) we conclude that $\left(\mathbb{E}(X_T^2)\right)^{1/2}$ is bounded as $T \leq 1$. Since $\phi_t \leq \sigma_t$, Cauchy-Schwarz inequality, Lemma 2.3.6 and Hypothesis (2.8) imply that

$$\begin{aligned}\mathbb{E}(\Lambda_s^2) &\leq C(T-s)\int_s^T \mathbb{E}(|D_s^W \phi_r^2|^2)dr \\ &= O\left((T-s)\int_s^T \frac{(T-r)^4}{T^4}(r-s)^{2H-1}dr\right) \\ &= O\left(\frac{(T-s)^{5+2H}}{T^4}\right).\end{aligned}$$

Finally, we conclude that

$$\mathbb{E}\int_0^T \frac{\Lambda_s}{v_s^2(T-s)}ds = O\left(\int_0^T (T-s)^{H-\frac{1}{2}}ds\right) = O\left(T^{H+\frac{1}{2}}\right),$$

which proves (2.14).

Similarly, in order to check (2.15), we use Lemma 2.3.6 together with Cauchy-Schwarz inequality, to get that

$$\begin{aligned}\frac{1}{T^2}\mathbb{E}\left(\frac{1}{v_0}\int_0^T\left(\int_s^T D_s^W\phi_r^2 dr\right)^2 ds\right) &\leq \frac{1}{T^2}\int_0^T (T-s)\int_s^T \mathbb{E}\left(\left(D_s^W\phi_r^2\right)^2\right)drds \\ &= O\left(\frac{C}{T^2}\int_0^T (T-s)\int_s^T \frac{(T-r)^4}{T^4}(r-s)^{2H-1}drds\right) \\ &= O\left(\int_0^T \frac{(T-s)^{5+2H}}{T^6}ds\right) \\ &= O(T^{2H}).\end{aligned}$$

Thus, condition (2.15) also holds and the proof is completed.

■

2.4.2 Proof of (2.11) in Theorem 2.2.9: ATM implied volatility skew

Proof. We will apply Theorem 2.3.2. We start checking hypothesis (2.16). Using (2.19), Lemma 2.3.6 and Hypothesis (2.8), we get that

$$\begin{aligned}&\mathbb{E}\left(\int_0^T\left(\int_s^T \phi_r^2 dr\right)^{-3}\Lambda_s\left(\int_s^T \Lambda_r dr\right)ds\right) \\ &= O\left(\mathbb{E}\left(\int_0^T \frac{X_T T^6}{(T-s)^9}\frac{T-s}{T}\int_s^t \frac{(T-r)^2}{T^2}|D_s^{W'}\sigma_r|dr\int_s^t \frac{T-r}{T}\int_r^T \frac{(T-u)^2}{T^2}|D_r^{W'}\sigma_u|dudr\right)\right) \\ &= O\left(\int_0^T \frac{1}{(T-s)^3}\int_s^t (r-s)^{H-\frac{1}{2}}dr\int_s^t\int_r^T (u-r)^{H-\frac{1}{2}}dudr\right) \\ &= O\left(\int_0^T (T-s)^{2H-1}\right) = O(T^{2H}).\end{aligned}$$

Thus, as $\lim_{T\to 0}\frac{T^{\max(\frac{1}{2}-H,0)}}{\sqrt{T}}T^{2H} = \lim_{T\to 0} T^{\max(H,2H-\frac{1}{2})} = 0$ for all $H \in (0,1)$, we get that (2.16) holds true for the leading terms of Lemma 2.3.6. The other terms can be treated similarly and we conclude that (2.16) holds true.

We next check (2.17). By the definition of Λ_s, we have

$$\begin{aligned}\int_s^T D_s^W \Lambda_r dr &= \int_s^T D_s^W \left(\phi_r \int_r^T D_r^W \phi_u^2 du\right) dr \\ &= \int_s^T \left((D_s^W \phi_r)\int_r^T D_r^W \phi_u^2 du + \phi_r \int_r^T D_s^W D_r^W \phi_u^2 du\right) dr,\end{aligned}$$

where

$$D_s^W D_r^W \phi_u^2 = 2(D_s^W \phi_u D_r^W \phi_u + \phi_u D_s^W D_r^W \phi_u).$$

Next, using Lemma 2.3.6 and Hypothesis 2.2.7, we get that the leading terms are in expectation of order

$$\begin{aligned}&\int_s^T D_s^W \phi_r \int_r^T D_r^W \phi_u^2 du dr \\ &= O\left(\int_s^T \frac{(T-r)(r-s)^{H-\frac{1}{2}}}{T}\int_r^T \frac{(T-u)^2(u-r)^{H-\frac{1}{2}}}{T^2} du dr\right) \\ &= O\left(\frac{(T-s)^{4+2H}}{T^3}\right),\end{aligned}$$

and

$$\begin{aligned}&\int_s^T D_s^W \phi_r \int_r^T D_r^W \phi_u^2 du dr \\ &= O\left(\int_s^T \frac{(T-r)}{T}\int_r^T \frac{(T-u)^2(u-r)^{H-\frac{1}{2}}(u-s)^{H-\frac{1}{2}}}{T^2} du dr\right) \\ &= O\left(\frac{(T-s)^{4+2H}}{T^3}\right).\end{aligned}$$

Then, we conclude that the leading terms satisfy that

$$\begin{aligned}&\mathbb{E}\left(\int_0^T \left(\int_s^T \phi_r^2 dr\right)^{-2} \phi_s \left(\int_s^T D_s^W \Lambda_r dr\right) ds\right) \\ &= O\left(\int_0^T \frac{(T^3}{(T-s)^5}\frac{(T-s)^{4+2H}}{T^3} ds\right) \\ &= O\left(\int_0^T (T-s)^{2H-1}\right) = O(T^{2H}).\end{aligned}$$

Following as above this proves (2.17).

We are left to check hypothesis (2.18). Similarly as above, we have that

$$\frac{T^{\max(\frac{1}{2}-H,0)}}{T^2}\mathbb{E}\left(\frac{1}{v_0^3}\int_0^T \Lambda_s ds\right) = O(1),$$

and thus the limit is finite. Therefore, all the hypotheses of Theorem 2.3.2 are satisfied.

We finally compute the limit of (2.18) to check that it coincides with (2.11). Using Lemma

2.3.6, we obtain

$$\begin{aligned}
&\lim_{T\to 0}\frac{1}{T^2}\mathbb{E}\left(\frac{T^{\max(\frac{1}{2}-H,0)}}{v_0^3}\int_0^T\phi_s\left(\int_s^T D_s^W\phi_r^2 dr\right)^2 ds\right)\\
&=\lim_{T\to 0}\mathbb{E}\Bigg(\frac{T^{\max(\frac{1}{2}-H,0)}}{T^2v_0^3}\int_0^T\frac{\sigma_0(T-s)}{T}\int_s^T\Bigg(\frac{2\sigma_0\rho(T-r)^2D_s^{W'}\sigma_r}{T^2}\\
&\quad+\frac{2(T-r)^2\sigma_0^3}{T^2}-\frac{2(T-r)^2(T-s)\sigma_0^3}{T^3}\Bigg)drds\Bigg)\\
&=\lim_{T\to 0}\mathbb{E}\left(\frac{2\sigma_0^2\rho T^{\max(\frac{1}{2}-H,0)}}{T^5v_0^3}\int_0^T\left((T-s)\int_s^T(T-r)^2D_s^{W'}\sigma_r dr\right)ds\right)\\
&\quad+\lim_{T\to 0}T^{\max(\frac{1}{2}-H,0)}\mathbb{E}\left(\frac{\sigma_0^4}{45v_0^3}\right).
\end{aligned}$$

Using (2.19) and dominated convergence we see that

$$\lim_{T\to 0}T^{\max(\frac{1}{2}-H,0)}\mathbb{E}\left(\frac{\sigma_0^4}{45v_0^3}\right)=\lim_{T\to 0}T^{\max(\frac{1}{2}-H,0)}\frac{\sqrt{3}\sigma_0}{60},$$

since v_0^2 converges a.s. towards $\frac{\sigma_0^2}{3}$ as $T\to 0$. In order to compute the remaining limit we write

$$\begin{aligned}
&\lim_{T\to 0}\mathbb{E}\left(\frac{2\sigma_0^2\rho T^{\max(\frac{1}{2}-H,0)}}{T^5v_0^3}\int_0^T\left((T-s)\int_s^T(T-r)^2D_s^{W'}\sigma_r dr\right)ds\right)\\
&\quad=\lim_{T\to 0}\mathbb{E}\left(\left(\frac{1}{v_0^3}-\frac{3\sqrt{3}}{\sigma_0^3}\right)A_T\right)+\lim_{T\to 0}\frac{3\sqrt{3}}{\sigma_0^3}\mathbb{E}\left(A_T\right),
\end{aligned}$$

where

$$A_T=\frac{2\rho\sigma_0^2T^{\max(\frac{1}{2}-H,0)}}{T^5}\int_0^T\left((T-s)\int_s^T(T-r)^2D_s^{W'}\sigma_r dr\right)ds.$$

By dominated convergence we see that

$$\lim_{T\to 0}\mathbb{E}\left(\left(\frac{1}{v_0^3}-\frac{3\sqrt{3}}{\sigma_0^3}\right)A_T\right)=0,$$

which concludes the proof of (2.11). ■

2.5 Numerical analysis

In this section we present numerical evidence of the adequacy of Theorems 2.2.9 in different settings.

2.5.1 The Black-Scholes model under constant volatility

We consider the Black-Scholes model (2.1) under constant volatility $\sigma>0$, that is,

$$dS_t=\sigma S_t dW_t,\qquad S_t=S_0e^{\sigma W_t-\frac{\sigma^2}{2}t}.$$

Appealing to Theorem 2.2.9 with $\rho=0$ and $H=\frac{1}{2}$, we conclude that the level and the skew of the at-the-money implied volatility satisfy that

$$\lim_{T\to 0}I(0,k^*)=\frac{\sigma}{\sqrt{3}}\quad\text{and}\quad\lim_{T\to 0}\partial_k I(0,k^*)=\frac{\sigma\sqrt{3}}{30}.$$

Notice that these results coincide with the ones obtained in Pirjol and Zhu [48], see Section 2.5.4 below.

We next proceed with numerical simulations with parameters

$$S_0 = 10, \qquad T = \frac{1}{252}, \qquad \sigma \in [0.1, 0.2, \ldots, 1.4].$$

We use the control variates method in order to get estimates of an Asian call option price. As a control variate we use a geometric Asian call option whose price is given by

$$BS_{GeomAsian} = e^{-\frac{1}{4}\sigma_G^2 T} S_0 N(d_1) - KN(d_2), \tag{2.25}$$

where

$$d_1 = \frac{\log \frac{S_0}{K} + \frac{1}{4}\sigma_G^2 T}{\sigma_G \sqrt{T}}, \quad d_2 = d_1 - \sigma_G \sqrt{T}, \quad \sigma_G = \frac{\sigma}{\sqrt{3}}.$$

Then, the Asian call option price estimator has the following form

$$\hat{BS}_{Asian} = \frac{1}{N}\sum_{i=1}^{N} V_T^i - c^* \frac{1}{N}\sum_{i=1}^{N} (\hat{BS}^i_{Asian} - BS_{GeomAsian}), \tag{2.26}$$

where

$$c^* = \frac{\sum_{i=1}^{N}(V_T^i - \frac{1}{N}\sum_{i=1}^{N} A_T^i)(\hat{BS}^i_{Asian} - BS_{GeomAsian})}{\sum_{i=1}^{N}(\hat{BS}^i_{Asian} - BS_{GeomAsian})^2},$$

and

$$\hat{BS}^i_{Asian} = \max(\sqrt{S_0^i S_1^i \ldots S_m^i} - K, 0),$$

where $N = 2000000$, $m = 50$, $V_T^i = \max(A_T^i - K, 0)$ and the sub-index i indicates the quantity estimated from a realisation of a path from Monte Carlo simulation.

In order to retrieve an estimation for the implied volatility $\hat{I}(0, k^*)$ from the estimated Asian call price we use the algorithm presented in Jäckel [39]. For the estimation of the skew, we use the following finite difference approximation

$$\partial_k \hat{I}(0, k^*) = \frac{\hat{I}(0, k^* \log(1 + \Delta k)) - \hat{I}(0, \frac{k^*}{\log(1+\Delta k)})}{2\log(1 + \Delta k)}, \tag{2.27}$$

where $\Delta k = 0.001$.

The at-the-money level and the skew of the implied volatility are presented at Figure 2.1. We conclude that the results of the numerical simulation are in line with the presented theoretical formulas.

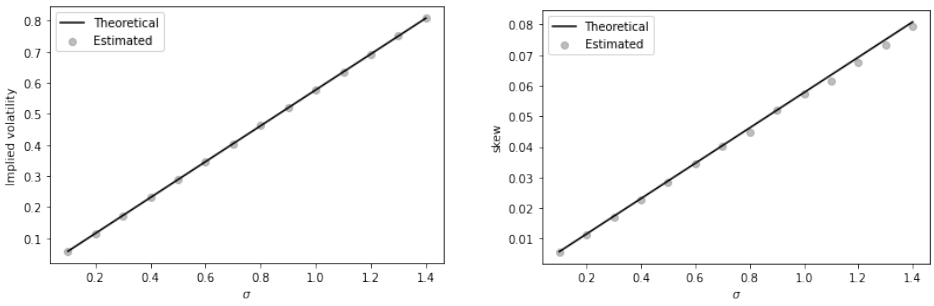

Figure 2.1: At-the-money level and skew of the IV under Black-Scholes

2.5.2 The SABR model

In this section we consider the SABR stochastic volatility model with the skewness parameter equal to 1, which is the most common case from a practical point of view. This corresponds to equation (2.1), where S_t denotes the forward price of the underlying asset and

$$d\sigma_t = \alpha \sigma_t dW_t', \qquad \sigma_t = \sigma_0 e^{\alpha W_t' - \frac{\alpha^2}{2} t}.$$

where $\alpha > 0$ is the volatility of volatility.

Notice that this model does not satisfy Hypothesis 2.2.1, so a truncation argument similar as in Section 5 in Alòs and Shiraya [11] is needed in order to check that Theorem 2.2.9 is true for this model. We define $\varphi(x) = \sigma_0 \exp(x)$. For every $n > 1$, we consider a function $\varphi_n \in C_b^2$ satisfying that $\varphi_n(x) = \varphi(x)$ for any $x \in [-n, n]$, $\varphi_n(x) \in [\varphi(-2n) \vee \varphi(x), \varphi(-n)]$ for $x \leq -n$, and $\varphi_n(x) \in [\varphi(n), \varphi(x) \wedge \varphi(2n)]$ for $x \geq n$. We set

$$\sigma_t^n = \varphi_n\left(\alpha W_t' - \frac{\alpha^2}{2}t\right).$$

It is easy to see that σ_t^n satisfies Hypotheses 2.2.1, 2.2.5, (2.8), and 2.2.8. In fact, for $r \leq t$, we have that

$$D_r^{W'}\sigma_t^n = \varphi_n'\left(\alpha W_t' - \frac{\alpha^2}{2}t\right)\alpha,$$

which implies that (2.8) holds with $H = \frac{1}{2}$ and Hypothesis 2.2.8 is satisfied with $\gamma < 1/2$. Therefore, appealing to Theorem 2.2.9 and using the fact that $\sigma_0^n = \sigma_0$, we conclude that

$$\lim_{T\to 0} I^n(0, k^*) = \frac{\sigma_0}{\sqrt{3}}. \tag{2.28}$$

where I^n denotes the implied volatility under the volatility process σ_t^n. We then write

$$I(0, k^*) = I^n(0, k^*) + I(0, k^*) - I^n(0, k^*).$$

By the mean value theorem,

$$\begin{aligned} I(0, k^*) - I^n(0, k^*) &= \partial_\sigma(BS^{-1}(0, X_0, X_0, \xi))(V_0 - V_0^n) \\ &= e^{-X_0 + \frac{\xi^2 T}{8}}\frac{\sqrt{2\pi}}{\sqrt{T}}(V_0 - V_0^n), \end{aligned}$$

for some $\xi \in (V_0, V_0^n)$, where V_0^n is the option price under σ^n. Thus, for $T \leq 1$ and $n > \alpha^2$,

$$\begin{aligned} |I(0, k^*) - I^n(0, k^*)| &\leq \frac{C_n}{\sqrt{T}}\mathbb{E}\left(|e^{X_T} - e^{X_T^n}|\mathbf{1}_{\sup_{s\in[0,T]}|\ln(\sigma_s/\sigma_0)|>n}\right) \\ &\leq \frac{C_n}{\sqrt{T}}\mathbb{E}[(|e^{X_T} + e^{X_T^n}|^2)]^{1/2}\left[\mathbb{P}\left(\sup_{s\in[0,T]}|\ln(\sigma_s/\sigma_0)| > n\right)\right]^{1/2} \\ &\leq \frac{C_n}{\sqrt{T}}\left[\mathbb{P}\left(\sup_{s\in[0,T]}|\alpha W_s' - \alpha^2 s/2| > n\right)\right]^{\frac{1}{2}} \\ &\leq \frac{C_n}{\sqrt{T}}\left[\mathbb{P}\left(\sup_{s\in[0,T]}|W_s| > \frac{n}{2\alpha}\right)\right]^{\frac{1}{2}}, \end{aligned}$$

for some constant $C_n > 0$ that changes from line to line. Then, Markov's inequality implies that for all $p > 2$,

$$|I(0, k^*) - I^n(0, k^*)| \leq \frac{C_n}{\sqrt{T}}\left(\frac{2\alpha}{n}\right)^{p/2}\left[\mathbb{E}\left(\sup_{s\in[0,T]}|W_s|^p\right)\right]^{1/2} \leq C_n T^{\frac{p}{2}-\frac{1}{2}},$$

Thus, taking $p > 4$, we conclude that

$$\lim_{T\to 0} I(0, k^*) = \frac{\sigma_0}{\sqrt{3}}.$$

On the other hand, for $s \leq r \leq t$, we have

$$D_s^{W'}D_r^{W'}\sigma_t^n = \varphi_n''\left(\alpha W_t' - \frac{\alpha^2}{2}t\right)\alpha^2,$$

which implies that (2.9) holds with $H = \frac{1}{2}$. Therefore, appealing to Theorem 2.2.9 we get that

$$\lim_{T\to 0} \partial_k I^n(0,k^*) = \frac{\sqrt{3}\rho\alpha\varphi_n'(\sigma_0)}{5\sigma_0^n} + \frac{\sqrt{3}\sigma_0^n}{30} = \frac{\sqrt{3}\rho\alpha}{5} + \frac{\sqrt{3}\sigma_0}{30}.$$

Next, similarly as above we can write

$$\partial_k I(0,k^*) = \partial_k I^n(0,k^*) + \partial_k(I(0,k^*) - I^n(0,k^*)).$$

By the mean value theorem,

$$\begin{aligned}\partial_k(I(0,k^*) - I^n(0,k^*)) &= \partial_\sigma\partial_k(BS^{-1}(0,X_0,X_0,\xi))(V_0 - V_0^n)\\ &= -e^{-X_0+\frac{\xi^2 T}{8}}\frac{\sqrt{2\pi}}{2}\xi(V_0 - V_0^n),\end{aligned}$$

for some $\xi \in (V_0, V_0^n)$. Thus, proceeding as above we conclude that

$$\lim_{T\to 0} \partial_k I(0,k^*) = \frac{\sqrt{3}\rho\alpha}{5} + \frac{\sqrt{3}\sigma_0}{30}.$$

We next proceed with some numerical simulations using the following parameters

$$S_0 = 10,\ T = \frac{1}{252},\ dt = \frac{T}{50},\ \alpha = 0.5,\ \rho = -0.3,\ \sigma_0 = (0.1, 0.2, \ldots, 1.4).$$

In order to get estimates of an Asian call option we use antithetic variates. The estimate of the price is defined as follows

$$\hat{V}_{sabr} = \frac{\frac{1}{N}\sum_{i=1}^N V_T^i + \frac{1}{N}\sum_{i=1}^N V_T^{i,A}}{2}, \tag{2.29}$$

where $N = 2000000$ and the sub-index A denotes the value of an Asian call option computed on the antithetic trajectory of a Monte Carlo path.

We use equation (2.27) in order to get estimates of the skew. In Figure 2.2 we present the results of a Monte Carlo simulation which aims to evaluate numerically the level and the skew of the at-the-money implied volatility of an Asian call option under the SABR model. Again, the numerical results fit the theoretical ones.

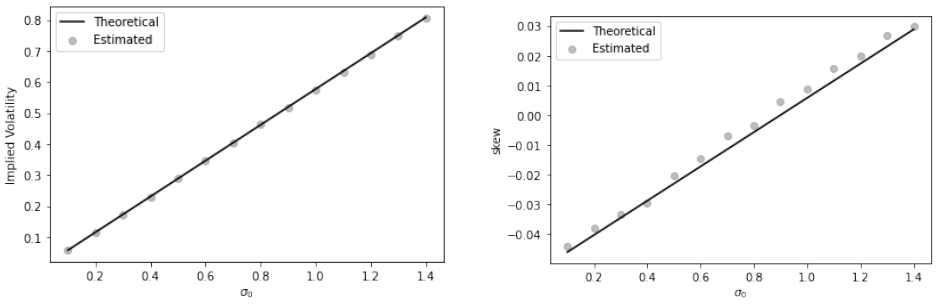

Figure 2.2: At-the-money level and skew of the IV under SABR model.

2.5.3 The fractional Bergomi model

The fractional Bergomi stochastic volatility model asssumes equation (2.1) with

$$\sigma_t^2 = \sigma_0^2 e^{v\sqrt{2H}Z_t - \frac{1}{2}v^2 t^{2H}}, \quad Z_t = \int_0^t (t-s)^{H-\frac{1}{2}} dW_s',$$

where $H \in (0,1)$ and $v > 0$, see Example 2.5.1 in Alòs and García-Lorite [5].

As for the SABR model, a truncation argument is needed in order to apply Theorem 2.2.9, as Hypothesis 2.2.1 is not satisfied. We define φ and φ_n as for the SABR model, and we set

$$\sigma_t^n = \varphi_n\left(\frac{1}{2}v\sqrt{2H}Z_t - \frac{1}{4}v^2t^{2H}\right).$$

It is easy to see that σ_t^n satisfies Hypotheses 2.2.1, 2.2.5, (2.8), and 2.2.8. In fact, for $r \le t$, we have that

$$D_r^{W'}\sigma_t^n = \varphi_n'\left(\frac{1}{2}v\sqrt{2H}Z_t - \frac{1}{4}v^2t^{2H}\right)\frac{1}{2}v\sqrt{2H}(t-r)^{H-\frac{1}{2}},$$

which implies that Hypothesis (2.8) holds and Hypothesis 2.2.8 is satisfied with $\gamma < H$. Moreover, for $s \le r \le t$, we have

$$D_s^{W'}D_r^{W'}\sigma_t^n = \varphi_n''\left(\frac{1}{2}v\sqrt{2H}Z_t - \frac{1}{4}v^2t^{2H}\right)\frac{1}{4}v^2\sqrt{4H^4}(t-r)^{H-\frac{1}{2}}(t-s)^{H-\frac{1}{2}},$$

which implies that (2.9) holds. Therefore, by Theorem 2.2.9 we get that (2.28) holds. Concerning the short maturity limit of the skew, we observe that

$$\mathbb{E}(D_r^{W'}\sigma_u) = e^{-\frac{1}{8}v^2u^{2H}}\frac{1}{2}\sigma_0 v\sqrt{2H}(u-r)^{H-\frac{1}{2}}.$$

which gives

$$\lim_{T\to 0}\partial_k I^n(0,k^*) = \begin{cases} \frac{\sqrt{3}\sigma_0}{30} & \text{if} \quad H > \frac{1}{2} \\ \frac{\sqrt{3}\rho v}{10} + \frac{\sqrt{3}\sigma_0}{30} & \text{if} \quad H = \frac{1}{2}, \end{cases} \tag{2.30}$$

and for $H < \frac{1}{2}$

$$\begin{aligned} &\lim_{T\to 0} T^{\frac{1}{2}-H}\left(\partial_k I^n(0,k^*) - \frac{\sqrt{3}\sigma_0}{30}\right) \\ &\qquad = \frac{3\sqrt{6H}\rho v}{(1+H-\frac{1}{2})(2+H-\frac{1}{2})(3+H-\frac{1}{2})(5+H-\frac{1}{2})}. \end{aligned} \tag{2.31}$$

Finally, similarly as for the SABR model one can easily show that for n sufficiently large but fixed,

$$\lim_{T\to 0}(I(0,k^*) - I^n(0,k^*)) = 0$$

and

$$\lim_{T\to 0}\partial_k(I(0,k^*) - I^n(0,k^*)) = 0,$$

so (2.28), (2.30), and (2.31) are also true for $I(0,k^*)$.

The parameters used for the Monte Carlo simulation are the following

$$S_0 = 10,\ T = 0.001,\ dt = \frac{T}{50},\ H = (0.4, 0.7),\ v = 0.5,\ \rho = -0.3,\ \sigma_0 = (0.1, 0.2, \ldots, 1.4).$$

In order to obtain an estimate of the price of an Asian call option under the fractional Bergomi model we use the combination of antithetic and control variates presented in equations (2.26) and (2.29). That is, we first sample the process from the Bergomi model and the antithetic analogue. We then average the payoffs calculated from both paths. Finally, use the geometric Asian as control variate assuming constant volatility model at level σ_0.

In Figure 2.3 we plot the estimates of the level of the ATMIV of the Asian call option and we observe that the result is independent of H as stated in Theorem 2.2.9.

In Figure 2.4 we simulate the ATMIV skew of the Asian call option as a function of the maturity as well as its least squares fit in order to observe the blow up to $-\infty$ for the case $H = 0.4$.

We then plot the quantities $T^{\frac{1}{2}-H}\partial_k\hat{I}(0,k^*)$ for $H = 0.4$ and $\partial_k\hat{I}(0,k^*)$ for $H = 0.7$ in Figure 2.5 as a function of σ_0. For $H = 0.4$, the line $-0.0243 + 0.032\sigma_0$ corresponds to the least square fit while formula (2.31) gives the line $-0.0286 + 0.029\sigma_0$. This difference is due to the numerical instability of the finite difference estimation at short maturity in the presence of rough noise and could be improved by increasing considerably the number of Monte Carlo samples or applying a variance reduction technique. For $H = 0.7$, we observe that formula (2.30) fits well the Monte Carlo estimates.

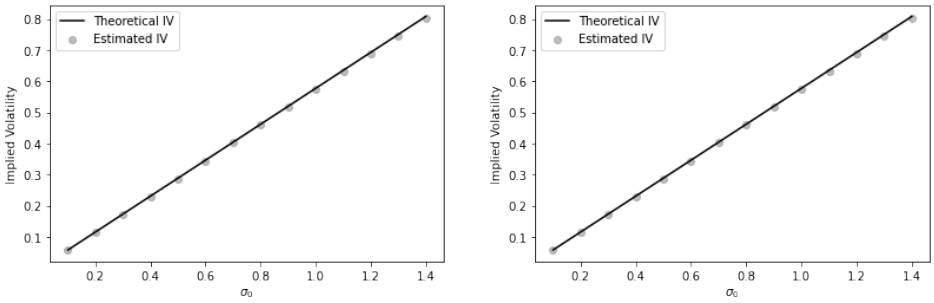

(a) H=0.4 (b) H=0.7

Figure 2.3: At-the-money level of the IV under fractional Bergomi model

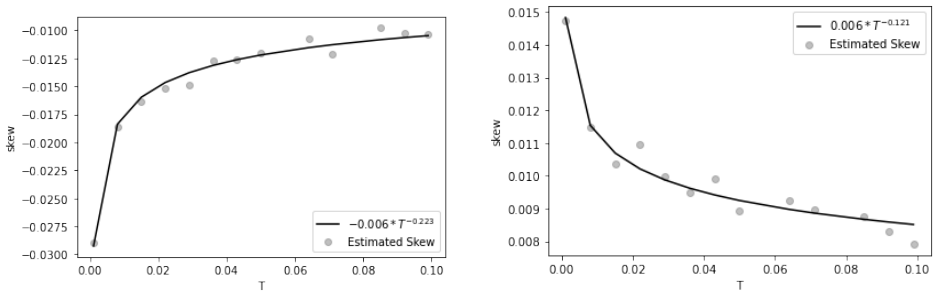

H=0.4 H=0.7

Figure 2.4: At-the-money IV skew as a function of T under fractional Bergomi model

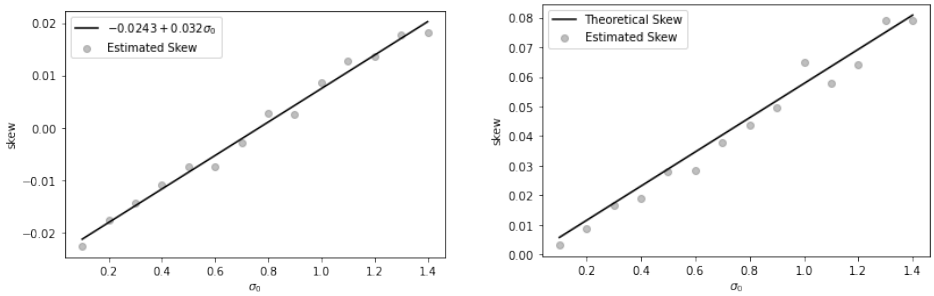

H=0.4 H=0.7

Figure 2.5: At-the-money IV skew as a function of σ_0 under fractional Bergomi model

2.5.4 Local volatility model

The short-maturity limit of the ATMIV level and skew of an Asian option under local volatility has already been computed in Pirjol and Zhu [48]. The aim of this section is to check that our Theorem 2.2.9 provides the same asymptotics as the ones obtained in that paper. We consider the local volatility model

$$dS_t = \sigma(S_t)S_t dW_t, \tag{2.32}$$

where $\sigma(.)$ is a twice differentiable function. In Proposition 19 of Pirjol and Zhu [48] they show that the following expansion holds for $x = \log(\frac{K}{S_0})$ around the ATM point

$$\lim_{T\to 0} I(0,k^*) = \frac{\sigma(S_0)}{\sqrt{3}}\left(1 + \left(\frac{1}{10} + \frac{3\sigma'(S_0)}{5\sigma(S_0)}S_0\right)x + O(x^2)\right). \tag{2.33}$$

Then, differentiating equation (2.33), we obtain that

$$\lim_{T\to 0} \partial_k I(0,k^*) = \frac{1}{\sqrt{3}}\left(\frac{1}{10}\sigma(S_0) + \frac{3}{5}S_0\sigma'(S_0)\right). \tag{2.34}$$

We next apply Theorem 2.2.9 in the case of the local volatility model (2.32) with $\sigma_t = \sigma(S_t)$ and $\rho = 1$ to verify that we obtain the same expressions as in (2.10) and (2.34). For the level, we directly see that when $\sigma(S_t)$ equals σ_t and $K = S_0$, (2.33) coincides with the limit in (2.10). For the skew, we need to compute $D_r\sigma(S_t)$. We have for $r \leq u$,

$$D_r\sigma(S_u) = \sigma'(S_u)D_r(S_u) = \sigma'(S_u)\left(\sigma(S_r)S_r + \int_r^u D_r(\sigma(S_s)S_s)dW_s\right).$$

In particular,

$$\mathbb{E}\left(D_r\sigma(S_u)\right) = \mathbb{E}\left(\sigma'(S_u)\sigma(S_r)S_r\right).$$

This can be written as

$$\begin{aligned}\mathbb{E}\left(D_r\sigma(S_u)\right) = \sigma'(S_0)\sigma(S_0)S_0 + \mathbb{E}\left((\sigma'(S_u) - \sigma'(S_0))\sigma(S_r)S_r\right) \\ + \sigma'(S_0)\mathbb{E}\left((\sigma(S_r) - \sigma(S_0))S_r\right).\end{aligned}$$

Then, using the mean value theorem and the fact that S_t has Hölder continuous sample paths of any order $\gamma < \frac{1}{2}$, we see that the last two terms of the last display will not contribute in the limit (2.11). Thus, (2.11) gives

$$\lim_{T\to 0} \partial_k I(0, k^*) = \frac{\sqrt{3}}{5}S_0\sigma'(S_0) + \frac{\sqrt{3}\sigma(S_0)}{30},$$

which is the same as in (2.34). This serves as one more evidence of the validity of Theorem 2.2.9.

2.5.5 Approximations for the Asian call price

In this last section we study numerically the adequacy of the linear approximation of the price of an Asian call option given in equation (2.13) in the case of the SABR and fractional Bergomi models.

We start considering the SABR model and we proceed with the following numerical experiment. We randomly sample the parameters as $\sigma_0 \sim U(0.2, 0.8)$, $\alpha \sim U(0.3, 1.5)$ and $\rho \sim U(-0.9, 0.9)$, where U stands for the uniform distribution. We fix $S_0 = 100$ and consider the following strikes $K = (90, 95, \ldots, 125)$ and maturities $T = (0.01, 0.1, 0.5, 1, 2)$. We then price the Asian call option using Monte Carlo with 100000 paths and discretization step 0.01 and then estimate the IV following the same approach as in Section 2.5.2. The approximation accuracy of the Monte Carlo for the IV is computed using the pointwise relative error with respect to the 95% Monte Carlo confidence interval and is presented in Table 2.1. We observe a high error in the case of short maturity deep OTM options with strike price equal to 120 and 125, which comes from the fact that in this region the price of the option is close to zero.

Maturity/Strike	90	95	100	105	110	115	120	125
0.01	6.78	1.41	0.97	1.09	2.41	6.69	104.39	105.01
0.10	1.58	1.18	1.07	1.00	1.04	1.16	1.36	1.66
0.50	1.82	1.16	1.02	0.97	1.08	1.41	1.91	2.74
1.00	2.07	1.85	1.72	1.64	1.60	1.59	1.61	1.68
2.00	3.26	3.20	3.02	2.94	2.87	2.87	2.90	2.92

Table 2.1: Median percentage error wrt the 95% Monte Carlo confidence interval for the SABR model.

We then compare the estimated IV with the approximation formula (2.13). We compute in Table 2.2 the median relative percentage error, the 90% quantile and the maximum of the relative percentage error of the Monte Carlo prices computed across 2000 random parameter combinations. We consider the 90% quantile in order to take into account the fact that we might generate 'bad' parameter combinations that may require more Monte Carlo samples to converge. In order to help the visualization of these quantities we also plot the heat map in Figure 2.6. We see that the suggested formula works the best for short dated options with strikes close to ATM level. As we increase the maturity the quality of the approximation decreases and the error can be very big.

We finally plot an implied volatility surface for different maturities in Figure 2.7 to see the typical shape of the IV under the SABR model. We see that that the level of the implied volatility

Maturity/Strike	90	95	100	105	110	115	120	125
0.01	4.07	0.40	0.24	0.28	0.55	1.19	2.93	5.44
0.10	0.78	0.46	0.34	0.40	0.56	0.88	1.29	1.79
0.50	215.50	216.26	216.60	216.12	215.27	214.31	213.39	212.64
1.00	2.79	2.43	2.27	2.38	2.59	2.89	3.36	3.78
2.00	4.48	4.10	3.89	3.86	4.02	4.33	4.81	5.27

(a) Median % error

Maturity/Strike	90	95	100	105	110	115	120	125
0.01	44.91	3.26	0.54	0.93	2.70	5.29	8.86	13.68
0.10	2.92	1.21	0.83	1.08	2.17	4.11	6.06	7.57
0.50	218.84	218.10	217.96	217.62	217.44	217.55	217.98	218.51
1.00	9.42	7.32	6.57	6.78	7.79	9.40	11.94	14.46
2.00	23.59	25.77	23.06	21.91	20.77	20.66	22.77	26.60

(b) 90th quantile % Error

Maturity/Strike	90	95	100	105	110	115	120	125
0.01	76.99	41.51	1.05	12.17	22.30	21.32	21.78	20.80
0.10	41.89	3.72	1.66	3.78	10.02	19.88	31.79	30.65
0.50	273.69	224.61	219.46	219.52	223.80	280.83	249.04	280.53
1.00	123.43	88.31	87.24	86.28	85.40	84.61	83.87	83.20
2.00	572.53	989.85	328.54	254.77	217.17	194.01	178.21	166.72

(c) Maximum % error

Table 2.2: Approximation error under the SABR model.

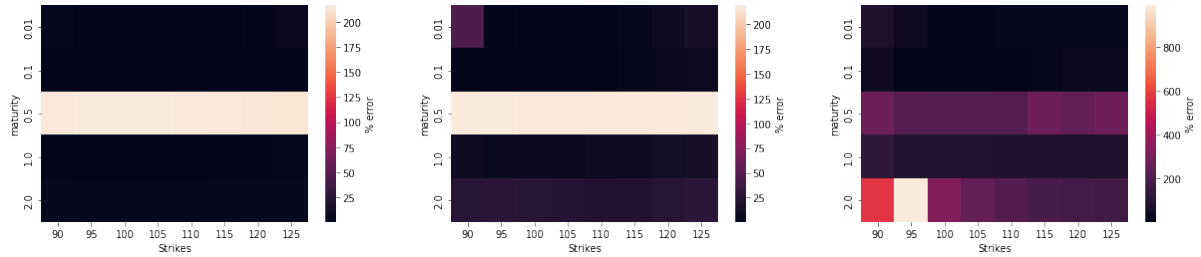

(a) Median (b) 90% Quantile (c) Maximum

Figure 2.6: Accuracy of the approximation (2.13) under the SABR model.

even for ATM options can shift considerably as we increase the maturity and is not necessarily linear.

Overall, we conclude that the suggested approximation formula is stable for short maturities and not too deep out and in-the-money options. Outside of these regions the quality of the approximation highly depends on the parameters of the model.

In the case of the fractional Bergomi model we randomly sample the parameters of the model as $\sigma_0 \sim U(0.2, 0.8)$, $v \sim U(0.3, 1.5)$ and $\rho \sim U(-0.9, 0.9)$. We fix $S_0 = 100$ and consider the strikes $K = (90, 95, \dots, 125)$ and maturities $T = (0.01, 0.1, 0.5, 1, 2)$. In order to investigate the influence of roughness of the volatility process we consider two values of $H = \{0.2, 0.7\}$. We price the Asian call option using Monte Carlo with 100000 paths and discretization step 0.01.

We start with the case $H = 0.2$. The approximation accuracy of the Monte Carlo for the implied volatility is computed using the corresponding pointwise median relative error with respect to the 95% Monte Carlo confidence interval and is presented at Table 2.3.

As for the SABR model, we compute the median relative percentage error, the 90% quantile and the maximum of relative percentage error across 1000 random parameter combinations in Table 2.4. The heat map is presented in Figure 2.8. We observe that the approximation works better

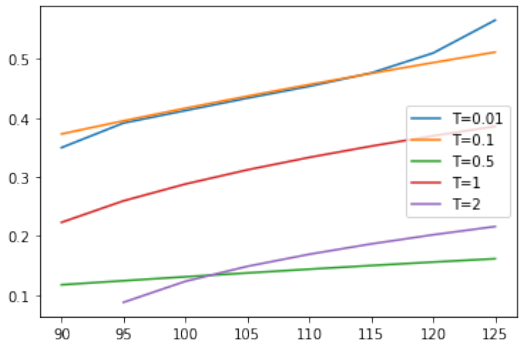

Figure 2.7: Implied volatility surface under the SABR model.

Maturity/Strike	90	95	100	105	110	115	120	125
0.01	5.10	1.41	0.99	1.12	2.35	4.58	9.60	10.95
0.10	1.47	1.18	1.09	1.03	1.08	1.22	1.48	1.79
0.50	1.55	1.41	1.32	1.26	1.23	1.24	1.28	1.35
1.00	1.77	1.64	1.55	1.48	1.44	1.43	1.44	1.46
2.00	2.25	2.11	2.01	1.93	1.89	1.86	1.84	1.86

Table 2.3: Median percentage error wrt the 95% Monte Carlo confidence interval of fractional Bergomi model with H=0.2.

for ATM options with short maturities. Additionally, we conclude that it exhibits an adequate performance in the range of 5% around the ATM strike for short dated options and quite a wide range of strikes for longer dated options.

Maturity/Strike	90	95	100	105	110	115	120	125
0.01	11.00	5.29	0.69	4.85	7.22	7.75	9.62	18.76
0.10	5.57	2.80	1.34	2.53	5.09	6.94	8.34	9.49
0.50	3.74	2.37	2.34	1.98	2.91	4.42	6.00	7.23
1.00	3.49	2.96	3.16	2.80	2.88	3.64	4.73	5.85
2.00	4.28	4.25	4.30	4.13	3.91	4.03	4.47	5.03

(a) Median % error

Maturity/Strike	90	95	100	105	110	115	120	125
0.01	42.98	14.75	1.33	12.96	26.83	38.08	49.11	60.95
0.10	16.39	8.49	2.80	7.91	13.38	18.16	25.08	32.56
0.50	11.84	7.48	5.26	7.05	10.40	13.58	16.56	18.68
1.00	11.40	8.38	7.04	8.10	10.16	12.59	14.96	17.09
2.00	13.28	11.26	10.33	11.19	12.35	13.51	15.30	16.68

(b) 90th quantile % error

Maturity/Strike	90	95	100	105	110	115	120	125
0.01	98.23	59.44	2.09	52.10	65.76	75.87	75.35	76.91
0.10	58.45	23.72	4.64	21.61	47.06	67.19	81.64	92.92
0.50	29.69	21.12	8.32	21.27	28.43	38.44	52.83	64.23
1.00	31.82	21.64	13.38	21.38	29.45	31.21	39.36	50.72
2.00	58.74	56.54	54.71	53.23	52.07	51.19	50.55	50.12

(c) Maximum % error

Table 2.4: The Approximation error of the IV under fractional Bergomi model with H=0.2.

As for the SABR model we plot in Figure 2.9 an IV surface for different maturities. We observe

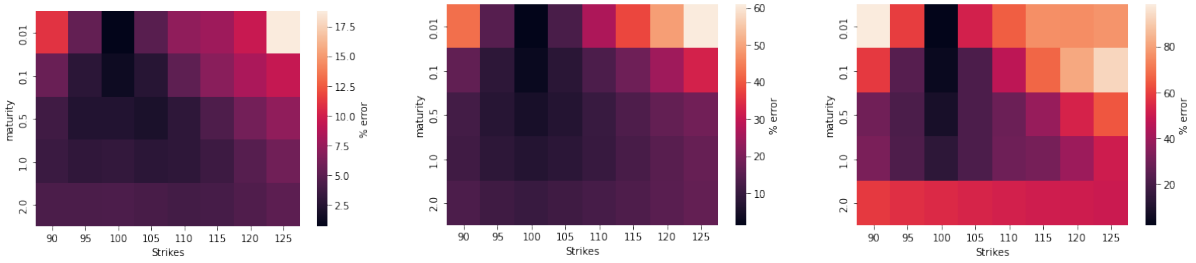

(a) Median (b) 90% Quantile (c) Maximum

Figure 2.8: Accuracy of the approximation (2.13) under fractional Bergomi with $H = 0.2$.

a considerable curvature for short maturity that smooths around the ATM values leading to the improvement in the behaviour of our approximation as maturity increases. This shape heavily depends on the parameters of the model, however this conclusion holds on average for our sample.

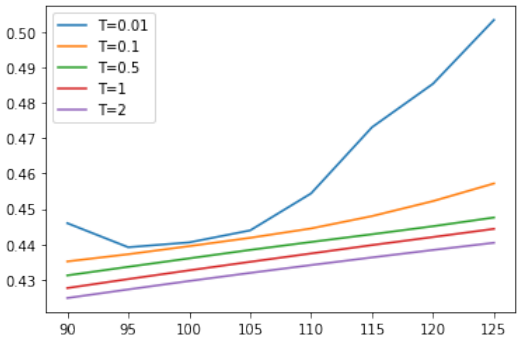

Figure 2.9: Implied volatility surface under the fractional Bergomi model with $H = 0.2$.

Finally, we follow the same approach the fractional Bergomi model with H=0.7. See Tables 2.5 and 2.6 and Figure 2.10. One can see that the behaviour of the errors is much better than in the case of $H = 0.2$. In general, the magnitudes of the errors turn out to be smaller. The approximation defined in equation (2.13) works quite well for a wide range of strikes and maturities. This fact is explained by the typical shape of the implied volatility of the considered model which is presented in Figure 2.11. We see that the curvature looks negligible as we increase the maturity of the option which makes linear approximation quite reasonable.

Maturity/Strike	90	95	100	105	110	115	120	125
0.01	5.52	1.34	0.97	1.07	2.46	6.41	104.51	105.28
0.10	1.36	1.12	1.06	0.98	1.00	1.07	1.30	1.62
0.50	1.44	1.32	1.24	1.17	1.13	1.13	1.15	1.19
1.00	1.65	1.53	1.45	1.38	1.34	1.32	1.32	1.34
2.00	2.27	2.13	2.03	1.96	1.91	1.89	1.88	1.88

Table 2.5: Median percentage error wrt the 95% Monte Carlo confidence interval of fractional Bergomi model with H=0.7.

In conclusion, the behaviour of the approximation (2.13) heavily depends on the model. For OTM and ITM options the quality gets better with the decrease in the curvature of the implied volatility surface. For ATM options, the quality of the approximation and behaviour are quite stable for the considered models and reasonably impairs with the increase of the maturity.

Maturity/Strike	90	95	100	105	110	115	120	125
0.01	2.58	0.40	0.27	0.32	0.51	1.11	2.84	10.22
0.10	0.40	0.35	0.35	0.33	0.30	0.31	0.33	0.40
0.50	0.78	0.86	0.87	0.81	0.71	0.65	0.60	0.57
1.00	1.65	1.77	1.78	1.72	1.59	1.33	1.20	1.13
2.00	3.94	4.06	4.07	4.00	3.81	3.54	3.16	2.78

(a) Median % error

Maturity/Strike	90	95	100	105	110	115	120	125
0.01	39.71	1.64	0.59	0.90	2.38	3.77	7.59	12.34
0.10	0.88	0.71	0.67	0.63	0.64	0.84	1.89	2.35
0.50	1.61	1.64	1.62	1.58	1.46	1.37	1.40	1.75
1.00	3.53	3.59	3.59	3.51	3.36	3.11	2.90	2.95
2.00	10.16	10.07	10.02	9.89	9.61	9.34	9.05	8.75

(b) 90th quantile % error

Maturity/Strike	90	95	100	105	110	115	120	125
0.01	57.59	16.07	1.10	15.35	28.43	30.11	15.95	18.70
0.10	3.68	1.18	1.09	1.05	2.96	6.83	11.84	18.08
0.50	2.71	2.65	2.60	2.52	2.45	2.35	6.40	11.29
1.00	7.81	7.58	7.39	7.24	7.12	7.00	6.87	8.77
2.00	77.63	76.58	75.66	74.85	74.14	73.52	72.98	72.51

(c) Maximum % Error

Table 2.6: Approximation error of the IV under fractional Bergomi model with H=0.7.

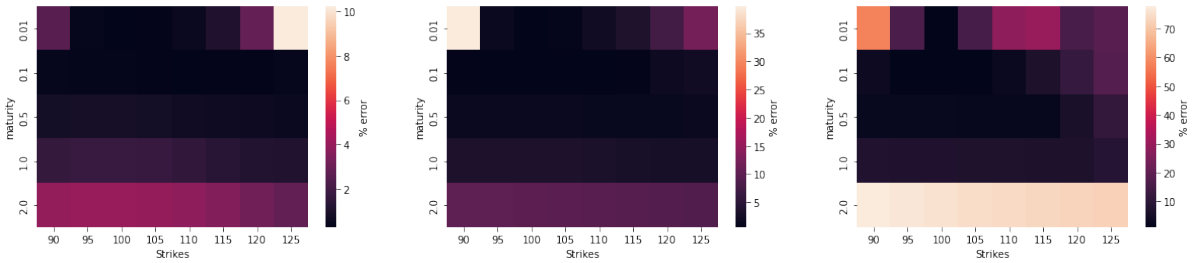

(a) Median (b) 90% Quantile (c) Maximum

Figure 2.10: Accuracy of the approximation (2.13) under fractional Bergomi with $H = 0.7$.

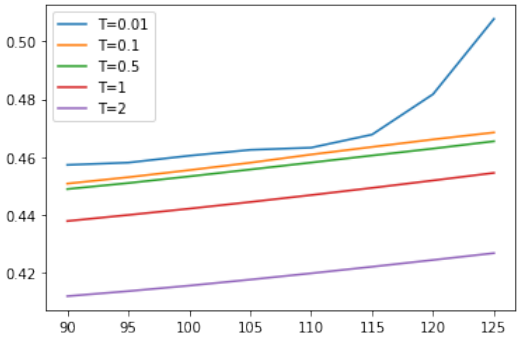

Figure 2.11: Implied volatility surface under fractional Bergomi model with $H = 0.7$.

Chapter 3

On the implied volatility of Inverse and Quanto Inverse options under stochastic volatility models

III

3.1 Introduction

Over the last several decades option pricing models were developed for conventional assets such as stocks, bonds, interest rates, foreign currencies, etc. Nowadays crypto derivatives is a new class of asset that has gain a lot of attention. Blockchain technology has started to prosper since the advent of Bitcoin. Since then the development of new much more powerful and scalable blockchains like Ethereum, Solana, Polygon, etc. has taken place. As a result, over the last decade we have seen the emergence of numerous exchanges that allow regular people, institutional investors and market professionals either to become a part of the innovation or speculate on it. For the introduction to this topic we refer to Fant et al. [22], Mukhopadhyay et al. [44] and Richards [49], among others.

The peculiarity of crypto derivatives is related to the idea of how one sees the cryptocurrency. Is it a security, currency or a commodity? As regards options, the answer to this question influences the pricing methodology. One can see a detailed discussion on this topic in Imeraj et al. [1]. Unfortunately, there is no clear legal answer to this question, see Bolotaeva et al.[16]. However, a detailed look at the topic allows us to incline to the following conclusions.

Cryptocurrency (at least Bitcoin and Ethereum) cannot be considered as a security since it is fully decentralised and no one has the power to control its emission, whereas securities are released by a central authority. Moreover, cryptocurrency cannot be treated as a conventional (fiat) currency. A question that one needs to understand is if its preserves key characteristics of money. Clearly, cryptocurrencies can be used to buy and sell things occasionally, however, they are not widely accepted as a means of payment. Secondly, by looking at the historical data one can observe enormous volatility of cryptocurrencies leading to the conclusion that its purchasing power is not stable enough over time. As a result, it can not be used as a means to store the value. However, the Central Bank Digital Currency solves the volatility issue by controlling the emission. Last but not least, despite the fact that some companies may accept cryptocurrencies as payment, the majority are still using regular currencies in order to measure the value of provided goods and services. See Hazlett and Luther [36] and Ammous [12] where authors provide an investigation about the similarity of cryptocurrencies to regular currencies.

On the other hand, if we consider the classical Garman and Kohlhagen [30] foreign exchange (FX) pricing model, the construction of the delta hedged portfolio is conceptually different for FX options than for regular options since we can not buy and sell units of the FX spot rate. As a result, hedging is conducted by buying and selling units of the underlying foreign bond. Notice that this completely undermines the idea of pricing crypto options using FX models since one can buy and sell crypto in a way similar to a regular tradable asset.

Alternatively, some people believe that Bitcoin is a digital gold, but how similar is it to the real commodity? In Goutte et al. [32] the authors define the following characteristics of hard commodities: they are costly to mine or extract, they are storable, no single government or institution controls their global supply, demand, or price and they have an intrinsic value, i.e., they can be consumed or used as inputs in the production of other consumable goods. The first three properties are naturally satisfied by Bitcoin, but the fourth one is still arguable. As a result, we can not conclude that the crypto is a commodity. See Ankenbrand and Bieri [13] and Gronwald [33] for more detailed discussion on the topic.

The aim of this chapter is to solve the pricing problem under a stochastic volatility model given only the payoff function, without assuming any specific property on the cryptocurrencies as an

asset. We consider as a crypto asset a cryptographically secured digital representation of value or contractual rights that uses a form of distributed ledger technology and can be transferred, stored, or traded electronically. Publicly traded crypto assets such as Bitcoin and Ethereum, etc., represent the main interest for us. Crypto derivative is a type of financial contract whose value is dependent on an underlying crypto asset. Some of the publicly traded crypto derivatives are coming directly from the regular exchanges, for instance, European type options and futures. However, some of them are unique and have been introduced due to specific characteristic of crypto world. In particular, one of the most traded crypto derivative is perpetual swap, which is a contract that allows traders to speculate on the future price movements of cryptocurrencies. Unlike a typical futures contract, perpetual swaps do not have expiration dates. For this reason, the price of perpetual contracts must be anchored to the spot prices of their underlying assets. Exchanges implement a price anchoring system called the funding rate mechanism. This mechanism balances the short and long positions of perpetual swaps by either encouraging or discouraging trades. In the case of a futures contract, you know that the price will converge to the spot value at expiry, whereas in the case of a perpetual swaps, you do not know that the price will converge to the spot at a certain point in time. In Section 3.2 we provide the mechanics of the perpetual swap market on Deribit exchange.

The main interest of this chapter is the analysis of a derivative which can be considered as a light exotic product and is called Inverse European option. The payoff at maturity of this product is given by

$$V_T^E = \max\left(\frac{S_T - K}{S_T}, 0\right),$$

where S_T denotes the price of the underlying at maturity and K is a fixed strike. In simple words, if the option becomes in-the-money then the payoff is payed in the crypto coin rather than fiat currency.

The Inverse European option is the main and the only type of options traded on Deribit exchange, which controls more than 80 percent of the global crypto options market. For instance, on June 10th 2023, the open interest in Bitcoin options on Deribit was 7.5 billion dollars, while on OKX and Binance, the closest competitors, it was 0.5 and 0.17 billion dollars, respectively. Therefore, the adequate pricing and hedging of Inverse European options is of high importance from a practical perspective. However, this turns out to be quite challenging due to the mechanics of Deribit exchange. We provide an overview of the Deribit trading mechanics in Section 3.2.

The Deribit does not allow the fiat currency and all the options are margined in cryptocurrency. This is quite beneficial for professional crypto traders. For instance, consider a crypto hedge fund or a crypto market maker. These are businesses which conduct deals exclusively with crypto assets. As a result, it is quite natural for them to manage their trading books in cryptocurrency rather than fiat currency. Clearly, they are exposed to the cryptocurrency depreciation risk, but it is much easier to deal with it on the level of the book rather than trade by trade basis. This is one of the main rationales which justifies the development of Inverse European options.

The literature related to the crypto derivatives is quite new. However, the topic attracts more and more attention to researchers. In general, most of the research is empirical and centered around the analysis of hedging crypto options under various stochastic volatility models. For instance, see Matic et al. [43] and Alexander and Imeraj [2]. The second most popular flow of research is empirical pricing of crypto options, see Hou et al. [38] and Siu and Elliott [51], among others.

However, the existing literature lacks rigorous analytical results about the price and the behaviour of the level and the skew of the implied volatility in the case of Inverse European options under stochastic volatility pricing models. As a result, the goal of this chapter is to fill the gap in the existing literature and to analyze the option pricing problem when we allow the volatility of the model to be a stochastic process.

Specifically, we present analytical results for the asymptotic behaviour of the at-the-money level and the skew of the implied volatility for a general stochastic volatility pricing model. Additionally, we provide the decomposition of the value of an Inverse European option into two components. The first component represents the price of the option in the case of zero correlation between the underlying and the volatility while the second component corrects for the correlation. This analysis allows us to make conclusions not only about Inverse European options, but also about Quanto Inverse European options which are briefly discussed in Section 3.3. Our main tool for proving

these results is the Malliavin calculus, see Appendix .1 for an introduction to this topic. The results of this chapter are extensions of Alòs [3], Muguruza et al. [6] and Alòs, Nualart, Pravosud [10].

The chapter is organized as follows. In Section 3.2 we provide details about the mechanics of a perpetual swap and Inverse European options markets. Section 3.3 is devoted to the statement of the problem and main results. Intermediary steps that allow us to prove the key theorems are presented in Sections 3.4 and 3.5. Finally, in Section 3.6 we present the numerical study in the case of the SABR and rough Bergomi models.

3.2 The mechanics behind perpetual swaps and Inverse European options

In this section we introduce in detail the following two main instruments on Deribit exchange: perpetual swap and Inverse European option.

In this chapter, we use Bitcoin as a particular example of basis asset. In general, the underlying asset used for these two instruments is Deribit BTC Index, which is defined as

$$\begin{aligned} med_t &= \text{median}(BTC_t^1, \dots, BTC_t^n), \\ \widehat{BTC_t^i} &= \min(\max(0.995 \times med_t, BTC_t^i), 1.005 \times med_t), \\ IDX_t &= \sum_{i=1}^{n} \omega_i \times \widehat{BTC_t^i}, \end{aligned}$$

where BTC_t^i is the quote mid point of the Bitcoin price on the exchange i, ω_i is the corresponding weight of the exchange (provided by Deribit) and n is the number of exchanges used for the calculation of the index. The complete list of exchanges can be found on Deribit website. It is worth to note that the list is updated quite often and criteria for including or excluding certain exchanges from the calculation of the index are not clearly indicated.

We next define a perpetual swap contract. As was mentioned before, the key characteristic of this contract is the associated funding payments. These payments have been introduced to keep the perpetual contract price as close as possible to the price of the underlying which is Deribit BTC Index. If perpetual contract trades at a price greater than the index value then traders that have long positions need to make funding payments to the traders having short positions. This will make perpetual swap less attractive to the long position holders and more attractive to the short position holders, pushing perpetual swap price to trade in line with the price of the index. If perpetual swap trades at a price lower than the index, the short position holders will have to pay the long position holders.

Deribit perpetual contracts features a continuous measurement of the difference between the mark price of the contract and the Deribit BTC Index. The percentage difference between these prices is the basis for the 8 hourly funding rate that is applied to all outstanding perpetual contracts. Funding payments are calculated every millisecond. The mark price is calculated as follows

$$\begin{aligned} x_t &= IDX_t + 30 \text{ seconds EMA of}(fair_t - IDX_t), \\ mark_t &= \begin{cases} 1.005 \times IDX_t & \text{if} \quad x_t \geq 1.005 \times IDX_t \\ 0.995 \times IDX_t & \text{if} \quad x_t \leq 0.995 \times IDX_t \\ x_t, & \text{otherwise.} \end{cases} . \end{aligned}$$

where EMA stands for exponential moving average which is recalculated every second with the smoothing factor which equals to 0.0645, $fair_t$ is the quote mid point between the fair impact bid and the fair impact ask prices. The fair impact bid is the average price of a 1 Bitcoin market sale order or the best bid price - 0.1%, whichever has a greater value. By analogy, the fair impact ask is the average price of a 1 Bitcoin market buy order or the best ask price + 0.1%, whichever has a lower value.

Additionally, Deribit restricts allowed trading bandwidth of perpetual swap meaning that ask and bid quotes have to be within certain distance around the Deribit BTC Index. The exact rule can be found on the Deribit website.

The funding rate is calculated as follows

$$rate_t = \frac{(mark_t - IDX_t)}{IDX_t} \times 100,$$
$$funding_t = \max(0.05\%, rate_t) + \min(-0.05\%, rate_t).$$

Notice that the $|funding_t| \leq 0.45\%$. Finally, the funding payment over the time interval between the changes in $funding_t$ is calculated as $funding_t \times$ Position Size in Bitcoins $\times$ Position Holding Time. Deribit does not charge any fees on funding payments and all payments are transferred between the holders of the perpetual contracts. This makes the funding transactions a zero-sum game, where longs receive all funding payments from shorts or the other way around.

We finally introduce the Inverse European call options. This option gives the right to buy 1 Bitcoin at the strike price at maturity. The payoff at maturity is given by

$$\widehat{V}_T = \max\left(\frac{\widehat{IDX_T} - K}{\widehat{IDX_T}}, 0\right),$$

where $\widehat{IDX_T}$ is the average of the Deribit BTC index (IDX_t) over the last 30 minutes before expiry. The option features cash settlement meaning that at expiry the writer of the option will pay profit if any to the buyer. The profit is payed in the units of Bitcoin.

We observe that this payoff can to be considered as exotic. Additionally, the underlying of the option is IDX_t, which is realistically non-tradable asset. Hence, one should use perpetual swap to hedge this option. The mechanics behind Inverse European option on Deribit leaves very little hope that this option can be priced analytically in a closed form.

In the next section we introduce the formal notation to the pricing problem. Instead of considering $\widehat{V}_T$ we use a more tractable quantity which is an upper bound of $\widehat{V}_T$.

3.3 Statement of the problem and main results

Let $T > 0$ and consider the following model for asset prices S_t (without lost of generality, we take the interest rate equal to zero for the sake of simplicity) in a time interval $[0, T]$

$$\begin{aligned} dS_t &= \sigma_t S_t dW_t \\ W_t &= \rho W'_t + \sqrt{(1-\rho^2)} B_t, \end{aligned} \tag{3.1}$$

where $S_0 > 0$ is fixed and W_t, W'_t, and B_t are three standard Brownian motions on $[0, T]$ defined on the same risk-neutral complete probability space $(\Omega, \mathcal{G}, \mathbb{P})$. We assume that W'_t and B_t are independent and $\rho \in [-1, 1]$ is the correlation coefficient between W_t and W'_t. When the volatility σ_t is constant, this model is the regular Black-Scholes model.

We consider the following hypotheses on the volatility process.

Hypothesis 3.3.1. *The process $\sigma = (\sigma_t)_{t\in[0,T]}$ is square integrable, adapted to the filtration generated by W', a.s. positive and continuous, and satisfies that for all $t \in [0, T]$,*

$$c_1 \leq \sigma_t \leq c_2,$$

for some positive constants c_1 and c_2.

Hypothesis 3.3.2. *For all $p \geq 1$ there exists $c > 0$ and $\gamma > 0$ such that for all $0 \leq s \leq r \leq T \leq 1$,*

$$(\mathbb{E}|\sigma_r - \sigma_s|^p)^{1/p} \leq c(r-s)^\gamma.$$

Hypothesis 3.3.3. *For $p \geq 2$, $\sigma \in \mathbb{L}^{2,p}_{W'}$ (see the Appendix .1 for the definition of this space).*

Hypothesis 3.3.4. *There exists $H \in (0, 1)$ and for all $p \geq 1$ there exist constants $c_1, c_2 > 0$ such that for all $0 \leq t \leq s \leq r \leq u \leq T \leq 1$*

$$\{\mathbb{E}(|D^{W'}_r \sigma_u|^p)\}^{1/p} \leq c_1(u-r)^{H-\frac{1}{2}} \tag{3.2}$$

and

$$\{\mathbb{E}(|D^{W'}_s D^{W'}_r \sigma_u|^p)\}^{1/p} \leq c_2(u-r)^{H-\frac{1}{2}}(u-s)^{H-\frac{1}{2}}, \tag{3.3}$$

where D denotes the Malliavin derivative defined in the Appendix .1.

Let $(V_t^E)_{t\in[0,T]}$ and $(V_t^{QE})_{t\in[0,T]}$ denote the values of an Inverse European call and a Quanto Inverse European call options with fixed strike K, respectively.

We have that

$$V_0^E = \mathbb{E}\left(\frac{S_T - K}{S_T}\right)_+ = K \times \mathbb{E}(\hat{K} - \hat{S}_T)_+,$$

where $\hat{K} = \frac{1}{K}$ and $\hat{S}_T = \frac{1}{S_T}$. Similarly,

$$V_0^{QE} = \mathbb{E}\left(\frac{\hat{R} \times (S_T - K)}{S_T}\right)_+ = K \times \hat{R} \times \mathbb{E}(\hat{K} - \hat{S}_T)_+,$$

where $\hat{R}$ is a fixed exchange rate. One can easily see that the difference between V_0^E and V_0^{QE} is due to the currency in which the options are quoted. In our case V_0^E is the crypto price of the option and V_0^{QE} is the dollar value of the option.

We denote by $BS(t, x, k, \sigma)$ the Black-Scholes price of an Inverse European call option with time to maturity $T - t$, log-underlying price x, log-strike price k and volatility σ. That is,

$$\begin{aligned} BS(t, x, k, \sigma) &= N(d_2(k, \sigma)) - e^{\sigma^2(T-t)} e^{k-x} N(d_1(k, \sigma)), \\ d_2(k, \sigma) &= \frac{x - k}{\sigma\sqrt{T - t}} - \frac{\sigma}{2}\sqrt{T - t}, \\ d_1(k, \sigma) &= d_2(k, \sigma) - \sigma\sqrt{T - t}, \end{aligned}$$

where N is the cumulative distribution function of the standard normal random variable. One can easily see that the Black-Scholes price of a Quanto Inverse European call is equal to $BS^{QE}(t, x, k, \sigma) = \hat{R} \times BS(t, x, k, \sigma)$. The derivation of these results is given in Imeraj et al. [1].

One can easily show that the Black-Scholes price satisfies the following PDE

$$\partial_t BS(t, x, k, \sigma) - \frac{1}{2}\sigma^2 \partial_x BS(t, x, k, \sigma) + \frac{1}{2}\sigma^2 \partial_{xx}^2 BS(t, x, k, \sigma) = 0. \tag{3.4}$$

Moreover, one can also easily show that the classical relationship between the Gamma, the Vega and the Delta holds, that is,

$$\frac{\partial_\sigma BS(t, x, k, \sigma)}{\sigma(T - t)} = (\partial_{xx}^2 BS(t, x, k, \sigma) - \partial_x BS(t, x, k, \sigma)). \tag{3.5}$$

Furthermore, the log-forward price $X_t = \log(S_t)$ satisfies

$$dX_t = \sigma_t dW_t - \frac{1}{2}\sigma_t^2 dt. \tag{3.6}$$

Next, we observe that, as $BS(T, x, k, \sigma) = e^k \times (e^{-k} - e^{-x})_+$ for every $\sigma > 0$, the price of an Inverse call option $V_t = e^k \times \mathbb{E}_t(e^{-k} - e^{-x})_+$ can be written as

$$V_t^E = \mathbb{E}_t(BS(T, X_T, k, v_T)), \qquad v_t = \sqrt{\frac{1}{T - t}\int_t^T \sigma_s^2 ds}. \tag{3.7}$$

In particular, $V_T^E = BS(T, X_T, k, v_T)$ and $V_t^{QE} = \hat{R} \times V_t^E$. This implies that the implied volatility level and the skew of Inverse and Quanto Inverse European call options are the same. Hence, we will only state the main results of this chapter for the Inverse options.

We define the implied volatility (IV) of an Inverse European call option as the quantity $I^E(t, k)$ satisfying

$$V_t^E = BS(t, X_t, k, I^E(t, k),$$

We denote by $I^E(t, k_t^*)$, where $k_t^* = X_t$, the corresponding at-the-money implied volatility (ATMIV) which, in the case of zero interest rates, takes the form $BS^{-1}(t, X_t, X_t, V_t^E)$.

The aim of this chapter is to apply the Malliavin calculus techniques developed in Alòs [3] in order to obtain formulas for

$$\lim_{T\to 0} I^E(0,k^*) \quad \text{and} \quad \lim_{T\to 0} \partial_k I^E(0,k^*)$$

under the general stochastic volatility model (3.1), where we have set $k^* = k_0^*$ for the sake of simplicity.

The main result of this chapter is the following theorem.

Theorem 3.3.5. *Assume Hypotheses 3.3.1-3.3.4. Then,*

$$\lim_{T\to 0} I^E(0,k^*) = \sigma_0. \tag{3.8}$$

Moreover,

$$\lim_{T\to 0} T^{\max(\frac{1}{2}-H,0)} \partial_k I^E(0,k^*) = \lim_{T\to 0} T^{\max(\frac{1}{2}-H,0)} \frac{\rho}{\sigma_0 T^2} \int_0^T \left(\int_r^T \mathbb{E}(D_r^{W'} \sigma_u) du \right) dr. \tag{3.9}$$

We observe that when prices and volatilities are uncorrelated then the short-time skew equals to zero. Observe also that if the term $\mathbb{E}(D_r^{W'}\sigma_u)$ is of order $(u-r)^{H-\frac{1}{2}}$, the limit of the right hand side of (3.9) will be 0 if $H > 1/2$ and it will converge to a constant when $H = \frac{1}{2}$. When $H < \frac{1}{2}$ we need to multiply by $T^{\frac{1}{2}-H}$ in order to obtain a finite limit.

The results of Theorem 3.3.5 can be used in order to derive approximation formulas for the price of an Inverse and Quanto Inverse European call options. Notice that, as

$$V_0^E = BS(0, X_0, k, I^E(0,k)).$$

Then, using Taylor's formula we can use the approximations

$$I^E(0,k) \approx I^E(0,k^*) + \partial_k I^E(0,k^*)(k-k^*).$$

The great utility of this relation is that we can use it to approximate the price of the European Inverse call option for a wide range of stochastic and fractional volatility models.

3.4 Preliminary results

In this section we provide closed form decomposition formulas for the price and for the ATM implied volatility skew of an Inverse call option under the stochastic volatility model (3.1). The main result of this section is the following theorem.

Theorem 3.4.1. *Assume Hypotheses 3.3.1-3.3.4. Then, the following relation holds for all $t \in [0,T]$,*

$$V_t^E = \mathbb{E}_t\left(BS(t,X_t,k,v_t)\right) + \mathbb{E}_t\left(\int_t^T H(s,X_s,k,v_s)\sigma_s \left(\int_s^T D_s^W \sigma_r^2 dr \right) ds \right),$$

where $H(s,X_s,k,v_s) = \frac{1}{2}(\partial^3_{xxx} BS(s,X_s,k,v_s) - \partial^2_{xx} BS(s,X_s,k,v_s))$.

Proof. We follow similarly as in Alòs [3]. Since $V_T = BS(T,X_T,k,v_T)$ the law of one price leads us to the conclusion that $V_t = \mathbb{E}_t(BS(T,X_T,k,v_T))$. Applying Theorem .1.2 in the Appendix to the function $BS(T,X_T,k,v_T)$ we get that

$$\begin{aligned}
BS(T,X_T,k,v_T) = BS(t,X_t,k,v_t) &+ \int_t^T \partial_s BS(s,X_s,k,v_s) ds \\
&+ \int_t^T \partial_x BS(s,X_s,k,v_s)\left(-\frac{1}{2}\sigma_s^2 ds + \sigma_s dW_s \right) \\
&+ \int_t^T \partial_\sigma BS(s,X_s,k,v_s)\left(\frac{v_s^2}{2(T-s)v_s} - \frac{\sigma_s^2}{2(T-s)v_s} \right) ds \\
&+ \int_t^T \partial^2_{\sigma x} BS(s,X_s,k,v_s) \frac{\sigma_s}{2(T-s)v_s} \left(\int_s^T D_s^W \sigma_r^2 dr \right) ds \\
&+ \frac{1}{2}\int_t^T \partial^2_{xx} BS(s,X_s,k,v_s)\sigma_s^2 ds.
\end{aligned}$$

By adding and subtracting $\frac{1}{2}\int_t^T v_s^2(\partial_{xx}^2 BS(s,X_s,k,v_s) - \partial_x BS(s,X_s,k,v_s))ds$ to the expression above we get that

$$\begin{aligned}
BS(T,X_T,k,v_T) &= BS(t,X_t,k,v_t) \\
&+ \int_t^T \left(\partial_s BS(s,X_s,k,v_s) - \frac{1}{2}v_s^2\partial_x BS(s,X_s,k,v_s) + \frac{1}{2}v_s^2\partial_{xx}^2 BS(s,X_s,k,v_s)\right)ds \\
&+ \int_t^T \partial_x BS(s,X_s,k,v_s)\sigma_s dW_s - \int_t^T \partial_\sigma BS(s,X_s,k,v_s)\frac{\sigma_s^2 - v_s^2}{2(T-s)v_s}ds \\
&+ \int_t^T \partial_{\sigma x}^2 BS(s,X_s,k,v_s)\frac{\sigma_s}{2(T-s)v_s}\left(\int_s^T D_s^W \sigma_r^2 dr\right)ds \\
&+ \frac{1}{2}\int_t^T (\partial_{xx}^2 BS(s,X_s,k,v_s) - \partial_x BS(s,X_s,k,v_s))(\sigma_s^2 - v_s^2)ds.
\end{aligned}$$

Notice that the second term in the above expression is equal to zero due to formula (3.4). Finally, using equation (3.5) and taking conditional expectation we complete the proof. ■

We next derive an expression for the ATM implied volatility skew of an Inverse European call option under the stochastic volatility model (3.1).

Proposition 3.4.2. *Assume Hypotheses 3.3.1-3.3.4. Then,*

$$\lim_{T\to 0}\partial_k I^E(0,k^*) = \lim_{T\to 0}\frac{\mathbb{E}\left(\int_0^T(\partial_k H(s,X_s,k^*,v_s) - H(s,X_s,k^*,v_s))\Lambda_s ds\right)}{\partial_\sigma BS(0,X_0,k^*,I^E(0,k^*))}, \tag{3.10}$$

where $H(s,x,k,\sigma) = \frac{1}{2}\left(\partial_{xxx}^3 BS(s,X_s,k,v_s) - \partial_{xx}^2 BS(s,X_s,k,v_s)\right)$ *and* $\Lambda_s = \sigma_s\int_s^T D_s^W\sigma_r^2 dr$.

Proof. This proof follows similarly as Theorem 4.2 in Alòs, León and Vives [7]. Since $V_t^E = BS(t,X_t,k,I^E(t,k))$, the following equation holds

$$\partial_k V_t^E = \partial_k BS(t,X_t,k,I^E(t,k)) + \partial_\sigma BS(t,X_t,k,I^E(t,k))\partial_k I^E(t,k).$$

On the other hand, using Theorem 3.4.1, we get that

$$\partial_k V_t^E = \partial_k \mathbb{E}_t\left(BS(t,X_t,k,v_t)\right) + \mathbb{E}_t\left(\int_t^T \partial_k H(s,X_s,k,v_s)\Lambda_s ds\right).$$

Combining both equations, we obtain that that the volatility skew $\partial_k I^E(t,k)$ is equal to

$$\frac{\mathbb{E}_t\left(\int_t^T \partial_k H(s,X_s,k,v_s)\Lambda_s ds\right) + \mathbb{E}_t\left(\partial_k BS(t,X_t,k,v_t)\right) - \partial_k BS(t,X_t,k,I(t,k))}{\partial_\sigma BS(t,X_t,k,I(t,k))}.$$

Finally, using the fact that

$$\partial_k BS(t,x,k_t^*,\sigma) = BS(t,x,k_t^*,\sigma) - \frac{1}{2}\mathrm{Erfc}\left(\frac{\sqrt{T-t}\sigma}{2\sqrt{2}}\right),$$

where $\mathrm{Erfc}(z) = 1 - \frac{2}{\sqrt{\pi}}\int_0^z e^{-t^2}dt$, and Theorem 3.4.1 we conclude that

$$\begin{aligned}
&\mathbb{E}\left(\partial_k BS(0,X_0,k^*,v_0)\right) - \partial_k BS(0,X_0,k^*,I^E(0,k^*)) \\
&= \left(\mathbb{E}(BS(0,X_0,k^*,v_0)) - V_0\right) + \frac{1}{2}\left(\mathrm{Erfc}\left(\frac{\sqrt{T}I(0,k^*)}{2\sqrt{2}}\right) - \mathrm{Erfc}\left(\frac{\sqrt{T}v_0}{2\sqrt{2}}\right)\right) \\
&= -\mathbb{E}\left(\int_0^T H(s,X_s,k^*,v_s)\Lambda_s ds\right) + \frac{1}{2}\left(\mathrm{Erfc}\left(\frac{\sqrt{T}I^E(0,k^*)}{2\sqrt{2}}\right) - \mathrm{Erfc}\left(\frac{\sqrt{T}v_0}{2\sqrt{2}}\right)\right).
\end{aligned}$$

By (3.8) $\lim_{T\to 0} I^E(0,k) = \sigma_0$. Moreover, by continuity, we have that $\lim_{T\to 0} v_0 = \sigma_0$. This completes the desired proof. ■

In order to compute the limit of the skew slope of the ATMI, we need to identify leading order terms of the numerator in equation (3.10). This result is provided in Proposition 3.4.3.

Proposition 3.4.3. *Assume Hypotheses 3.3.1-3.3.4. Then, for all $t \leq T$,*

$$\begin{aligned}\mathbb{E}_t\left(\int_t^T G(s,X_s,k,v_s)\Lambda_s ds\right) &= \mathbb{E}_t\left(G(t,X_t,k,v_t)J_t\right)\\ &+ \mathbb{E}_t\left(\frac{1}{2}\int_t^T(\partial^3_{xxx}-\partial^2_{xx})G(s,X_s,k,v_s)J_s\Lambda_s ds\right)\\ &+ \mathbb{E}_t\left(\int_t^T \partial_x G(s,X_s,k,v_s)\sigma_s D^- J_s ds\right),\end{aligned} \tag{3.11}$$

where $G(t,X_t,k,v_t) = (\partial_k H(t,X_t,k,v_t) - H(t,X_t,k,v_t))$, $J_t = \int_t^T \Lambda_s ds$, and $D^- J_s = \int_s^T D_s^W \Lambda_r dr$.

Proof. The proof follows similarly as in Alòs, León and Vives [7]. Applying Theorem .1.2 to the function $(\partial_k H(t,X_t,k,v_t) - H(t,X_t,k,v_t))\int_t^T \Lambda_s ds$, we obtain that

$$\begin{aligned}\int_t^T G(s,X_s,k,v_s)\Lambda_s ds &= G(t,X_t,k,v_t)J_t\\ &+ \int_t^T\left(\partial_s G(s,X_s,k,v_s) + \frac{v_s^2}{2(T-s)v_s}\partial_v G(s,X_s,k,v_s)\right)J_s ds\\ &+ \int_t^T \partial_x G(s,X_s,k,v_s)J_s\left(-\frac{1}{2}\sigma_s^2 ds + \sigma_s dW_s\right)\\ &- \int_t^T \partial_v G(s,X_s,k,v_s)J_s\frac{\sigma_s^2}{2(T-s)v_s}ds + \int_t^T \partial^2_{vx}G(s,X_s,k,v_s)J_s\Lambda_s\frac{1}{2(T-s)v_s}ds\\ &+ \int_t^T \partial_x G(s,X_s,k,v_s)\sigma_s D^- J_s ds + \frac{1}{2}\int_t^T \sigma_s^2\partial^2_{xx}G(s,X_s,k,v_s)J_s ds.\end{aligned}$$

By adding and subtracting the term $\frac{1}{2}\int_t^T v_s^2(\partial^2_{xx}G(s,X_s,k,v_s) - \partial_x G(s,X_s,k,v_s))ds$ to the expression above we get that

$$\begin{aligned}\int_t^T G(s,X_s,k,v_s)\Lambda_s ds &= G(t,X_t,k,v_t)J_t\\ &+ \int_t^T(\partial_s G(s,X_s,k,v_s) + \frac{1}{2}v_s^2(\partial^2_{xx}G(s,X_s,k,v_s) - \partial_x G(s,X_s,k,v_s)))J_s ds\\ &+ \int_t^T \frac{1}{2}(\partial^2_{xx}G(s,X_s,k,v_s) - \partial_x G(s,X_s,k,v_s))(\sigma_s^2 - v_s^2)J_s ds\\ &- \int_t^T \partial_v G(s,X_s,k,v_s)\frac{\sigma_s^2 - v_s^2}{2(T-s)v_s}J_s ds + \int_t^T \partial_x G(s,X_s,k,v_s)J_s\sigma_s dW_s\\ &+ \int_t^T \partial^2_{vx}G(s,X_s,k,v_s)J_s\Lambda_s\frac{1}{2(T-s)v_s}ds + \int_t^T \partial_x G(s,X_s,k,v_s)\sigma_s D^- J_s ds.\end{aligned}$$

Next, equations (3.4) and (3.5) imply that

$$\begin{aligned}&\partial_s G(s,X_s,k,v_s) - \frac{1}{2}v_s^2\partial_x G(s,X_s,k,v_s) + \frac{1}{2}v_s^2\partial^2_{xx}G(s,X_s,k,v_s) = 0,\\ &\partial^2_{xx}G(s,X_s,k,v_s) - \partial_x G(s,X_s,k,v_s) = \frac{\partial_v G(s,X_s,k,v_s)}{v_s(T-s)}.\end{aligned}$$

Finally, taking conditional expectations and noticing that by Lemma 3.4.4 all conditional expectations are finite, we complete the desired proof. ■

We conclude this section with the following lemma. See Lemma 6.3.1 in [6] for the standard European call option case.

Lemma 3.4.4. *Assume Hypotheses 3.3.1-3.3.4. Then, there exist positive constants C and C' such that for all $T < 1$,*

$$|(\partial_x G(s, X_s, k, v_s)| \leq C \left(\int_s^T \sigma_u^2 du \right)^{-2},$$
$$\left|(\partial_{xxx}^3 - \partial_{xx}^2) G(s, X_s, k, v_s)\right| \leq C' \left(\int_s^T \sigma_u^2 du \right)^{-3}.$$

Proof. Straightforward differentiation give us that

$$|\partial_x G(s, x, k, v_s)| = \exp\left(-\frac{\left(2(k-x) + (T-s)v_s^2\right)^2}{8(T-s)v_s^2} \right) \times$$
$$\left| \frac{\left(8(k-x)^3 - 2(k-x+2)(T-s)^2 v_s^4 + 4(k-x-6)(k-x)(T-s)v_s^2 - (T-s)^3 v_s^6\right)}{16\sqrt{2\pi}(T-s)^{7/2} v_s^7} \right|.$$

Then, due to Hypothesis 3.3.1, we get that

$$\begin{aligned}
|\partial_x G(s, x, k, v_s)| &\leq \frac{1}{(T-s)^2 v_s^4} \exp\left(-c_0 \left(y + v_s\sqrt{T-s} \right)^2 \right) \times \\
&\quad \left(c_1 |y|^3 + c_2 |y|^2 + c_3 |y| + c_4 (T-s)^{3/2} v_s^3 \right) \\
&\leq \frac{1}{(T-s)^2 v_s^4} \exp\left(-c_0 \left(y + v_s\sqrt{T-s} \right)^2 \right) \times \\
&\quad \left(c_1' \left(\left| y + v_s\sqrt{T-s} \right|^3 + \left(v_s\sqrt{T-s} \right)^3 \right) + c_2' \left(\left| y + v_s\sqrt{T-s} \right|^2 + \left(v_s\sqrt{T-s} \right)^2 \right) \right. \\
&\left. + c_3' \left(\left| y + v_s\sqrt{T-s} \right| + v_s\sqrt{T-s} \right) + c_4' \right),
\end{aligned}$$

where $y = \frac{(k-x)}{\sqrt{(T-s)}v_s}$.

Finally, since for any $c \geq 0$ and $d > 0$ the function $x^c e^{-dx^2}$ is bounded and $T < 1$ we conclude that

$$|\partial_x G(s, x, k, v_s)| \leq C \left(\int_s^T \sigma_u^2 du \right)^{-2},$$

which proves the first inequality.

Similarly, we have that

$$\begin{aligned}
&\left|(\partial_{xxx}^3 - \partial_{xx}^2) G(s, x, k, v_s)\right| \leq \frac{1}{(T-s)^3 v_s^6} \exp\left(-c_0 \left(y + v_s\sqrt{T-s} \right)^2 \right) \times \\
&\left(c_1 |y|^5 + c_2 |y|^4 + c_3 |y|^3 + c_4 |y|^2 + c_5 |y| + c_6 (T-s)^{7/2} v_s^5 \right),
\end{aligned}$$

and the same argument as in the case of first inequality allows us to complete the proof. ■

3.5 Proof of Theorem 3.3.5

3.5.1 Proof of (3.8) in Theorem 3.3.5: ATM implied volatility level

This section is devoted to the proof of (3.8) in Theorem 3.3.5. The proof follows the ideas initially presented in Alòs and Shiraya [11].

3.5.1.1 The uncorrelated case

Notice that, if $\rho = 0$, Theorem 3.4.1 gives us that the option price can be written as $V_t^E = \mathbb{E}_t\left(BS(t, X_t, k_t^*, v_t)\right)$. Then the implied volatility satisfies the following

$$\begin{aligned} I_E^0(0,k^*) = BS^{-1}(k^*, V_0^E) = \mathbb{E}\left(BS^{-1}(k^*, \mathbb{E}BS(0, X_0, k^*, v_0))\right) = \\ = \mathbb{E}\left(BS^{-1}(k^*, \Phi_0) - BS^{-1}(k^*, \Phi_T)\right) + \mathbb{E}\left(v_0\right), \end{aligned}$$

where $\Phi_r := \mathbb{E}_r\left(BS\left(0, X_0, k^*, v_0\right)\right)$.

Thus, $\Phi_r = \mathbb{E}\left(BS\left(0, X_0, k^*, v_0\right)|\mathcal{F}_r^{W'}\right)$ and $(\Phi_r)_{r\geq 0}$ is a martingale with respect to the filtration $(\mathcal{F}_r^{W'})_{r\geq 0}$. By the martingale representation theorem, there exists a square integrable and $\mathcal{F}^{W'}$-adapted process $(U_r)_{r\geq 0}$ such that

$$\Phi_r = \Phi_0 + \int_0^r U_s dW_s'.$$

Clark-Ocone-Haussman (Theorem .1.1) formula gives us the following representation,

$$\begin{aligned} U_r = \mathbb{E}\left(D_r^{W'} BS(0, X_0, k^*, v_0)|\mathcal{F}_r^{W'}\right) = \mathbb{E}\left(\frac{\partial BS}{\partial \sigma}(0, X_0, k^*, v_0)) D_r^{W'} v_0 | \mathcal{F}_r^{W'}\right) = \\ = \mathbb{E}\left(\frac{\partial BS}{\partial \sigma}(0, X_0, k^*, v_0) \frac{\int_r^T D_r^{W'} \sigma_s^2 ds}{2v_0} | \mathcal{F}_r^{W'}\right). \end{aligned}$$

Then, a direct application of the classical Itôs formula gives us

$$\begin{aligned} \mathbb{E}\left(BS^{-1}(k^*, \Phi_0) - BS^{-1}(k^*, \Phi_T)\right) = -\mathbb{E}\left(\int_0^T (BS^{-1})'(k^*, \Phi_r) U_r dW_r'\right) + \\ + \mathbb{E}\left(\frac{1}{2}\int_0^T (BS^{-1})''(k^*, \Phi_r) U_r^2 dr\right) \\ = \mathbb{E}\left(\frac{1}{2}\int_0^T (BS^{-1})''(k^*, \Phi_r) U_r^2 dr\right), \end{aligned}$$

where $(BS^{-1})'$ and $(BS^{-1})''$ denote, respectively, the first and second derivatives of BS^{-1} with respect to Φ_r.

Straightforward differentiation gives us the following expression

$$\partial_\sigma BS(0, X_0, k^*, \sigma) = -\sigma T e^{\sigma^2 T} \mathrm{Erfc}\left(\frac{3\sigma\sqrt{T}}{2\sqrt{2}}\right) + \frac{e^{-\frac{1}{8}\sigma^2 T}\sqrt{T}}{\sqrt{2\pi}}.$$

Notice that

$$\begin{aligned} (BS^{-1})'(k^*, \Phi_r) = \frac{1}{\partial_\sigma BS(0, X_0, k^*, BS^{-1}(k^*, \Phi_r)))}, \\ (BS^{-1})''(k^*, \Phi_r) = -\frac{\partial^2_{\sigma\sigma} BS(0, X_0, k^*, BS^{-1}(k^*, \Phi_r)))}{\left(\partial_\sigma BS(0, X_0, k^*, BS^{-1}(k^*, \Phi_r)))\right)^3}. \end{aligned} \tag{3.12}$$

By Lemma .4.2 (see the Appendix .4), $\left|(BS^{-1})''(k^*, \Phi_r)\right| \leq CT^{-\frac{1}{2}}$.

Hence, for $T < 1$ due to Hypothesis 3.3.1 we conclude that $|\partial_\sigma BS(0, X_0, k^*, v_0)| \leq C\sqrt{T}$.

Finally, using Hypotheses 3.3.1 and 3.3.4 and Hölder's and Jensen inequalities we get

$$\begin{aligned}
\mathbb{E}\left|\frac{1}{2}\int_0^T (BS^{-1})''(k^*,\Phi_r)U_r^2 dr\right| &\leq CT^{-\frac{1}{2}}\int_0^T \mathbb{E}U_r^2 dr \\
&\leq CT^{\frac{1}{2}}\int_0^T \mathbb{E}\left(\mathbb{E}\left(\int_r^T \left|D_r^{W'}\sigma_s^2\right| ds\mathcal{F}_r^{W'}\right)\right)^2 dr \\
&\leq CT^{\frac{1}{2}}\int_0^T\int_r^T (T-r)\,\mathbb{E}\left(\mathbb{E}\left(\left|D_r^{W'}\sigma_s^2\right|\mathcal{F}_r^{W'}\right)\right)^2 dsdr \\
&\leq CT^{\frac{3}{2}}\int_0^T\int_r^T \mathbb{E}\left(D_r^{W'}\sigma_s^2\right)^2 dsdr \\
&\leq CT^{\frac{3}{2}}\int_0^T\int_r^T (s-r)^{2H-1} dsdr
\end{aligned} \tag{3.13}$$

Hence, we conclude that $\lim_{T\to 0}\mathbb{E}\left(\frac{1}{2}\int_0^T (BS^{-1})''(k^*,\Phi_r)U_r^2 dr\right) = 0$. Which under Hypothesis 3.3.1 and Dominated Convergence theorem lead to

$$\lim_{T\to 0} I_E^0(0,k^*) = \lim_{T\to 0}\mathbb{E}(v_0) = \sigma_0.$$

3.5.1.2 The correlated case

Using the similar idea as in the uncorrelated case we get the following

$$\begin{aligned}
I^E(0,k^*) = BS^{-1}(k^*,V_0^E) &= \mathbb{E}\left(BS^{-1}(k^*,\Gamma_T) + BS^{-1}(k^*,\Gamma_0) - BS^{-1}(k^*,\Gamma_0)\right) = \\
&= \mathbb{E}\left(BS^{-1}(k^*,\Gamma_T) - BS^{-1}(k^*,\Gamma_0)\right) + I_E^0(0,k^*) = \\
&= \mathbb{E}\left(BS^{-1}(k^*,\Gamma_T) - BS^{-1}(k^*,\Gamma_0)\right) + I_E^0(0,k^*),
\end{aligned}$$

where $\Gamma_s := \mathbb{E}\left(BS(0,X_0,k^*,v_0)\right) + \frac{\rho}{2}\mathbb{E}\left(\int_0^s H(r,X_r,k^*,v_r)\Lambda_r dr\right)$.

Then, a direct application of the Itôs formula gives us

$$\begin{aligned}
I^E(0,k^*) = I_E^0(0,k^*) + \mathbb{E}\left(\int_0^T (BS^{-1})'(k^*,\Gamma_s)H(s,X_s,k^*,v_s)\Lambda_s ds\right) \leq \\
\leq I_E^0(0,k^*) + \int_0^T O((T-s)^{H-\frac{1}{2}})ds.
\end{aligned}$$

The last line follows from the following observations. Using Hypothesis 3.3.1 and Appendix .4, we conclude that $|H(s,X_s,k^*,v_s)| \leq C(T-s)^{-\frac{3}{2}}$. Additionally, from Appendix .4 one can see that $\left|(BS^{-1})'(k^*,\Gamma_s)\right| \leq CT^{-\frac{1}{2}}$. Finally, due to Hypothesis 3.3.4 we conclude that $\mathbb{E}\left(|\Lambda_s|\right) \leq C(T-s)^{\frac{3}{2}+H}$.

As a result, we get $\lim_{T\to 0}\mathbb{E}\left(\int_0^T (BS^{-1})'(k^*,\Gamma_s)H(s,X_s,k^*,v_s)\Lambda_s ds\right) = 0$. Then, the result in the previous section gives us that

$$I^E(0,k^*) \to \sigma_0$$

as $T \to 0$, as we wanted to prove.

We summarise the presented steps in the following corollary.

Corollary 3.5.1. *Under Hypotheses 3.3.1-3.3.4 the following holds*

$$I^E(0,k^*) = I_E^0(0,k^*) + \mathbb{E}\left(2\rho\int_0^T (B_E^{-1})'(k^*,\Gamma_s)H(s,M_s,k^*,v_s)\left(\sigma_s\int_s^T \sigma_r D_s^{W'}\sigma_r dr\right)ds\right).$$

3.5.2 Proof of (3.9) in Theorem 3.3.5: ATM implied volatility skew

Appealing to Propositions 3.4.2 and 3.4.3 we have that

$$\begin{aligned}\mathbb{E}\left(\int_0^T G(s,X_s,k,v_s)\Lambda_s ds\right) &= \mathbb{E}\left(G(0,X_0,k,v_0)J_0\right)\\ &+\mathbb{E}\left(\frac{1}{2}\int_0^T(\partial^3_{xxx}-\partial^2_{xx})G(s,X_s,k,v_s)J_s\Lambda_s ds\right)\\ &+\mathbb{E}\left(\int_0^T \partial_x G(s,X_s,k,v_s)\sigma_s D^- J_s ds\right).\end{aligned} \tag{3.14}$$

We proceed in a series of steps and start by bounding the second term in (3.14).

Step 1. Using Hypotheses 3.3.1 and 3.3.4 with Hölder's inequality we get the following

$$\begin{aligned}\mathbb{E}(|J_s\Lambda_s|) &\le C\mathbb{E}\left(\left(\int_s^T\left|D_s^{W'}\sigma_r\right|dr\right)\left(\int_s^T\int_u^T\left|D_u^{W'}\sigma_r\right|drdu\right)\right)\\ &\le C\sqrt{\mathbb{E}\left(\int_s^T|D_s^{W'}\sigma_r|\,dr\right)^2\mathbb{E}\left(\int_s^T\int_u^T|D_u^{W'}\sigma_r|\,drdu\right)^2}\\ &\le C\sqrt{\mathbb{E}\left(\sqrt{(T-s)\int_s^T(D_s^{W'}\sigma_r)^2dr}\right)^2\mathbb{E}\left(\sqrt{(T-s)\int_s^T\left(\int_u^T|D_u^{W'}\sigma_r|\,dr\right)^2du}\right)^2}\\ &\le C\sqrt{\left((T-s)\int_s^T\mathbb{E}(D_s^{W'}\sigma_r)^2dr\right)\left((T-s)\int_s^T\mathbb{E}\left(\int_u^T|D_u^{W'}\sigma_r|\,dr\right)^2du\right)}\\ &\le C\sqrt{(T-s)^{2H+1}\left((T-s)\int_s^T(T-u)^{2H+1}du\right)}\\ &= C\sqrt{(T-s)^{4H+4}} = C(T-s)^{2H+2}.\end{aligned} \tag{3.15}$$

Next, by Lemma 3.4.4 we know that

$$\begin{aligned}\mathbb{E}\left(\left|(\partial^3_{xxx}-\partial^2_{xx})G(s,X_s,k,v_s)\right|\right) &\le C\left(\int_s^T\sigma_u^2du\right)^{-3},\\ \mathbb{E}\left(|(\partial_x G(s,X_s,k,v_s)|\right) &\le C\left(\int_s^T\sigma_u^2du\right)^{-2}.\end{aligned} \tag{3.16}$$

Finally, using Hypothesis 3.3.1, equations (3.15) and (3.16) we conclude that

$$\begin{aligned}\mathbb{E}\left(\frac{1}{2}\int_0^T\left|(\partial^3_{xxx}-\partial^2_{xx})G(s,X_s,k,v_s)J_s\Lambda_s\right|ds\right) &\le C\int_0^T(T-s)^{2H-1}ds\\ &= O(T^{2H}).\end{aligned} \tag{3.17}$$

Step 2. Calculating the Malliavin derivative of $D_s^W\Lambda_r$ we get the following

$$\begin{aligned}\int_s^T D_s^W\Lambda_r dr &= \int_s^T D_s^W\left(\sigma_r\int_r^T D_r^W\sigma_u^2du\right)dr\\ &= \int_s^T\left(\left(D_s^W\sigma_r\right)\int_r^T D_r^W\sigma_u^2du+\sigma_r\int_r^T D_s^W D_r^W\sigma_u^2du\right)dr,\end{aligned} \tag{3.18}$$

where

$$D_s^W D_r^W \sigma_u^2 = 2(D_s^W \sigma_u D_r^W \sigma_u + \sigma_u D_s^W D_r^W \sigma_u).$$

Using Hypothesis 3.3.1 we get the following

$$\left|D_s^W D_r^W \sigma_u^2\right| \leq C \left|D_s^{W'} \sigma_u D_r^{W'} \sigma_u + D_s^{W'} D_r^{W'} \sigma_u\right|$$

Next, using Hypothesis 3.3.4, Hölder's inequality and equation (3.15) we conclude that

$$\begin{aligned}
\mathbb{E}\left(\sigma_r \int_r^T \left|D_s^W D_r^W \sigma_u^2\right| du\right) &\leq C \int_r^T \left((u-r)^{H-\frac{1}{2}}(u-s)^{H-\frac{1}{2}}\right) du \\
&\leq C(T-s)^{2H+1}, \\
\mathbb{E}\left(\left|D_s^W \sigma_r \int_r^T D_r^W \sigma_u^2 du\right|\right) &\leq C\mathbb{E}\left(\left|D_s^{W'} \sigma_r \int_r^T D_r^{W'} \sigma_u^2 du\right|\right) \\
&\leq C\sqrt{\mathbb{E}(D_s^{W'}\sigma_r)^2 \mathbb{E}\left(\int_r^T \left|D_r^{W'}\sigma_u^2\right| du\right)^2} \\
&\leq C(r-s)^{H-\frac{1}{2}}(T-r)^{H+\frac{1}{2}}.
\end{aligned} \tag{3.19}$$

Substituting the result from the equation (3.19) into the equation (3.18) we conclude that

$$\begin{aligned}
\mathbb{E}\left(\int_s^T \left|D_s^W \Lambda_r\right| dr\right) &\leq C \int_s^T \left((r-s)^{H-\frac{1}{2}}(T-s)^{H+\frac{1}{2}} + (T-s)^{2H+1}\right) dr \\
&\leq C\left((T-s)^{2H+1} + (T-s)^{2H+2}\right) = O\left((T-s)^{2H+1}\right).
\end{aligned} \tag{3.20}$$

Finally, Hypothesis 3.3.1, equations (3.16) and (3.20) allow us to conclude that

$$\begin{aligned}
\mathbb{E}\left(\int_0^T \left|\partial_x G(s, X_s, k, v_s)\sigma_s D^- J_s\right| ds\right) &\leq C \int_0^T (T-s)^{2H-1} ds \\
&= O(T^{2H}).
\end{aligned} \tag{3.21}$$

Step 3. Direct differentiation gives us the following expressions

$$\begin{aligned}
\partial_\sigma BS(0, X_0, k^*, \sigma) &= -\sigma T e^{\sigma^2 T} \mathrm{Erfc}\left(\frac{3\sigma\sqrt{T}}{2\sqrt{2}}\right) + \frac{e^{-\frac{1}{8}\sigma^2 T}\sqrt{T}}{\sqrt{2\pi}}, \\
G(0, X_0, k^*, v_0) &= \frac{e^{-\frac{1}{8}Tv_0^2}\left(Tv_0^2 + 4\right)}{8\sqrt{2\pi}T^{3/2}v_0^3}.
\end{aligned} \tag{3.22}$$

Combining Propositions 3.4.2 and 3.4.3, equations (3.17) and (3.21) we get the following

$$\lim_{T\to 0} T^{\frac{1}{2}-H}\partial_k I^E(0, k^*) = \lim_{T\to 0} \frac{\sqrt{2\pi}T^{\frac{1}{2}-H}}{\sqrt{T}} \mathbb{E}\left(G(0, X_0, k^*, v_0) J_0\right). \tag{3.23}$$

Notice that

$$\mathbb{E}J_0 = \mathbb{E}\int_0^T 2\rho \left((\sigma_0 + (\sigma_s - \sigma_0)) \int_s^T (\sigma_0 + (\sigma_r - \sigma_0)) D_s^{W'} \sigma_r dr\right) ds.$$

Hence, using Hypothesis 3.3.1 and Hölder's inequality we get the following

$$\left|\mathbb{E}J_0 - 2\rho\sigma_0^2 \int_0^T \int_s^T \mathbb{E}\left(D_s^{W'}\sigma_r\right) dr ds\right| = O\left(T^{\frac{3}{2}+H+\gamma}\right). \tag{3.24}$$

Finally, under Hypothesis 3.3.1 and equation (3.24) apply Lebesgue dominated convergence theorem to equation (3.23) and conclude that

$$\lim_{T\to 0} T^{\frac{1}{2}-H}\partial_k I^E(0, k^*) = \lim_{T\to 0} \frac{\rho T^{\frac{1}{2}-H}}{\sigma_0 T^2} \int_0^T \left(\int_r^T \mathbb{E}\left(D_r^{W'}\sigma_u\right) du\right) dr. \tag{3.25}$$

One can see that the limit in equation (3.25) under Hypotheses 3.3.1 - 3.3.4 is well defined.

3.6 Numerical analysis

In this section we justify Theorem 3.3.5 with numerical simulations. Notice that the SABR and rough Bergomi models do not satisfy Hypothesis 3.3.1. However, truncation argument justifies the application of Theorem 3.3.5 in these cases. In simple words, truncation argument allows us to pretend that the the volatility process satisfies Hypothesis 3.3.1 and apply the results of Theorem 3.3.5 in a straightforward way. The step by step application of truncation argument is presented in Section 2.5 and we safely omit it in this section.

3.6.1 The SABR model

We consider the SABR stochastic volatility model with skewness parameter equal to 1, which is the most common case from a practical point of view. This corresponds to equation (3.1), where S_t denotes the forward price of the underlying asset and

$$d\sigma_t = \alpha\sigma_t dW'_t, \qquad \sigma_t = \sigma_0 e^{\alpha W'_t - \frac{\alpha^2}{2}t}.$$

where $\alpha > 0$ is the volatility of volatility.

For $r \leq t$, we have that $D_r^{W'}\sigma_t = \alpha\sigma_t$ and $\mathbb{E}\left(D_r^{W'}\sigma_t\right) = \alpha\sigma_0$. Therefore, applying Theorem 3.3.5 we conclude that

$$\lim_{T\to 0} \partial_k I^E(0,k^*) = \frac{1}{2}\rho\alpha.$$

We next proceed with some numerical simulations using the following parameters

$$S_0 = 100,\ T = 0.001,\ dt = \frac{T}{50},\ \alpha = 0.3,\ \sigma_0 = (0.1, 0.2, \ldots, 1.4).$$

In order to get estimate of the price of the Inverse European call option we use antithetic variates. The estimate of the price is calculated as follows

$$\hat{V}_{sabr} = \frac{\frac{1}{N}\sum_{i=1}^N V_T^i + \frac{1}{N}\sum_{i=1}^N V_T^{i,A}}{2}, \tag{3.26}$$

where $N = 2000000$ and the sub-index A denotes the value of a call option computed on the antithetic trajectory of a Monte Carlo path.

In order to retrieve the implied volatility we use Brent's method. For the estimation of the skew, we use the following expression which allows us to avoid a finite difference approximation of the first order derivative.

$$\partial_k \hat{I}(0,k^*) = \frac{-\partial_k BS(0,X_0,k^*,I(0,k^*)) - \mathbb{E}\left(e^{k^*-X_T}1_{X_T\geq k^*}\right)}{\partial_\sigma BS(0,X_0,k^*,I(0,k^*))}. \tag{3.27}$$

In Figures 3.1 and 3.2 we present the results of a Monte Carlo simulation which aims to estimate numerically the skew and the level of the at-the-money implied volatility of the Inverse European call option under the SABR model. We conclude that numerical results fit the theoretical ones.

3.6.2 The fractional Bergomi model

The rough Bergomi stochastic volatility model asssumes equation (3.1) with

$$\sigma_t^2 = \sigma_0^2 e^{v\sqrt{2H}Z_t - \frac{1}{2}v^2 t^{2H}},$$
$$Z_t = \int_0^t (t-s)^{H-\frac{1}{2}} dW'_s,$$

where $H \in (0,1)$ and $v > 0$.

Moreover, for $r \leq u$, we have

$$D_r^{W'}\sigma_u = \frac{1}{2}\sigma_u v\sqrt{2H}(u-r)^{H-\frac{1}{2}},$$
$$\mathbb{E}(D_r^{W'}\sigma_u) = e^{-\frac{1}{8}v^2u^{2H}}\frac{1}{2}\sigma_0 v\sqrt{2H}(u-r)^{H-\frac{1}{2}},$$

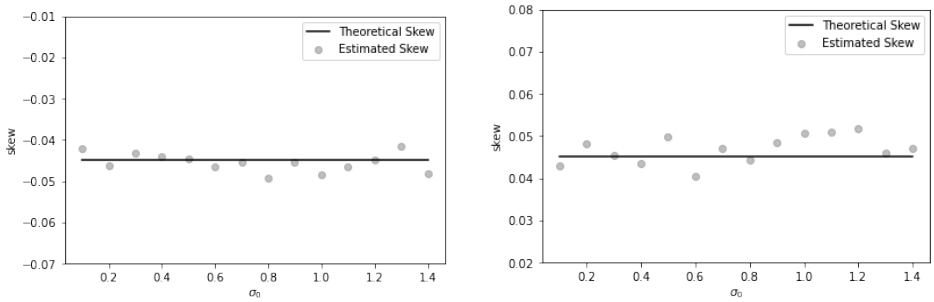

(a) ρ=-0.3 (b) ρ=0.3

Figure 3.1: At-the-money skew of the IV under the SABR model.

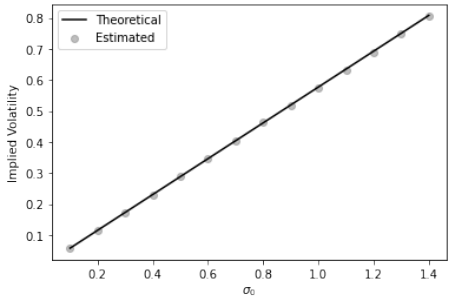

Figure 3.2: At-the-money level of the IV under the SABR model.

which gives

$$\lim_{T\to 0} \partial_k I^E(0,k^*) = \begin{cases} 0 & \text{if} \quad H > \frac{1}{2} \\ \frac{\rho v}{4} & \text{if} \quad H = \frac{1}{2}. \end{cases} \tag{3.28}$$

and for $H < \frac{1}{2}$

$$\lim_{T\to 0} T^{\frac{1}{2}-H} \partial_k I^E(0,k^*) = \frac{2\rho v\sqrt{2H}}{(3+4H(2+H))}. \tag{3.29}$$

The parameters used for the Monte Carlo simulation are the following

$$S_0 = 100,\ T = 0.001,\ dt = \frac{T}{50},\ H = (0.4, 0.7),\ v = 0.5,\ \rho = -0.3,\ \sigma_0 = (0.1, 0.2, \ldots, 1.4).$$

In order to get estimate of the price of the Inverse European call option under the rough Bergomi model we use antithetic variates presented in equations (3.26). We use equation (3.27) for the estimation of the skew.

In Figure 3.3 we present the ATM implied volatility skew as a function of maturity of the Inverse European call option for two different values of H, where we observe the blow up to $-\infty$ for the case $H = 0.4$.

Due to the blow up of the at-the-money implied volatility skew of the Inverse European call option when $H < \frac{1}{2}$ we also plot the quantities $T^{\frac{1}{2}-H}\partial_k \hat{I}(0,k^*)$ for $H = 0.4$ and $\partial_k \hat{I}(0,k^*)$ for $H = 0.7$ on Figure 3.4. And in Figure 3.5 we present the estimates of ATM IV level. In general, we conclude that theoretical results are in line with values provided by Theorem 3.3.5.

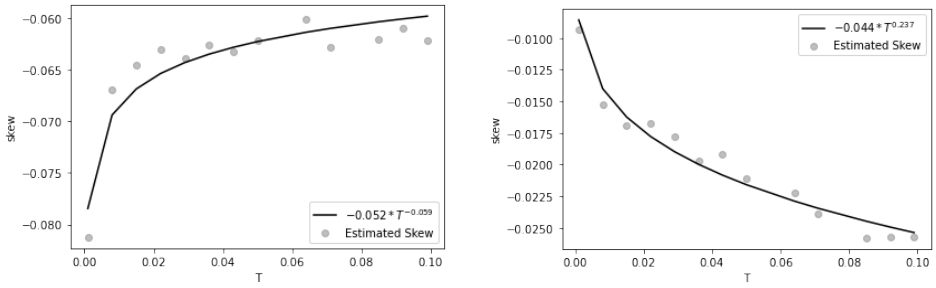

(a) H=0.4, $\sigma_0 = 0.3$ (b) H=0.7, $\sigma_0 = 0.3$

Figure 3.3: At-the-money IV skew as a function of T under rough Bergomi model

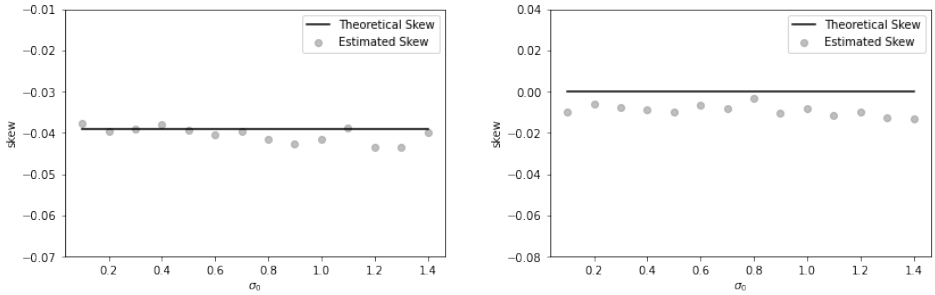

(a) H=0.4 (b) H=0.7

Figure 3.4: At-the-money IV skew as a function of σ_0 under rough Bergomi model

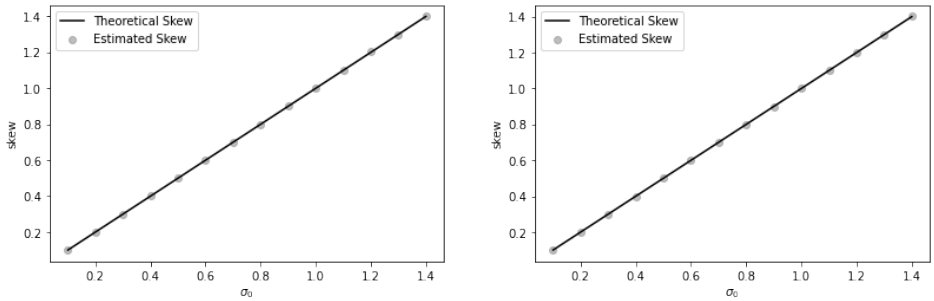

(a) H=0.4 (b) H=0.7

Figure 3.5: At-the-money IV level as a function of σ_0 under rough Bergomi model.

Chapter 4

On the skew and curvature of the implied and local volatilities

4.1 Introduction

Local volatilities are the main tool in real market practice, see Dupire [21], since they are the simplest models that capture the empirical implied volatility surface. They are an example of mimicking process, see Gyöngy [34], in the sense that they are one-dimensional models that can reproduce the marginal distributions of asset prices S_t. In the local volatility model the volatility process is a deterministic function $\sigma(t, S_t)$ of time and the underlying asset price. The values of this function can be computed via Dupire's formula, see Dupire [21].The plot of this function σ, is called the local volatility surface.

One challenging problem in this context is the study of the relationship between the implied and local volatilities. Even when both surfaces are similar, we can easily notice that short-end local volatility smiles are more pronounced than implied volatility smiles. In fact, some empirical studies, see Derman, Kani, and Zou [20], state that for short and intermediate maturities the ATM implied volatility skew is approximately half of the skew of the local volatility (a property that is known as the *one over two* rule).

There have been many attempts to address this phenomena from the analytical point of view. Classical proofs of this property for stochastic volatility models can be found in the literature. For example, in Derman, Kani, and Zou [20] or in Gatheral [31], this property is deduced from the expression of the implied volatilities as averaged local volatilities. In Lee [41], the expansion of the implied and local volatilities allow to prove this property by a direct comparison. In Alòs and García-Lorite [5], Malliavin calculus techniques give a representation of the short-limit at-the-money (ATM) implied volatility skew as averaged local volatility skew, from where the one over two rule follows directly.

Nevertheless, recent studies, see Bourgey, De Marco, Friz, and Pigato [17], state that the one over two rule is not true for rough volatility models, where the volatility process is driven by a fractional Brownian motion with Hurst parameter $H < \frac{1}{2}$. More precisely, the ATM short-end implied volatility skew is $\frac{1}{H+\frac{3}{2}}$ the ATM short-end local volatility skew, a result that is obtained via large deviations techniques.

In this chapter, we see how Malliavin calculus leads to an easy proof of this $\frac{1}{H+\frac{3}{2}}$ rule. On the other hand, we study the relationship between the curvature of implied and local volatilities. In particular, we show how the ATM short-end implied volatility curvature can be written in terms of the ATM short-limit skew and curvature of the local volatility, and vice versa. Moreover, we explain why $\frac{1}{H+\frac{3}{2}}$ rule is not incompatible with real market data, where the short-end local volatility is usually computed via a regularization procedure.

This chapter is organized as follows. In Section 4.2 we introduce the notation of the problem. Section 4.3 is devoted to the study of the at-the-money skew for the local volatility model. In Section 4.4 we analyze the relationship between the curvatures of the implied and local volatilities. Finally, we present some numerical examples in Section 4.5.

4.2 Malliavin calculus for local volatilities

In this section we recall the key tools of Malliavin calculus in application to the local volatility function. We refer to Alòs and García-Lorite [5] for a deeper introduction to this topic and its applications to finance.

Consider the local volatility model of the form

$$S_t = S_0 + \int_0^t \sigma(u, S_u) S_u dW_u, \tag{4.1}$$

where W_t is a Brownian motion on $[0,T]$ defined on the risk-neutral complete probability space $(\Omega, \mathcal{F}, \mathbb{P})$. We assume that interest rate $r = 0$ for the sake of simplicity. In order to study the Malliavin differentiability of the asset price S_t, let us consider the following hypotheses.

Hypothesis 4.2.1. *σ is continuous and there exist two constants $c_1, c_2 > 0$ such that, for all $(t,x) \in [0,T] \times \mathbb{R}$,*

$$c_1 < \sigma(t,x) < c_2.$$

Hypothesis 4.2.2. *There exist two constants $C > 0$ and $\gamma \in (0, \frac{1}{2})$ such that, for all $t \in [0,T]$, $\sigma(t,\cdot)$ is differentiable and*

$$S_t \partial_x \sigma(t, S_t) \leq C t^{-\gamma}.$$

Remark 4.2.3. *Notice that Hypothesis 4.2.2 is equivalent to*

$$\partial_x \hat{\sigma}(t, X_t) \leq C t^{-\gamma},$$

where $\hat{\sigma}$ denotes the local volatility in terms of the log-price of the underlying that is $\hat{\sigma}(t,x) = \sigma(t, e^x)$.

According to (45), the Malliavin derivative of the random variable S_t for $r \leq t$ is given by

$$D_r^W S_t = \sigma(r, S_r) S_r + \int_r^t a(u, S_u) D_r^W S_u dW_u,$$

where $a(u, S_u) = \partial_x \sigma(u, S_u) S_u + \sigma(u, S_u)$. Notice that, as σ is bounded and Hypothesis 4.2.1 holds, for all $p \geq 2$, Burkhölder and Holder inequalities give us that

$$\begin{aligned} \mathbb{E}(D_r^W S_t)^p &\leq c_p \left(\mathbb{E}(\sigma(r,S_r)S_r)^p + \left(\int_r^t u^{-2\gamma} \mathbb{E}(D_r^W S_u)^2 du \right)^{\frac{p}{2}} \right) \\ &\leq c_p \left(\mathbb{E}(\sigma(r,S_r)S_r)^p + \left(\int_r^t u^{-\frac{2\gamma p}{(p-2)}} du \right)^{\frac{p-2}{2}} \left(\int_r^t \mathbb{E}(D_r^W S_u)^p du \right) \right), \end{aligned} \tag{4.2}$$

for some positive constant c_p. This implies, by Gronwall's lemma, that, for all $t < T$, $\mathbb{E}(D_r^W S_t)^p \leq c_p \mathbb{E}(\sigma(r,S_r)S_r)^p$, which implies that $\mathbb{E}(D_r^W S_t)^p \leq c_p'$, for some positive constant c_p'. Moreover, a direct application of Itô's lemma gives us that

$$D_r^W S_t = \sigma(r, S_r) S_r \exp\left(-\frac{1}{2} \int_r^t a^2(u, S_u) du + \int_r^t a(u, S_u) dW_u \right). \tag{4.3}$$

In order to study the second Malliavin derivative of S, let us consider the following hypothesis:

Hypothesis 4.2.4. *There exist two constants $C > 0$ and $\gamma \in (0, \frac{1}{4})$ such that, for all $t \in [0,T]$, $\sigma(t,\cdot)$ is twice differentiable and*

$$S_t^2 \partial_{xx}^2 \sigma(t, S_t) \leq C t^{-2\gamma}.$$

Then, under hypotheses 4.2.1, 4.2.2, and 4.2.4, for $\theta < r$ the second Malliavin derivative of the random variable S_t is given by

$$\begin{aligned} D_\theta^W D_r^W S_t = a(r, S_r) D_\theta^W S_r &+ \int_r^t \partial_x a(u, S_u) D_r^W S_u D_\theta^W S_u dW_u \\ &+ \int_r^t a(u, S_u) D_\theta^W D_r^W S_u dW_u. \end{aligned} \tag{4.4}$$

Notice that, as Hypotheses 4.2.1, 4.2.2, and 4.2.4 hold, the stochastic integrals are well defined. Then, similar arguments as for the first Malliavin derivative give us that $\mathbb{E}(D_\theta^W D_r^W S_t)^p \leq c_p$ for

some positive constant c_p. Moreover,

$$\begin{aligned} D_\theta^W D_r^W S_t &= a(r,S_r) D_\theta^W S_r \exp\left(-\frac{1}{2}\int_r^t a^2(u,S_u)du + \int_r^t a(u,S_u)dW_u\right) \\ &\quad + \sigma(r,S_r) S_r \exp\left(-\frac{1}{2}\int_r^t a^2(u,S_u)du + \int_r^t a(u,S_u)dW_u\right) \\ &\quad \times \left(-\frac{1}{2}\int_r^t D_\theta^W(a^2(u,S_u))du + \int_r^t D_\theta^W(a(u,S_u))dW_u\right) \\ &= a(r,S_r)\sigma(\theta,S_\theta) S_\theta \exp\left(-\frac{1}{2}\int_\theta^t a^2(u,S_u)du + \int_\theta^t a(u,S_u)dW_u\right) \\ &\quad + \sigma(r,S_r) S_r \exp\left(-\frac{1}{2}\int_r^t a^2(u,S_u)du + \int_r^t a(u,S_u)dW_u\right) \\ &\quad \times \left(-\frac{1}{2}\int_r^t D_\theta^W(a^2(u,S_u))du + \int_r^t D_\theta^W(a(u,S_u))dW_u\right). \end{aligned} \tag{4.5}$$

Remark 4.2.5. *Consider $t > 0$. Notice that, under the above hypotheses and as $\theta, r \to t$,*

$$D_r^W S_t \to \sigma(t,S_t) S_t, \tag{4.6}$$

and

$$D_\theta^W D_r^W S_t \to a(t,S_t)\sigma(t,S_t) S_t = \sigma(t,S_t)\partial_x\sigma(t,S_t) S_t^2 + \sigma^2(t,S_t) S_t, \tag{4.7}$$

a.s.

Finally, let us consider the following hypothesis

Hypothesis 4.2.6. *There exist two constants $C > 0$ and $\gamma \in (0, \frac{1}{6})$ such that, for all $t \in [0,T]$, $\sigma(t,\cdot)$ is three-times differentiable and*

$$S_t^3 \partial^3_{xxx}\sigma(t,S_t) \le C t^{-3\gamma}.$$

Using the same arguments as before, one can see that, under this hypothesis, $E|D_u^W D_\theta^W D_r^W S_t|^p \le c_p$ for some positive constant c_p, and for all $u < \theta < r < t$.

4.3 The skew

Consider a risk-neutral probability model for asset prices of the form

$$dS_t = \sigma_t S_t(\rho dW_+ \sqrt{1-\rho^2} dB_t), \tag{4.8}$$

where we assume the interest rate to be zero, $\rho \in [-1,1]$, W and B are two independent Brownian motions. We denote by $\mathcal{F}^W$ and $\mathcal{F}^B$ the σ-algebra generated by W and B, respectively, and $\mathcal{F} := \mathcal{F}^W \vee \mathcal{F}^B$. Moreover, σ is a stochastic process adapted to the filtration generated by W. Notice that (4.8) includes the cases of local volatilities, classical stochastic volatility models, where σ is assumed to be a diffusion, and fractional volatilities, where σ is driven by a fractional Brownian motion. In particular, it includes the case of rough volatilities, fractional volatilities with Hurst parameter $H < \frac{1}{2}$.

We denote by $BS(t, X_t, k, \sigma)$ the Black-Scholes price at time t of a European call with time to maturity T, log-underlying X_t and log-strike price $k := \ln K$, and by $I(t,k)$ the corresponding Black-Scholes implied volatility. Moreover, we denote as $k^* = \ln(S_t)$ the at-the-money strike.

Now we introduce the general results on the short-end behaviour of the volatility skew that we use in this chapter.

4.3.1 Short-end limit of the skew slope

Let us fix $t \in [0,T]$. Consider the following hypotheses.

Hypothesis 4.3.1. *The process $\sigma = (\sigma_s)_{s\in[t,T]}$ is positive and continuous a.s., and satisfies that for all $s \in [t,T]$,*

$$c_1 \leq \sigma_s \leq c_2,$$

for some positive constants c_1 and c_2.

Hypothesis 4.3.2. *$\sigma \in \mathbb{L}_W^{2,2}$, and there exist $C_1 > 0$, $C_2 > 0$ and $H \in (0,1)$ such that for all $t \leq \tau \leq \theta \leq r \leq u \leq T$ and for all $p > 0$*

$$(E|(D_\theta^W \sigma_r^2)|^p)^{\frac{1}{p}} \leq C_1 (r-\theta)^{H-\frac{1}{2}},$$
$$(E|(D_\theta^W D_r^W \sigma_u^2)|^p)^{\frac{1}{p}} \leq C_2 (u-r)^{H-\frac{1}{2}} (u-\theta)^{H-\frac{1}{2}}.$$

Hypothesis 4.3.3. *Hypothesis 4.2.6 holds and the following quantity*

$$\frac{1}{(T-t)^{\frac{3}{2}+H}} \mathbb{E}_t \int_t^T \left(\int_s^T D_s^W \sigma_u^2 du \right) ds$$

where $\mathbb{E}_t$ denotes the expectation with respect to $\mathcal{F}_t$, has a finite limit as $T \to t$.

Under the above hypotheses, the at-the-money short-end skew slope of the implied volatility can be computed from the following adaptation of Theorem 6.3 in Alòs, León and Vives [7].

Theorem 4.3.4. *Assume that Hypotheses 4.3.1, 4.3.2 and 4.3.3, hold for some $t \in [0,T]$. Then*

$$\lim_{T\to t} (T-t)^{\frac{1}{2}-H} \partial_k I(t,k^*) = \frac{\rho}{2\sigma_t^2} \lim_{T\to t} \frac{1}{(T-t)^{\frac{3}{2}+H}} \mathbb{E}_t \left(\int_t^T \left(\int_r^T D_r^W \sigma_u^2 du \right) dr \right). \tag{4.9}$$

4.3.2 The skew in local volatility models

Now we consider a local volatility model defined in equation (4.1). Firstly, we analyse the case of differentiable local volatilities with bounded derivatives.

4.3.2.1 Regular local volatilities

If the local volatility function is bounded with bounded derivatives, the model (4.1) satisfies Hypotheses 4.3.1, 4.3.2 and 4.3.3 for any $t \in [0,T]$, with $\sigma_u = \sigma(u, S_u)$ and $H = 0$. Then Theorem 4.3.4 gives us that, for every fixed t, $\lim_{T\to t} \partial_k I(t,k^*)$ is finite. Moreover, as

$$D_r^W \sigma^2(u, S_u) = 2\sigma(u,S_u) \partial_x \sigma(u, S_u) D_r^W S_u$$

and $D_r^W S_u \to \sigma(u,S_u) S_u$ as $r \to u$, we get (see Alòs and García-Lorite (2021))

$$\begin{aligned}
\lim_{T\to t} \partial_k I(t,k^*) &= \frac{1}{2\sigma^2(t,S_t)} \lim_{T\to t} \frac{1}{(T-t)^2} \mathbb{E}_t \left(\int_t^T \left(\int_r^T D_r^W \sigma^2(u,S_u) du \right) dr \right) \\
&= \frac{1}{\sigma^2(t,S_t)} \lim_{T\to t} \frac{1}{(T-t)^2} \mathbb{E}_t \left(\int_t^T \left(\int_r^T \partial_x \sigma(u,S_u) \sigma(u,S_u) D_r^W S_u du \right) dr \right) \\
&= \lim_{T\to t} \frac{1}{(T-t)^2} \mathbb{E}_t \left(\int_t^T \left(\int_r^T \partial_x \sigma(u,S_u) S_u du \right) dr \right) \\
&= \lim_{T\to t} \frac{1}{(T-t)^2} \mathbb{E}_t \left(\int_t^T \partial_x \sigma(u,S_u) S_u \left(\int_t^u dr \right) du \right).
\end{aligned} \tag{4.10}$$

Recall that $S_u\partial_x\sigma(u,S_u) = \partial_X\hat{\sigma}(u,X_u)$, where $\hat{\sigma}$ denotes the local volatility function in terms of the log-price X. Then we get the following

$$\begin{aligned}\lim_{T\to t}\partial_k I(t,k^*) &= \lim_{T\to t}\frac{1}{(T-t)^2}\mathbb{E}_t\left(\int_t^T \partial_x\hat{\sigma}(u,X_u)\left(\int_t^u dr\right)du\right)\\ &= \frac{1}{2}\partial_X\hat{\sigma}(t,X_t).\end{aligned}$$

Remark 4.3.5. *The above is consistent with the one-half rule, a heuristic relationship introduced by Derman, Kani, and Zou [20]. According to this rule, in the short end, the local volatility varies with the asset price twice as fast as the implied volatility varies with the strike. This rule has been proved for stochastic volatility models via different techniques (see Gatheral [31], Lee [41], or Alòs and García-Lorite [5]).*

4.3.2.2 The rough local volatility case

Now, assume that Hypotheses 4.2.1, 4.2.2, and 4.2.4 hold for some $\gamma > 0$. Under these hypotheses, the local volatility has a singularity at $(0,S_0)$, and then we refer to it as a 'rough local volatility'. Since

$$D_\theta^W\sigma_u^2 = 2\sigma(u,S_u)\partial_x\sigma(u,S_u)D_\theta^W S_u$$

and

$$\begin{aligned}D_\theta^W D_r^W\sigma^2(u,S_u) &= 2(\partial_x\sigma(u,S_u))^2 D_\theta^W S_u D_r^W S_u + 2\sigma(u,S_u)\partial_{xx}^2\sigma(u,S_u)D_\theta^W S_u D_r^W S_u\\ &\quad + 2\sigma(u,S_u)\partial_x\sigma(u,S_u)D_\theta^W D_r^W S_u,\end{aligned} \tag{4.11}$$

a direct computation leads to the following bounds

$$(\mathbb{E}(D_\theta^W\sigma_u^2)^p)^{\frac{1}{p}} \le Cu^{-\gamma}$$

and

$$(\mathbb{E}(D_\theta^W D_r^W\sigma_u^2)^p)^{\frac{1}{p}} \le Cu^{-2\gamma}.$$

Notice that, if $t > 0$, $u^{-\gamma} < t^{-\gamma}$ and then Hypothesis 4.3.2 holds with $H = \frac{1}{2}$, which implies that the one-half rule is satisfied. Nevertheless, if $t = 0$, this hypothesis holds with $H = \frac{1}{2} - \gamma$. Then, the one-half rule is not true in this case, and we have the following result

Theorem 4.3.6. *Consider a local volatility model satisfying Hypotheses 4.2.1, 4.2.2, 4.2.4, 4.2.6, and 4.3.3 with $t = 0$. Then*

$$\lim_{T\to 0} T^{\frac{1}{2}-H}\partial_k I(0,k^*) = \frac{1}{\frac{3}{2}+H}\lim_{T\to 0} T^{\frac{1}{2}-H}\partial_x\hat{\sigma}(T,X_T),$$

where $\hat{\sigma}$ denotes the local volatility function in terms of the log-price X and $H = \frac{1}{2} - \gamma$.

Proof. As

$$D_r^W\sigma^2(u,S_u) = 2\sigma(u,S_u)D_r^W(\sigma(u,S_u)) = 2\sigma(u,S_u)\partial_x\sigma(u,S_u)D_r^W S_u. \tag{4.12}$$

Then, a direct application of Theorem 4.3.4 and equation (4.3) give us that

$$\lim_{T\to 0} T^{\frac{1}{2}-H}\partial_k I(0,k^*) = \frac{1}{2\sigma(0,S_0)^2}\lim_{T\to 0}\frac{1}{T^{\frac{3}{2}+H}}\mathbb{E}\left(\int_0^T\int_r^T 2\sigma(u,S_u)\partial_x\sigma(u,S_u)\sigma(r,S_r)S_r dudr\right). \tag{4.13}$$

Due to the continuity of the local volatility function σ and the asset price S we can write

$$\lim_{T\to 0} T^{\frac{1}{2}-H}\partial_k I(0,k^*) = \lim_{T\to 0}\frac{1}{T^{\frac{3}{2}+H}}\mathbb{E}\left(\int_0^T\int_r^T S_u\partial_x\sigma(u,S_u)dudr\right). \tag{4.14}$$

Since $S_u\partial_x\sigma(u,S_u) = \partial_X\hat{\sigma}(u,X_u)$ we get the following

$$\begin{aligned}\lim_{T\to 0} T^{\frac{1}{2}-H}\partial_k I(0,k^*) &= \lim_{T\to 0}\frac{1}{T^{\frac{3}{2}+H}}\mathbb{E}\left(\int_0^T\int_r^T \partial_x\hat{\sigma}(u,x_u)dudr\right)\\ &= \lim_{T\to 0}\frac{1}{T^{\frac{3}{2}+H}}\mathbb{E}\left(\int_0^T u\partial_x\hat{\sigma}(u,X_u)du\right).\end{aligned} \tag{4.15}$$

Direct application of l'Hôpital rule allow us to conclude that

$$\begin{aligned}\lim_{T\to 0} T^{\frac{1}{2}-H}\partial_k I(0,k^*) &= \lim_{T\to 0}\frac{1}{T^{\frac{3}{2}+H}}\mathbb{E}\left(\int_0^T u\partial_x\hat{\sigma}(u,X_u)du\right)\\ &= \lim_{T\to 0}\frac{1}{(\frac{3}{2}+H)}T^{-\frac{1}{2}-H}T\partial_x\hat{\sigma}(T,X_T)du\\ &= \frac{1}{\frac{3}{2}+H}\lim_{T\to 0} T^{\frac{1}{2}-H}\partial_x\hat{\sigma}(T,X_T),\end{aligned} \tag{4.16}$$

as we wanted to prove. ■

Remark 4.3.7. *The above result recovers the recent results by Bourgey, De Marco, Friz, and Pigato (2022).*

Remark 4.3.8. *This relationship between the local and implied volatility implies that, given a model for the volatility process σ, the local and the implied skew slopes follow the same power law.*

Remark 4.3.9. *The above result seems to be in contradiction with real market practice, where the one-half rule is observed (see Derman, Kani, and Zou [20]). However, the truth is that both facts are compatible. Even when a rough local volatility satisfies the above $\frac{1}{H+\frac{3}{2}}$ rule, local volatilities computed in real market practice are never 'rough', rather they are regularized near maturity, as we can see in the following example.*

Example 4.3.10. In Figure 4.1 we present empirical ratio between the at-the-money skew slope of the implied and local volatilities corresponding to the Stox50 index on July 13 2023. The shortest observed market maturity is $T = 0.03$. Then, the computation of the local volatility from $T = 0$ up to $T = 0.03$ is done via a regularization procedure, which leads to a regular local volatility function with finite skew slope limit.

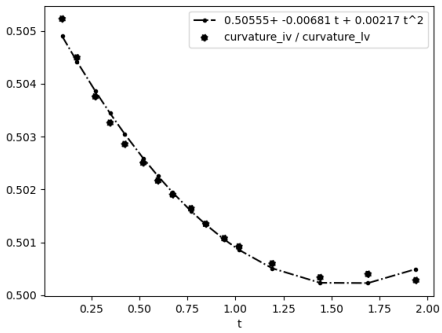

Figure 4.1: Empirical $\frac{\partial_k I_0(T,k^*)}{\partial_x\hat{\sigma}(T,X_T)}$ for market data of EUROSTOXX50E index.

4.4 The curvature

Fix $t \in [0,T]$ and assume the following hypotheses

Hypothesis 4.4.1. *There exists $H \in (0,1)$ such that, for all $t < \tau < \theta < r < u$,*

$$(E|(D^W_\tau D^W_\theta D^W_r \sigma^2_u)|^p)^{\frac{1}{p}} \leq C(u-r)^{H-\frac{1}{2}}(u-\theta)^{H-\frac{1}{2}}(u-\tau)^{H-\frac{1}{2}}.$$

Hypothesis 4.4.2. *There exists $H \in (0,1)$ such that for every fixed $t \in [0,T]$ the following quantities have a finite limit as $T \to t$*

$$\frac{1}{(T-t)^{2+2H}}\mathbb{E}_t \int_t^T \left(\mathbb{E}_r \int_r^T D_r^W \sigma_u^2 du\right)^2 dr$$

$$\frac{1}{(T-t)^{2+2H}}\mathbb{E}_t \int_t^T \left(\int_s^T D_s^W \left(\sigma_r \int_s^T D_s^W \sigma_u^2 du\right) dr\right) ds$$

We recall the following result which is an adaptation of Theorem 4.6 in Alòs and León [9].

Theorem 4.4.3. *Take $t \in [0,T]$, then under Hypothesis 4.3.1-4.4.2 for every fixed $t \in [0,T]$,*

$$\begin{aligned}
&\lim_{T\to t}(T-t)^{1-2H}\partial_{kk}^2 I(t,k^*) \\
&= \frac{1}{4\sigma_t^5}\lim_{T\to t}\frac{1}{(T-t)^{2+2H}}\mathbb{E}_t\left(\int_t^T\left(\mathbb{E}_r\int_r^T D_r^W\sigma_u^2 du\right)^2 dr\right) \\
&- \frac{3\rho^2}{2\sigma_t^5}\lim_{T\to t}\frac{1}{(T-t)^{3+2H}}\mathbb{E}_t\left(\int_t^T\left(\int_r^T D_r^W\sigma_u^2 du\right)dr\right)^2 \\
&+ \frac{\rho^2}{\sigma_t^4}\lim_{T\to t}\frac{1}{(T-t)^{2+2H}}\mathbb{E}_t\left(\int_t^T\int_s^T D_s^W\left(\sigma_r\int_r^T D_r^W\sigma_u^2 du\right)drds\right).
\end{aligned} \tag{4.17}$$

Similar arguments as in Section 4.3 give us that for fixed $t > 0$ and under Hypotheses 4.2.1-4.2.6, conditions 4.3.1-4.4.2 are satisfied with $\gamma = 0$. Hence, $\partial_{kk}^2 I(t,k^*)$ tends to finite quantity. Nevertheless, if $t = 0$, 4.3.1-4.4.2 hold for $H = \frac{1}{2} - \gamma$. In this case we can prove the following result

Theorem 4.4.4. *Under Hypothesis 4.2.1- 4.2.6,*

$$\begin{aligned}
\lim_{T\to 0} T^{1-2H}\partial_{kk}^2 I(0,k^*) &= \frac{(H+\frac{1}{2})(H-\frac{3}{2})}{\sigma(0,S_0)(H+1)(H+\frac{3}{2})^2}\lim_{T\to 0} T^{1-2H}(\partial_x\hat{\sigma}(T,X_T))^2 \\
&+ \frac{1}{2(1+H)}\lim_{T\to 0} T^{1-2H}\partial_{xx}^2\hat{\sigma}(T,X_T),
\end{aligned} \tag{4.18}$$

where $H = \frac{1}{2} - \gamma$.

Proof. Because of Theorem 4.4.3, we know that the limit

$$\lim_{T\to 0} T^{1-2H}\partial_{kk}^2 I(0,k^*)$$

is finite. Moreover, as local volatilities replicate vanilla prices, the result in Theorem 4.4.3 is also true if we replace the spot volatility σ_u by the local volatility $\sigma(u,S_u)$. Then we can write

$$\begin{aligned}
&\lim_{T\to 0} T^{1-2H}\partial_{kk}^2 I(0,k^*) \\
&= \frac{1}{4\sigma(0,S_0)^5}\lim_{T\to 0}\frac{1}{T^{2+2H}}\mathbb{E}\left(\int_0^T\left(\mathbb{E}_r\int_r^T D_r^W\sigma^2(u,S_u)du\right)^2 dr\right) \\
&- \frac{3}{2\sigma(0,S_0)^5}\lim_{T\to 0}\frac{1}{T^{3+2H}}\mathbb{E}\left(\int_0^T\left(\int_r^T D_r^W\sigma^2(u,S_u)du\right)dr\right)^2 \\
&+ \frac{1}{\sigma(0,S_0)^4}\lim_{T\to 0}\frac{1}{T^{2+2H}}\mathbb{E}\left(\int_0^T\int_s^T D_s^W\left(\sigma(r,S_r)\int_r^T D_r^W\sigma^2(u,S_u)du\right)drds\right) \\
&= T_1 + T_2 + T_3.
\end{aligned} \tag{4.19}$$

Now the proof is decomposed into several steps.

Step 1 We start with the study of the term T_1. Since

$$D_r^W \sigma^2(u, S_u) = 2\sigma(u, S_u)\partial_x \sigma(u, S_u) D_r^W S_u,$$

and because of the continuity of σ and S, we get

$$\begin{aligned} T_1 &= \frac{1}{\sigma(0,S_0)} \lim_{T\to 0} \frac{1}{T^{2+2H}} \mathbb{E}\left(\int_0^T \left(\mathbb{E}_r \int_r^T \partial_x \sigma(u, S_u) S_u du \right)^2 dr \right) \\ &= \frac{1}{\sigma(0,S_0)} \lim_{T\to 0} \frac{1}{T^{2+2H}} \mathbb{E}\left(\int_0^T \left(\mathbb{E}_r \int_r^T \partial_x \hat{\sigma}(u, X_u) du \right)^2 dr \right). \end{aligned} \tag{4.20}$$

Due to the Theorem 4.3.6 we know that $u^{\frac{1}{2}-H}\partial_x \hat{\sigma}(u, X_u)$ tends to a finite limit. Then we can write

$$\begin{aligned} T_1 &= \frac{1}{\sigma(0,S_0)} \lim_{u\to 0} u^{1-2H} (\partial_x \hat{\sigma}(u, X_u)))^2 \lim_{T\to 0} \frac{\int_0^T \left(\int_r^T u^{H-\frac{1}{2}} du \right)^2 dr}{T^{2+2H}} \\ &= \frac{1}{\sigma(0,S_0)} \lim_{u\to 0} u^{1-2H} (\partial_x \hat{\sigma}(u, X_u))^2 \lim_{T\to 0} \frac{\int_0^T \left(T^{H+\frac{1}{2}} - r^{H+\frac{1}{2}} \right)^2 dr}{(H+\frac{1}{2})^2 T^{2+2H}} \\ &= \frac{1}{\sigma(0,S_0)(H+\frac{1}{2})^2} \left(1 - \frac{2}{(H+\frac{3}{2})} + \frac{1}{2H+2} \right) \lim_{u\to 0} u^{1-2H} (\partial_x \hat{\sigma}(u, X_u)))^2. \end{aligned} \tag{4.21}$$

Notice that

$$1 - \frac{2}{(H+\frac{3}{2})} + \frac{1}{2H+2} = \frac{(H+\frac{1}{2})^2}{(H+\frac{3}{2})(H+1)}.$$

Finally, we get the following expression

$$T_1 = \frac{1}{\sigma(0,S_0)} \frac{1}{(H+\frac{3}{2})(H+1)} \lim_{T\to 0} T^{1-2H} (\partial_x \hat{\sigma}(T, X_T)))^2. \tag{4.22}$$

Step 2 In a similar way we get the following representation

$$\begin{aligned} T_2 &= -\frac{6}{\sigma(0,S_0)} \lim_{u\to 0} u^{1-2H} (\partial_x \hat{\sigma}(u, X_u)))^2 \lim_{T\to 0} \frac{1}{T^{3+2H}} \left(\int_0^T \left(\int_r^T u^{H-\frac{1}{2}} du \right) dr \right)^2 \\ &= -\frac{6}{\sigma(0,S_0)} \frac{1}{(H+\frac{3}{2})^2} \lim_{T\to 0} T^{1-2H} (\partial_x \hat{\sigma}(T, X_T)))^2. \end{aligned} \tag{4.23}$$

Step 3 Let us now study the term T_3. Similar arguments as before allow us to write

$$\begin{aligned} T_3 &= \frac{1}{\sigma(0,S_0)^4} \lim_{T\to 0} \frac{1}{T^{2+2H}} \mathbb{E}\left(\int_0^T \int_s^T D_s^W \left(\sigma(r, S_r) \int_r^T D_r^W \sigma^2(u, S_u) du \right) drds \right) \\ &= \frac{1}{\sigma(0,S_0)^4} \lim_{T\to 0} \frac{1}{T^{2+2H}} \mathbb{E}\left(\int_0^T \int_s^T \left(D_s^W \sigma(r, S_r) \int_r^T D_r^W \sigma^2(u, S_u) du \right) drds \right) \\ &+ \frac{1}{\sigma(0,S_0)^4} \lim_{T\to 0} \frac{1}{T^{2+2H}} \mathbb{E}\left(\int_0^T \int_s^T \left(\sigma(r, S_r) \int_r^T D_s^W D_r^W \sigma^2(u, S_u) du \right) drds \right) \\ &= T_3^1 + T_3^2. \end{aligned} \tag{4.24}$$

As $D_s^W \sigma(r, S_r) = \partial_x \sigma(r, S_r) D_s^W S_r$, the continuity of σ and S allows us to write

$$\begin{aligned} T_3^1 &= \frac{2}{\sigma(0,S_0)} \lim_{T\to 0} \frac{1}{T^{2+2H}} \mathbb{E}\left(\int_0^T \int_s^T \left(\partial_x \sigma(r, S_r) S_r \int_r^T \partial_x \sigma(u, S_u) S_u du \right) drds \right) \\ &= \frac{2}{\sigma(0,S_0)} \lim_{T\to 0} \frac{1}{T^{2H+2}} \mathbb{E}\left(\int_0^T \int_s^T \left(\partial_x \hat{\sigma}(r, X_r) \int_r^T \partial_x \hat{\sigma}(u, X_u) du \right) drds \right). \end{aligned} \tag{4.25}$$

Since $u^{\frac{1}{2}-H}\partial_x\hat{\sigma}(u,X_u)$ has a finite limit we get the following

$$\begin{aligned} T_3^1 &= \frac{2}{\sigma(0,S_0)}\lim_{u\to 0}u^{1-2H}(\partial_x\hat{\sigma}(u,X_u))^2\times\frac{1}{T^{2+2H}}\left(\int_0^T\int_s^T r^{H-\frac{1}{2}}\left(\int_r^T u^{H-\frac{1}{2}}du\right)drds\right) \\ &= \frac{1}{\sigma(0,S_0)}\frac{1}{(H+\frac{3}{2})(H+1)}\lim_{T\to 0}T^{1-2H}(\partial_x\hat{\sigma}(T,X_T))^2. \end{aligned} \tag{4.26}$$

Next, we move to the analysis of term T_3^2. The following holds

$$\begin{aligned} T_3^2 &= \frac{1}{\sigma(0,S_0)^4}\lim_{T\to 0}\frac{1}{T^{2+2H}}\mathbb{E}\left(\int_0^T\int_s^T\left(\sigma(r,S_r)\int_r^T D_s^W D_r^W\sigma^2(u,S_u)du\right)drds\right) \\ &= \frac{1}{\sigma(0,S_0)^3}\lim_{T\to 0}\frac{1}{T^{2+2H}}\mathbb{E}\left(\int_0^T\int_s^T\left(\int_r^T D_s^W D_r^W\sigma^2(u,S_u)du\right)drds\right). \end{aligned} \tag{4.27}$$

Direct computation of Malliavin derivative gives us the following

$$\begin{aligned} D_\theta^W D_r^W\sigma^2(u,S_u) &= 2(\partial_x\sigma(u,S_u))^2 D_\theta^W S_u D_r^W S_u + 2\sigma(u,S_u)\partial_{xx}^2\sigma(u,S_u)D_\theta^W S_u D_r^W S_u \\ &\quad + 2\sigma(u,S_u)\partial_x\sigma(u,S_u)D_\theta^W D_r^W S_u. \end{aligned} \tag{4.28}$$

When $\theta, r\to u$ the continuity of σ and S together with equations (4.6) and (4.7) allow us to get the following representation

$$\begin{aligned} D_\theta^W D_r^W\sigma^2(u,S_u) &\to 2\sigma(u,S_u)^2(\partial_x\sigma(u,S_u)S_u)^2 + 2\sigma(u,S_u)^3\partial_{xx}^2\sigma(u,S_u)S_u^2 \\ &\quad + 2\sigma(u,S_u)\partial_x\sigma(u,S_u)\left(\sigma(u,S_u)\partial_x\sigma(u,S_u)S_u^2 + \sigma^2(u,S_u)S_u\right) \\ &= 4\sigma(u,S_u)^2(\partial_x\sigma(u,S_u)S_u)^2 + 2\sigma(u,S_u)^3\left(\partial_{xx}^2\sigma(u,S_u)S_u^2 + \partial_x\sigma(u,S_u)S_u\right). \end{aligned} \tag{4.29}$$

Next, using the above equations we get the following representation

$$\begin{aligned} T_3^2 &= \frac{4}{\sigma(0,S_0)}\lim_{u\to 0}u^{1-2H}(\partial_x\hat{\sigma}(u,X_u))^2\times\frac{1}{T^{2+2H}}\left(\int_0^T\int_s^T\int_r^T u^{2H-1}dudrds\right) \\ &\quad + 2\lim_{T\to 0}\frac{1}{T^{2+2H}}\mathbb{E}\left(\int_0^T\int_s^T\int_r^T\left(\partial_{xx}^2\sigma(u,S_u)S_u^2 + \partial_x\sigma(u,S_u)S_u\right)dudrds\right) \\ &= \frac{1}{\sigma(0,S_0)(H+1)}\lim_{u\to 0}u^{1-2H}(\partial_x\hat{\sigma}(u,X_u))^2 \\ &\quad + 2\lim_{T\to 0}\frac{1}{T^{2+2H}}\mathbb{E}\left(\int_0^T\int_s^T\int_r^T\left(\partial_{xx}^2\sigma(u,S_u)S_u^2 + \partial_x\sigma(u,S_u)S_u\right)dudrds\right) \\ &= \frac{1}{\sigma(0,S_0)(H+1)}\lim_{u\to 0}u^{1-2H}(\partial_x\hat{\sigma}(u,X_u))^2 \\ &\quad + \lim_{T\to 0}\frac{1}{T^{2+2H}}\mathbb{E}\left(\int_0^T\partial_{xx}^2\hat{\sigma}(u,X_u)u^2du\right). \end{aligned} \tag{4.30}$$

The last line in the equation (4.30) follows from the following observation

$$\begin{aligned} \int_0^T\int_s^T\int_r^T\partial_{xx}^2\hat{\sigma}(u,X_u)dudrds &= \int_0^T\int_s^T\partial_{xx}^2\hat{\sigma}(u,X_u)(u-s)duds \\ &= \int_0^T\partial_{xx}^2\hat{\sigma}(u,X_u)\int_0^u(u-s)dsdu \\ &= \frac{1}{2}\int_0^T\partial_{xx}^2\hat{\sigma}(u,X_u)u^2du. \end{aligned} \tag{4.31}$$

Finally, since all the limits in the equation (4.30) are well defined, direct application of l'Hôpital rule allows us to conclude

$$T_3^2 = \frac{1}{\sigma(0,S_0)(H+1)}\lim_{T\to 0}T^{1-2H}(\partial_x\hat{\sigma}(T,X_T))^2 + \frac{1}{2(1+H)}\lim_{T\to 0}T^{1-2H}\partial_{xx}^2\hat{\sigma}(T,X_T). \tag{4.32}$$

Combining equations (4.22), (4.23), (4.26), and (4.32) we get that

$$\begin{aligned}\lim_{T\to 0} T^{1-2H}\partial^2_{kk} I(0,k^*) = &\frac{(H+\frac{1}{2})(H-\frac{3}{2})}{\sigma(0,S_0)(H+1)(H+\frac{3}{2})^2}\lim_{T\to 0} T^{1-2H}(\partial_x\hat{\sigma}(T,X_T))^2 \\ &+\frac{1}{2(1+H)}\lim_{T\to 0} T^{1-2H}\partial^2_{xx}\hat{\sigma}(T,X_T),\end{aligned} \tag{4.33}$$

as we wanted to prove. ■

Remark 4.4.5. *Notice that, if $H=\frac{1}{2}$, the above reduces to*

$$\lim_{T\to 0} T^{1-2H}\partial^2_{kk} I(0,k^*) = -\frac{1}{6\sigma(0,S_0)}\lim_{u\to 0} u^{1-2H}(\partial_x\hat{\sigma}(u,X_u))^2 + \frac{1}{3}\lim_{T\to 0} T^{1-2H}\partial^2_{xx}\hat{\sigma}(T,X_T), \tag{4.34}$$

according to Equation (8.4.3) in Alòs and García-Lorite [5]. On the other hand, in the uncorrelated case $\rho=0$ it reads

$$\lim_{T\to 0}\partial^2_{kk} I(0,k^*) = \frac{1}{2(H+1)}\lim_{T\to 0}\partial^2_{xx}\hat{\sigma}(T,X_T). \tag{4.35}$$

In particular, if $\rho=0$ and $H=\frac{1}{2}$, we get

$$\lim_{T\to 0}\partial^2_{kk} I(0,k^*) = \frac{1}{3}\lim_{T\to 0}\partial^2_{xx}\hat{\sigma}(T,X_T), \tag{4.36}$$

according to the results in Hagan, Kumar, Lesniewski, and Woodward (2002).

Remark 4.4.6. *As*

$$\lim_{T\to 0} T^{1-2H}(\partial_x\hat{\sigma}(T,X_T))^2 = \left(\frac{3}{2}+H\right)^2\lim_{T\to 0} T^{1-2H}(\partial_k I(0,k^*))^2$$

the result in Theorem 4.4.4 can be written as

$$\begin{aligned}\frac{1}{2(1+H)}\lim_{T\to 0} T^{1-2H}\partial^2_{xx}\hat{\sigma}(T,X_T) = &\lim_{T\to 0} T^{1-2H}\partial^2_{kk} I(0,k^*) \\ &-\frac{(H+\frac{1}{2})(H-\frac{3}{2})}{\sigma(0,S_0)(H+1)}\lim_{T\to 0} T^{1-2H}(\partial_k I(0,k^*))^2.\end{aligned} \tag{4.37}$$

Remark 4.4.7. *This relationship between the local and the implied volatility implies that, given a model for the volatility process σ, the local and the implied curvature satisfy the same power law.*

4.5 Numerical Results

This section is devoted to study numerically the relationship between the skews and curvatures of local and implied volatilities. Towards this end, we generate local volatility models satisfying the hypotheses required in the previous section, and we compare with the corresponding implied volatility behaviour.

Example 4.5.1 (The skew)**.** Consider a rough Bergomi model. That is, assume that the volatility process is given by

$$\sigma_u = \sigma_0 \exp\left(\nu\sqrt{2H}W^H_t - \frac{1}{2}\nu^2 t^{2H}\right),$$

where $W^H_t = \int_0^t (t-s)^{H-\frac{1}{2}} dW_s$ (see Bayer, Friz, and Gatheral [15]). The set of parameters using in the simulation is: $S_0=100$, $\nu=1.1$, $\sigma_0=0.3$, and $\rho=-0.6$. We will estimate the corresponding at-the-money implied and local volatility skews of a European call option as a function of maturity. It is easy to show that the next representation of $\sigma^2(T,K)$ holds:

$$\sigma^2(T,K) = \frac{\mathbb{E}_t\left(\sigma_t^2\phi(d(t,T,S_t,K))\right)}{\mathbb{E}_t\left(\phi(d(t,T,S_t,K))\right)} \tag{4.38}$$

where $\phi(\cdot)$ is PDF of a standard Gaussian variable, $d(t,T,S_t,K) = \frac{\log(\frac{K}{S_t})+\frac{(T-t)v_{t,T}}{2}-\rho\int_t^T \sigma_u dB_u}{\sqrt{1-\rho^2}\sqrt{T-t}v_{t,T}}$ and $v_{t,T} = \sqrt{\frac{\int_t^T \sigma_u^2 du}{T-t}}$. To compute the at-the-money skew for the local volatility, we take ∂_K in (4.38)

$$\partial_K \sigma(T,K) = \frac{\mathbb{E}_t\left(\frac{\sigma_T^2 d(t,T,x_t,K,v_{t,T})}{v_t^2 K\sqrt{T-t}}\phi(d(t,T,x_t,K,v_{t,T}))\right) - \sigma^2(T,K)\mathbb{E}_t\left(\frac{d(t,T,x_t,K,v_{t,T})\phi(d(t,T,x_t,K,v_{t,T}))}{Kv_t^2\sqrt{T-t}}\right)}{2\sigma(T,K)\mathbb{E}_t\left(\frac{\phi(d(t,T,x_t,K,v_{t,T}))}{v_{t,T}}\right)} \tag{4.39}$$

To compute at-the-money skew for the implied volatility, we use finite difference method[1]

$$\partial_K I(T,K) \approx \frac{I(T,K+h) - I(T,K-h)}{2h}.$$

Finally, we compute the ratio of the implied volatility skew over the local volatility skew for $H = \frac{1}{2}$ and $H = 0.2$, in order to show that in the limit goes to $\frac{1}{H+\frac{3}{2}} = 0.588$ as we stated in Theorem 4.3.6 and Remark 4.3.8. The result is presented in Figure 4.2.

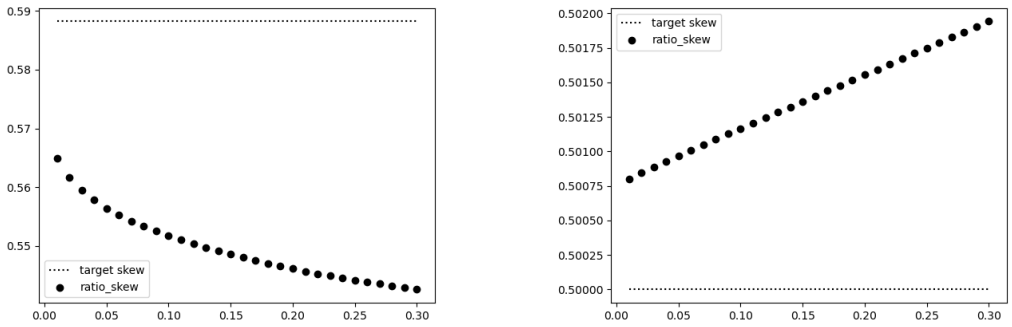

(a) $H = 0.2$ (b) $H = 0.5$

Figure 4.2: $\frac{\partial_k I(T,k^*)}{\partial_x^2 \hat{\sigma}(T,X_T)}$ as a function of T

Example 4.5.2. The goal of this example is to show that the behaviour of the curvature in the case of the SABR model satisfies Remark 4.4.5. Recall that the SABR model is defined by

$$dF_t = \sigma_t F_t^\beta(\rho dW_t + \sqrt{1-\rho^2}dB_t),$$

where we study $\beta = 1$, and the volatility is given by

$$\sigma_t = \alpha \exp\left(-\frac{\nu^2}{2}t + \nu B_t\right),$$

We use the following approximation of the local volatility equivalent (see [35] for more details) for a log-normal SABR model

$$\sigma(T,K) \approx \alpha\sqrt{1 + 2\rho\nu y(K) + \nu^2 y^2(K)}$$

[1]Another way to get the skew is to take the derivative with respect to K in

$$\mathbb{E}\left((S_T - K)^+\right) = BS(T,K,I(T,K)).$$

Then we get the next expression for the skew

$$\partial_k I(T,K) = -\frac{\mathbb{E}\left(I(S_T > K)\right) - \partial_K BS(T,K,I(T,K)}{\partial_\sigma BS(T,K,I(T,K))}.$$

We must observe, that the term $\mathbb{E}\left(I(S_T > K)\right)$ can be estimated in the same simulation where we get the price of the option. We have checked both approaches and we have seen they lead to identical results.

with $y(K) = \frac{\log(\frac{K}{S_0})}{\alpha}$. Then, we have that the skew and curvature are given by

$$\partial_K \sigma(T,K) = \frac{\alpha^2 y'(K)\left(\rho\nu + \nu^2 y(K)\right)}{\sigma(T,K)}$$
$$\partial_{K,K}\sigma(T,K) = \frac{\alpha^2 y''(K)(\rho\nu + \nu y(K)) + (\alpha\nu y'(K))^2 - (\partial_K\sigma(T,K))^2}{\sigma(T,K)}$$

Therefore, we have that

$$\partial_{k,k}\hat{\sigma}(T,k) = K\partial_K\sigma(T,K) + K^2\partial_{K,K}\sigma(T,K). \tag{4.40}$$

In addition, we use the approximation for the implied volatility proposed in [35] for the log-normal case

$$I(T,K) \approx \alpha\frac{z}{x(z)}\left(1 + \left(\frac{1}{4}\rho\nu\alpha + \frac{2-3\rho^2}{24}\nu^2\right)T\right)$$

where $z = \frac{\nu}{\alpha}\log\left(\frac{S_0}{K}\right)$ and $x(z) = \log\left(\frac{\sqrt{1-2\rho z+z^2}}{1-\rho}\right)$. It is easy to show with a little bit of algebra that

$$\partial_K I(T,K) = -\nu\frac{f'(z)}{K}m(T)$$
$$\partial_{K,K}I(T,K) = \left(\nu\frac{f'(z)}{K^2} + \nu^2\frac{f''(z)}{\alpha K^2}\right)m(T)$$

with $m(T) = 1 + \left(\frac{1}{4}\rho\nu\alpha + \frac{2-3\rho^2}{24}\nu^2\right)T$ and $f(z) = \frac{z}{x(z)}$. Therefore

$$\partial_{k,k}I(T,k^*) = K^*\partial_K I(T,K^*) + K^2\partial_{K,K}I(T,K^*). \tag{4.41}$$

where $K^* = \exp(k^*)$. Firstly, we must note that from Remark 4.4.5, we have that the curvature of the local volatility is bigger than the curvature of the implied volatility and that the difference between curvatures for the SABR model in the short term is equal to $\frac{\rho^2\nu^2}{6\alpha}$. In order to check it, we use the next set of parameters for the SABR model $\alpha = 0.3, \nu = 0.6, \rho = -0.6$ and $S_0 = 100$. The result is presented in Figure 4.3. On other hand, Remark 4.4.5, gives us that for $\rho = 0$

$$\lim_{T\to 0}\partial^2_{kk}I(0,k^*) = \frac{1}{3}\lim_{T\to 0}\partial^2_{xx}\hat{\sigma}(T,X_T)$$

This property can be observed in Figure 4.4.

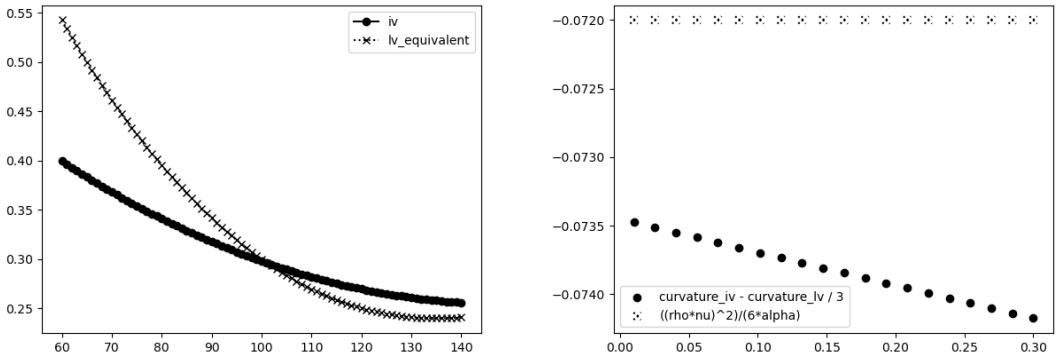

(a) Local volatility Vs Implied volatility at $T = 0.5$ (b) $\partial^2_{kk}I(T,k^*) - \partial^2_{xx}\hat{\sigma}(T,X_T)$ as a function of T

Figure 4.3: Local volatility equivalent Vs Implied volatility and differences between the curvatures in the short end.

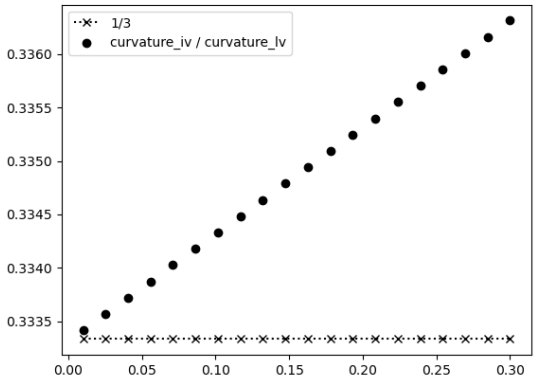

Figure 4.4: $\frac{\partial^2_{kk} I(T,k^*)}{\partial^2_{xx} \hat{\sigma}(T,X_T)}$ as a function of T, with $\rho = 0$.

Example 4.5.3. In this example, we show that the power law followed by the curvature of the implied volatility and the equivalent local volatility is the order $(T-t)^{1-2H}$ when $0 \leq H < \frac{1}{2}$ for a rough Bergomi model. In order to compute the curvature of the implied volatility avoiding the noise of the Monte Carlo simulation, we use the approximation for implied volatility proposed by the authors in [28]. In this paper the following dynamics for the underlying is given

$$\begin{aligned} \frac{S_t}{\beta(s_t)} &= \sigma_t dW_t \\ \frac{d\xi_t(s)}{\xi_t(s)} &= k(s-t)dB_t \quad t < s. \end{aligned}$$

where $\sigma_t = \sqrt{\xi_t(t)}$, β is a positive continuous function, $\xi_t(s) = \mathbb{E}_t\left(\xi_s(s)\right)$ and $k(\tau) = \eta\sqrt{2H}t^{H-\frac{1}{2}}$. We must note that different choices of H and $\beta(\cdot)$ lead to different models. For example when $\beta(s) = s$ we recover the rough Bergomi model, which is our case of interest. The implied volatility approximation proposed in [28] is

$$I(T,k) = I(T,0)\frac{|y(T,k)|}{\sqrt{G_A(y(k_\beta(k),T))}}$$

where

$$\begin{aligned} y(T,k) &= \frac{k(T-t)}{U_t(T)} \\ U_t(T) &= \sqrt{\frac{1}{T-t}\int_t^T \xi_t(s)ds} \\ k &= \log(K) - k^* \\ k_\beta(k) &= \int_s^k \frac{ds}{\beta(s)} \end{aligned}$$

To estimate $\partial_k I(T,k)$ and $\partial_{k,k} I(T,k)$ we use finite differences

$$\begin{aligned} \partial_k I(T,k) &= \frac{I(T,k+h) - I(T,k-h)}{2h} \\ \partial_{k,k} I(T,k) &= \frac{I(T,k+h) - 2I(T,k) + I(T,k-h)}{h^2} \end{aligned}$$

On other hand, to estimate the local volatility equivalent and the skew we use (4.38) and (4.39) respectively. The curvature is also estimated by finite differences

$$\partial_{K,K}\sigma(T,K) \approx \frac{\partial_K \sigma(T,K+h) - \partial_K \sigma(T,K-h)}{2h}.$$

In Figure 4.5 we see that the power law for curvature of the implied volatility and local volatility is the same. In the Monte Carlo simulation we used the following set of parameters $H = 0.1$, $\nu = 1.1$ and $\rho = -0.6$. We conclude that both curvatures satisfy the same power law in accordance with Remark 4.4.7.

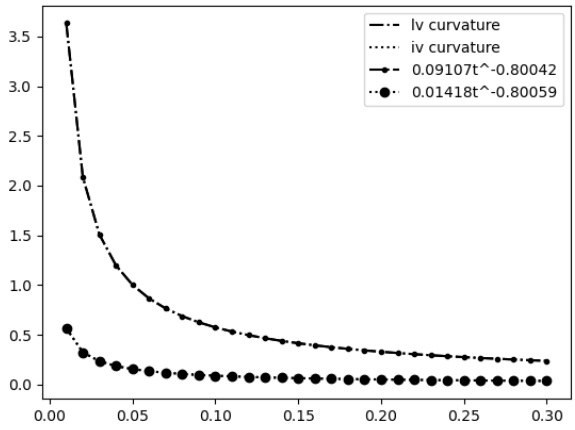

Figure 4.5: $\frac{\partial^2_{kk} I(T,k^*)}{\partial^2_{xx} \hat{\sigma}(T,X_T)}$ at the short-term with $\rho = -0.6$

Appendices

.1 A primer on Malliavin Calculus

We introduce the elementary notions of the Malliavin calculus used in this thesis (see Nualart and Nualart [46]). Let us consider a standard Brownian motion $Z = (Z_t)_{t\in[0,T]}$ defined on a complete probability space $(\Omega, \mathcal{F}, \mathbb{P})$ and we done by $\mathcal{F}_t$ the filtration generated by Z_t. Let $\mathcal{S}^Z$ be the set of random variables of the form

$$F = f(Z(h_1), \dots, Z(h_n)), \tag{42}$$

with $h_1, \dots, h_n \in L^2([0,T])$, $Z(h_i)$ denotes the Wiener integral of the function h_i, for $i = 1, .., n$, and $f \in C_b^\infty(\mathbb{R}^n)$ (i.e., f and all its partial derivatives are bounded). Then the Malliavin derivative of F, $D^Z F$, is defined as the stochastic process given by

$$D_s^Z F = \sum_{j=1}^n \frac{\partial f}{\partial x_j}(Z(h_1), \dots, Z(h_n))h_j(s), \quad s \in [0,T].$$

This operator is closable from $L^p(\Omega)$ to $L^p(\Omega; L^2([0,T]))$, for all $p \geq 1$, and we denote by $\mathbb{D}_Z^{1,p}$ the closure of $\mathcal{S}^Z$ with respect to the norm

$$||F||_{1,p} = \left(\mathbb{E}\,|F|^p + \mathbb{E}||D^Z F||^p_{L^2([0,T])}\right)^{1/p}.$$

We also consider the iterated derivatives $D^{Z,n}$ for all integers $n > 1$ whose domains will be denoted by $\mathbb{D}_Z^{n,p}$, for all $p \geq 1$. We will use the notation $\mathbb{L}_Z^{n,p} := L^p([0,T]; \mathbb{D}_Z^{n,p})$. One of the main results in Malliavin calculus is the Clark-Ocone-Haussman formula:

Theorem .1.1. *Let $F \in \mathbb{D}_Z^{1,2}$. Then*

$$F = E(F) + \int_0^T E_s(D_r^Z(F))dZ_r.$$

The following theorem is an extension of the classical Itô's Lemma for non-anticipating processes, see Proposition 4.3.1 in Alòs and García-Lorite [5].

Theorem .1.2 (Anticipating Itô's Formula)**.** *Consider a process of the form*

$$X_t = X_0 + \int_0^t u_s dZ_s + \int_0^t v_s ds,$$

where X_0 is an $\mathcal{F}_0$-measurable random variable and u and v are $\mathcal{F}_t$-adapted processes in $L^2([0,T]\times\Omega)$. Consider also a process $Y_t = \int_t^T \theta_s ds$, for some $\theta \in \mathbb{L}_Z^{1,2}$. Let $F : [0,T]\times\mathbb{R}^2 \to \mathbb{R}$ be a $C^{1,2}([0,T]\times\mathbb{R}^2)$ function such that there exists a positive constant C such that, for all $t \in [0,T]$, F and its derivatives evaluated in (t, X_t, Y_t) are bounded by C. Then it follows that for all $t \in [0,T]$,

$$\begin{aligned} F(t, X_t, Y_t) = F(0, X_0, Y_0) &+ \int_0^t \partial_s F(s, X_s, Y_s)ds + \int_0^t \partial_x F(s, X_s, Y_s)u_s dZ_s \\ &+ \int_0^t \partial_x F(s, X_s, Y_s)v_s ds + \int_0^t \partial_y F(s, X_s, Y_s)dY_s \\ &+ \int_0^t \partial^2_{xy} F(s, X_s, Y_s)u_s D^- Y_s ds + \frac{1}{2}\int_0^t \partial^2_{xx} F(s, X_s, Y_s)u_s^2 ds, \end{aligned}$$

where $D^- Y_s = \int_s^T D_s^Z \theta_r dr$ and the integral $\int_0^t \partial_x F(s, X_s, Y_s)u_s dZ_s$ is defined in the Skorohod sense since the process $\partial_x F(s, X_s, Y_s)u_s$ is not adapted.

Notice that the Malliavin derivative operator satisfies the *chain rule*. That is, given $f \in C^{1,2}$, and $F \in \mathbb{D}_Z^{1,2}$, the random variable $f(F)$ belongs to $\mathbb{D}_Z^{1,2}$, and $D^Z f(F) = f'(F)D^Z F$.

The adjoint of the derivative operator D^Z is the divergence operator δ^Z, which coincides with the Skorohod integral. Its domain, denoted by Dom δ, is the set of processes $u \in L^2(\Omega \times [0,T])$ such that there exists a random variable $\delta^Z(u) \in L^2(\Omega)$ such that

$$E(\delta^Z(u)F) = E\left(\int_0^T (D_s^Z F)u_s ds\right), \qquad \text{for every } \ F \in \mathcal{S}^Z. \tag{43}$$

We use the notation $\delta^Z(u) = \int_0^T u_s dZ_s$. It is well known that δ is an extension of the Itô integral. That is, δ, applied to an adapted and square integrable processes, coincides with the classical Itô integral. Moreover, the space $\mathbb{L}_Z^{1,2}$ is included in the domain of δ.

From the above relationship between the operators D^Z and δ^Z, it is easy to see that, for an Itô process of the form

$$X_t = X_0 + \int_0^t v_s ds + \int_0^t u_s dZ_s,$$

where a and b are adapted processes in $\mathbb{L}_Z^{1,2}$, its Malliavin derivative for $r \leq t$ is given by

$$D_r^Z X_t = \int_r^t D_r^Z v_s ds + u_r \mathbf{1}_{[0,t]}(r) + \int_r^t D_r^Z u_s dZ_s. \tag{44}$$

Then, if we consider an equation of the form

$$X_t = X_0 + \int_0^t a(s, X_s) ds + \int_0^t b(s, X_s) dZ_s,$$

where $a(s, \cdot)$ and $b(s, \cdot)$ are differentiable functions with uniformly bounded derivatives, a direct application of (44) allows us to see that

$$D_u^Z X_t = \int_u^t \frac{\partial a}{\partial x}(s, X_s) D_u^Z X_s ds + b(u, X_u) + \int_u^t \frac{\partial b}{\partial x}(s, X_s) D_u^Z X_s dZ_s. \tag{45}$$

Notice that the above equality also holds, for example, if a and b are globally Lipschitz functions with polynomial growth (see Theorem 2.2.1 in Nualart [45]), replacing $\frac{\partial a}{\partial x}$ and $\frac{\partial b}{\partial x}$ by an adequate processes.

.2 Computation of Malliavin derivatives

In this appendix we provide the computations of the first and second Malliavin derivatives of the processes S_t, M_t and ϕ_t defined in Chapter 2.

Using the fact that σ_t is adapted to the filtration of W' and the formula for the derivative of a stochastic integral (see for example (3.6) in Nualart and Nualart [46]), we get that, for $0 \leq s \leq r \leq T$,

$$\begin{aligned}
D_s^{W'} S_r &= S_r \left(\rho\sigma_s - \frac{1}{2}\int_s^r D_s^{W'}\sigma_u^2 du + \int_s^r D_s^{W'}\sigma_u dW_u \right), \\
D_s^{B} S_r &= S_r \sigma_s \sqrt{1-\rho^2}, \\
D_s^{W'} M_r &= \frac{\rho\sigma_s S_s (T-s)}{T} + \int_s^r \frac{(T-u) D_s^{W'}(\sigma_u S_u)}{T} dW_u, \\
D_s^{B} M_r &= \frac{\sqrt{1-\rho^2}\sigma_s S_s (T-s)}{T} + \int_s^r \frac{(T-u)\sigma_u D_s^{B}(S_u)}{T} dW_u.
\end{aligned}$$

Moreover, appealing to (2.7), we find that

$$\begin{aligned}
D_s^{W} S_r &= \rho S_r \left(-\frac{1}{2}\int_s^r D_s^{W'}\sigma_u^2 du + \int_s^r D_s^{W'}\sigma_u dW_u \right) + S_r\sigma_s, \\
D_s^{W} M_r &= \frac{\sigma_s S_s (T-s)}{T} + \rho\int_s^r \frac{(T-u) D_s^{W'}(\sigma_u S_u)}{T} dW_u \\
&\quad + \sqrt{1-\rho^2}\int_s^r \frac{(T-u) D_s^{B}(\sigma_u S_u)}{T} dW_u.
\end{aligned}$$

Finally, from the definition of ϕ_t, we conclude that

$$\begin{aligned}
D_s^{W}\phi_r &= \frac{\rho(T-r) D_s^{W'}(\sigma_r S_r)}{T M_r} - \frac{\rho(T-r) S_r\sigma_r D_s^{W'} M_r}{T M_r^2} \\
&\quad + \frac{\sqrt{1-\rho^2}(T-r) D_s^{B}(\sigma_r S_r)}{T M_r} - \frac{\sqrt{1-\rho^2}(T-r) S_r\sigma_r D_s^{B} M_r}{T M_r^2}.
\end{aligned} \tag{46}$$

We next compute the second Malliavin derivatives. Similarly as before, using the fact that we can differentiate Lebesgue integrals of stochastic processes (see for example Proposition 3.4.3 in Nualart and Nualart [46]), we get that, for $0 \leq s \leq r \leq u \leq T$,

$$\begin{aligned}
D_s^{B} D_r^{W'} S_u &= S_u\sigma_s\sqrt{1-\rho^2}\left(\rho\sigma_r - \frac{1}{2}\int_r^u D_r^{W'}\sigma_v^2 dv + \int_r^u D_r^{W'}\sigma_v dW_v \right), \\
D_s^{W'} D_r^{W'} S_u &= S_u \left(\rho\sigma_s - \frac{1}{2}\int_s^u D_s^{W'}\sigma_v^2 dv + \int_s^u D_s^{W'}\sigma_v dW_v \right) \\
&\qquad \times \left(\rho\sigma_r - \frac{1}{2}\int_r^u D_r^{W'}\sigma_v^2 dv + \int_r^u D_r^{W'}\sigma_v dW_v \right) \\
&\quad + S_u \left(\rho D_s^{W'}\sigma_r - \frac{1}{2}\int_r^u D_s^{W'} D_r^{W'}\sigma_v^2 dv + \int_r^u D_s^{W'} D_r^{W'}\sigma_v dW_v \right), \\
D_s^{W'} D_r^{B} S_u &= \sqrt{1-\rho^2} S_u D_s^{W'}\sigma_r + \sqrt{1-\rho^2}\sigma_r D_s^{W'} S_u, \\
D_s^{W'} D_r^{W'} M_u &= \frac{\rho(T-r) D_s^{W'}(\sigma_r S_r)}{T} + \int_r^u \frac{(T-v) D_s^{W'} D_r^{W'}(\sigma_v S_v)}{T} dW_v, \\
D_s^{B} D_r^{W'} M_u &= \frac{\rho(T-r)\sigma_r D_s^{B} S_r}{T} + \int_r^u \frac{(T-v) D_s^{B} D_r^{W'}(\sigma_v S_v)}{T} dW_v, \\
D_s^{W'} D_r^{B} M_u &= \frac{\sqrt{1-\rho^2}(T-r) D_s^{W'}(\sigma_r S_r)}{T} + \int_r^u \frac{(T-v) D_s^{W'}(\sigma_v D_s^{B} S_v)}{T} dW_v, \\
D_s^{B} D_r^{B} M_u &= \frac{\sqrt{1-\rho^2}(T-r)\sigma_r D_s^{B}(S_r)}{T} + \int_r^u \frac{(T-v)\sigma_v D_s^{B} D_r^{B} S_v}{T} dW_v,
\end{aligned} \tag{47}$$

and

$$
\begin{aligned}
D_s^W D_r^W \phi_u &= \frac{\rho^2(T-u)D_s^{W'}D_r^{W'}(\sigma_u S_u)}{TM_u} - \frac{\rho^2(T-u)D_s^{W'}(\sigma_u S_u)D_s^{W'}M_u}{TM_u^2} \\
&- \frac{\rho^2(T-u)D_s^{W'}\left(\sigma_u S_u D_r^{W'}M_u\right)}{TM_u^2} + \frac{2\rho^2(T-u)\sigma_u S_u D_s^{W'}M_u D_r^{W'}M_u}{TM_u^3} \\
&+ \frac{\rho\sqrt{1-\rho^2}(T-u)D_s^{W'}D_r^{B}(\sigma_u S_u)}{TM_u} - \frac{\rho\sqrt{1-\rho^2}(T-u)D_r^{B}(\sigma_u S_u)D_s^{W'}M_u}{TM_u^2} \\
&- \frac{\rho\sqrt{1-\rho^2}(T-u)D_s^{W'}\left(\sigma_u S_u D_r^{B}M_u\right)}{TM_u^2} + \frac{2\rho\sqrt{1-\rho^2}(T-u)\sigma_u S_u D_r^{B}M_u D_s^{W'}M_u}{TM_u^3} \\
&+ \frac{\rho\sqrt{1-\rho^2}(T-u)D_s^{B}D_r^{W'}(\sigma_u S_u)}{TM_u} - \frac{\rho\sqrt{1-\rho^2}(T-u)D_r^{W'}(\sigma_u S_u)D_s^{B}M_u}{TM_u^2} \\
&- \frac{\rho\sqrt{1-\rho^2}(T-u)D_s^{B}\left(\sigma_u S_u D_r^{W'}M_u\right)}{TM_u^2} + \frac{\rho\sqrt{1-\rho^2}(T-u)\sigma_u S_u D_r^{W'}M_u D_s^{B}M_u}{TM_u^3} \\
&+ \frac{(1-\rho^2)(T-u)D_s^{B}D_r^{B}(\sigma_u S_u)}{TM_u} - \frac{(1-\rho^2)(T-u)D_r^{B}(\sigma_u S_u)D_s^{B}M_u}{TM_u^2} \\
&- \frac{(1-\rho^2)(T-u)D_s^{B}\left(S_u\sigma_u D_r^{B}M_u\right)}{TM_u^2} + \frac{2(1-\rho^2)(T-u)S_u\sigma_u D_r^{B}M_u D_s^{B}M_u}{TM_u^3}.
\end{aligned}
\tag{48}
$$

.3 The Price of an Asian Call Option under the Bachelier Model

In this appendix we derive closed form formula for the price of an arithmetic Asian call option under the constant volatility Bachelier model.

Theorem .3.1. *Consider the model (1.1) in the case of constant volatility σ. Then, the price of an arithmetic Asian call option for $t \in [0,T]$ satisfies*

$$B_A(t,S_t,y_t,k,\sigma) = \left(S_t\frac{T-t}{T} + \frac{y_t}{T} - k\right) N(d_A(k,\sigma)) + \left(\frac{\sigma(T-t)\sqrt{T-t}}{T\sqrt{3}}\right) n(d_A(k,\sigma)),$$

where

$$d_A(k,\sigma) = \frac{S_t\frac{T-t}{T} + \frac{y_t}{T} - k}{\left(\frac{\sigma(T-t)\sqrt{T-t}}{T\sqrt{3}}\right)},$$

T is the maturity, S_t is the stock price at time t, k is the strike price, and $y_t = \int_0^t S_u du$ is the state variable.

Proof. Firstly, notice the following representation

$$\begin{aligned}\frac{1}{T}\int_0^T S_t dt &= \frac{1}{T}\int_0^T \left(S_0 + \int_0^t \sigma dW_u\right) dt = S_0 + \frac{\sigma}{T}\int_0^T W_s ds = \\ &= S_0 + \frac{\sigma}{T}\int_0^t (T-s) dW_s + \frac{\sigma}{T}\int_t^T (T-s) dW_s.\end{aligned}$$

The last term on the right hand side is normally distributed with mean zero and variance equal to

$$\mathbb{E}\left(\frac{\sigma}{T}\int_t^T (T-s)dW_s\right)^2 = \frac{\sigma^2}{T^2}\int_t^T (T-s)^2 ds = \frac{\sigma^2(T-t)^3}{3T^2}.$$

Due to the risk neutral pricing argument we know that

$$B_A(t,S_t,y_t,k,\sigma) = \mathbb{E}_t\left(\frac{1}{T}\int_0^T S_t dt - k\right)_+.$$

Therefore, using the above formulas this can be equivalently written as

$$\begin{aligned}\mathbb{E}_t\left(\frac{1}{T}\int_0^T S_t dt - k\right)_+ &= \mathbb{E}_t\left(S_t\frac{T-t}{T} + \frac{y_t}{T} - k + \frac{\sigma}{T}\int_t^T (T-s)dW_s\right)_+ = \\ &= \frac{1}{\sqrt{2\pi}}\int_{\frac{k-u_t}{z_t}}^{\infty} (u_t - k + z_t x)\, e^{-\frac{x^2}{2}} dx = \\ &= (u_t - k)\, N\left(\frac{u_t-k}{z_t}\right) + z_t n\left(\frac{u_t-k}{z_t}\right),\end{aligned}$$

where $u_t = S_t\frac{T-t}{T} + \frac{y_t}{T}$ and $z_t = \frac{\sigma(T-t)\sqrt{T-t}}{T\sqrt{3}}$.

The last step allows us to complete the proof. ∎

.4 Extra steps in the proof of (3.8) in Theorem 3.3.5

Lemma .4.1. *Under Hypothesis 3.3.1*

$$|(BS^{-1})'(k^*, \Gamma_s)| \leq O\left(T^{-\frac{1}{2}}\right), \tag{49}$$

where $\Gamma_s = \mathbb{E}\left(BS(0, X_0, k^*, v_0)\right) + \frac{\rho}{2}\mathbb{E}\left(\int_0^s H(r, X_r, k^*, v_r)\Lambda_r dr\right)$.

Proof. One can show the following

$$(BS^{-1})'(k^*, \Gamma_s) = \frac{1}{\partial_\sigma BS(t, X_t, k_t^*, BS^{-1}(k_t^*, \Gamma_s)))}. \tag{50}$$

Straightforward differentiation gives that ATM Vega is

$$\partial_\sigma BS(0, X_0, k^*, \sigma) = \sqrt{T}\left(-ye^{y^2}\text{Erfc}\left(\frac{3y}{2\sqrt{2}}\right) + \frac{e^{-\frac{1}{8}y^2}}{\sqrt{2\pi}}\right) =: g(y)\sqrt{T}, \tag{51}$$

where $y = \sigma\sqrt{T}$ and $\text{Erfc}(z) = 1 - \frac{2}{\sqrt{\pi}}\int_0^z e^{-t^2}dt$. Then, using equations (50) and (51) we get

$$(BS^{-1})'(k^*, \Gamma_s) = \frac{1}{g(y)\sqrt{T}},$$

where $y = BS^{-1}\left(k^*, \Gamma_s\right)\sqrt{T}$. Notice that

$$\lim_{y \to 0.916269^-} g(y) = \infty$$

Recall that ATM value of an Inverse call option is given by

$$BS(0, x, k^*, \sigma) = \frac{1}{2}\left(\text{Erfc}\left(\frac{\sigma\sqrt{T}}{2\sqrt{2}}\right) - e^{\sigma^2 T}\text{Erfc}\left(\frac{3\sigma\sqrt{T}}{2\sqrt{2}}\right)\right)$$

Additionally, one can see that for $T > 0$

$$\lim_{\sigma \to \infty} BS(0, x, k^*, \sigma) = 0.$$

Using non-arbitrage argument we get $\mathbb{E}\left(BS(0, X_0, k^*, v_0)\right) + \frac{\rho}{2}\mathbb{E}\left(\int_0^s H(r, X_r, k^*, v_r)\Lambda_r dr\right) \neq 0$ (otherwise if ATM option has zero value and non-zero probability to become in the money we get Free Lunch). Hence, we conclude that

$$BS^{-1}(k^*, \Gamma_s) < \infty.$$

As a result, we can assume that there exists U such that for all $T < U$ we have $0 \leq y < 0.91$. Notice that function $g(y)$ is non-negative and monotonically decreasing over this interval, which allows us to conclude the proof. ■

Lemma .4.2. *Under Hypothesis 3.3.1*

$$|(BS^{-1})''(k^*, \Phi_r)| \leq O\left(T^{-\frac{1}{2}}\right). \tag{52}$$

Proof. Using equation (50) we get

$$(BS^{-1})''(k_t^*, \Phi_r) = -\frac{\partial^2_{\sigma\sigma} BS(t, X_t, k_t^*, BS^{-1}(k_t^*, \Phi_r)))}{\left(\partial_\sigma BS(t, X_t, k_t^*, BS^{-1}(k_t^*, \Phi_r))\right)^3}. \tag{53}$$

Then, using equations (50) and (51) we get

$$\begin{aligned}\left|(BS^{-1})''(k^*, \Phi_r)\right| &= \left|\frac{11\sqrt{2}\pi e^{\frac{y^2}{4}} y - 8\pi^{3/2} e^{\frac{11y^2}{8}}\left(2y^2 + 1\right)\text{erfc}\left(\frac{3y}{2\sqrt{2}}\right)}{\sqrt{T}\left(2\sqrt{\pi}e^{\frac{9y^2}{8}} y\text{Erfc}\left(\frac{3y}{2\sqrt{2}}\right) - \sqrt{2}\right)^3}\right| \\ &= f(y)T^{-\frac{1}{2}},\end{aligned}$$

where $y = BS^{-1}(k^*, \mathbb{E}_r BS(0, X_0, k^*, v_0))\sqrt{T}$. Notice that

$$\lim_{y \to 0.916269^-} \left(2\sqrt{\pi} e^{\frac{9y^2}{8}} y \text{Erfc}\left(\frac{3y}{2\sqrt{2}} \right) - \sqrt{2} \right) = 0.$$

Additionally, one can see that for $T > 0$

$$\lim_{\sigma \to \infty} BS(0, x, k^*, \sigma) = 0.$$

Under Hypothesis 4.2.1 we have $\mathbb{E}_r BS(0, X_0, k^*, v_0) \neq 0$. Hence, we conclude that

$$BS^{-1}(k^*, \mathbb{E}_r BS(0, X_0, k^*, v_0)) < \infty.$$

As a result, we can assume that there exists U such that for all $T < U$ we have $0 \leq y \leq 0.91$. Notice that function $f(y)$ is non-negative and monotonically increasing over this interval, which allows us to conclude the proof. ■

The behaviour of $g(y)$ and $\frac{1}{g(y)}$ are presented at Figure .6.

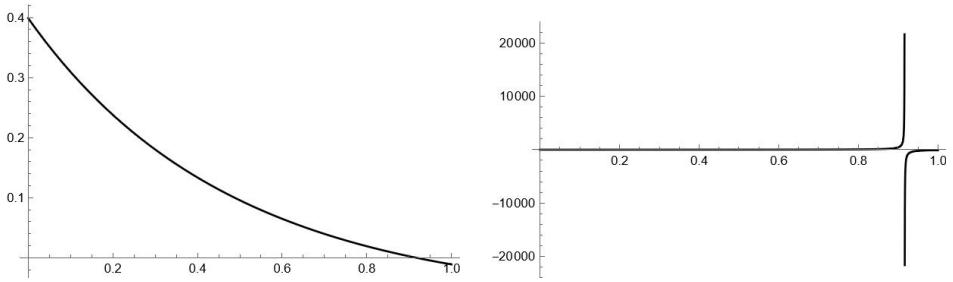

(a) $g(y)$ (b) $\frac{1}{g(y)}$

Figure .6: The behaviour of $g(y)$ and $\frac{1}{g(y)}$.

The corresponding plot of $f(y)$ for $0 \leq y \leq 0.91$ is presented at Figure .7.

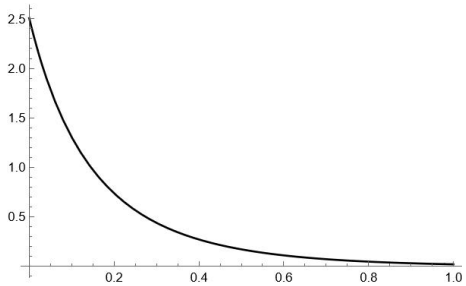

Figure .7: The behaviour of $f(y)$.

Finally, recall that $2H(s, x, k, \sigma) = \left(\partial^3_{xxx} BS(s, X_s, k, v_s) - \partial^2_{xx} BS(s, X_s, k, v_s)\right)$. Straightfor-

ward differentiation gives us the following

$$
\begin{aligned}
2H(s,x,k,\sigma) = \frac{1}{2}&\left(\text{Erfc}\left(\frac{y_1}{2\sqrt{2}}\right)e^{k+\sigma^2(T-s)-x} - \frac{2\sqrt{\frac{2}{\pi}}e^{k+\sigma^2(T-s)-x-\frac{y_1^2}{8}}}{\sigma\sqrt{T-s}}\right) + \\
&+\frac{1}{2}\left(\text{Erfc}\left(\frac{y_1}{2\sqrt{2}}\right)e^{k+\sigma^2(T-s)-x} + \frac{3y_1e^{k+\sigma^2(T-s)-x-\frac{y_1^2}{8}}}{\sqrt{2\pi}\sigma^2(T-s)}\right) + \\
&+\frac{1}{2}\left(\frac{y_1e^{k+\sigma^2(T-s)-x-\frac{y_1^2}{8}}}{\sqrt{2\pi}\sigma^2(T-s)} - \frac{e^{-\frac{y_2^2}{8}}y_2}{\sqrt{2\pi}\sigma^2(T-s)}\right) + \\
&+\frac{1}{2}\left(-\frac{3\sqrt{\frac{2}{\pi}}e^{k+\sigma^2(T-s)-x-\frac{y_1^2}{8}}}{\sigma\sqrt{T-s}} - \frac{\sqrt{\frac{2}{\pi}}e^{-\frac{y_2^2}{8}}}{\sigma^3(T-s)^{3/2}}\right) - \\
&-\frac{1}{2}\left(\frac{e^{-\frac{y_1^2}{8}}y_1^2}{2\sqrt{2\pi}\sigma^3(T-s)^{3/2}} + \frac{e^{-\frac{y_2^2}{8}}y_2^2}{2\sqrt{2\pi}\sigma^3(T-s)^{3/2}} - \frac{\sqrt{\frac{2}{\pi}}e^{-\frac{y_1^2}{8}}}{\sigma^3(T-s)^{3/2}}\right)e^{k+\sigma^2(T-s)-x},
\end{aligned}
$$

where $y_1 = \frac{2k+3\sigma^2(T-s)-2x}{\sigma\sqrt{T-s}}$ and $y_2 = \frac{2k+\sigma^2(T-s)-2x}{\sigma\sqrt{T-s}}$.

Using Hypothesis 3.3.1 and Lemma 1, provided in Alós, Nualart and Pravosud [10], one can see that $e^{k-X_s+v_s^2(T-s)}$ is bounded. Finally, using the fact that for $c>0$ and $d>0$ the function $x^ce^{-dx^2}$ is bounded we conclude that $H(s,X_s,k,v_s) \leq Cv_s^{-3}(T-s)^{-\frac{3}{2}}$.

Bibliography

[1] Alexander, C., Chen, D., and Imeraj, A. "Crypto quanto and inverse options". In: *Mathematical Finance* vol. 33, no. 5 (2023), pp. 1005–1043.

[2] Alexander, C. and Imeraj, A. "Delta Hedging Bitcoin Options with a Smile". In: *Quantitative Finance* vol. 23, no. 5 (2023), pp. 799–817.

[3] Alòs, E. "A generalization of the Hull and White formula with applications to option pricing approximation". In: *Finance and Stochastics* vol. 10, no. 3 (2006), pp. 353–365.

[4] Alòs, E., García, D., and Pravosud, M. "On the Skew and Curvature of the Implied and Local Volatilities". In: *Applied Mathematical Finance* vol. 30, no. 1 (2023), pp. 47–67.

[5] Alòs, E. and García Lorite, D. *Malliavin Calculus in Finance*. Chapman and Hall, 2021.

[6] Alòs, E., García-Lorite, D., and Muguruza, A. "On Smile Properties of Volatility Derivatives: Understanding the VIX Skew". In: *SIAM Journal on Financial Mathematics* vol. 13, no. 1 (2022), pp. 32–69.

[7] Alòs, E., León, J. A., and Vives, J. "On the short-time behavior of the implied volatility for jump-diffusion models with stochastic volatility". In: *Finance and Stochastics* vol. 11, no. 4 (2007), pp. 571–589.

[8] Alòs, E. and León, J. A. "A note on the implied volatility of floating strike Asian options". In: *Decisions in Economics and Finance* vol. 42, no. 2 (2019), pp. 743–758.

[9] Alòs, E. and León, J. A. "On the Curvature of the Smile in Stochastic Volatility Models". In: *SIAM Journal on Financial Mathematics* vol. 8, no. 1 (2017), pp. 373–399.

[10] Alòs, E., Nualart, E., and Pravosud, M. "On the implied volatility of Asian options under stochastic volatility models". In: (2022). arXiv: 2208.01353.

[11] Alòs, E. and Shiraya, K. "Estimating the Hurst parameter from short term volatility swaps: a Malliavin calculus approach". In: *Finance and Stochastics* vol. 23, no. 2 (2019), pp. 423–447.

[12] Ammous, S. "Can cryptocurrencies fulfil the functions of money?" In: *The Quarterly Review of Economics and Finance* vol. 70 (2018), pp. 38–51.

[13] Ankenbrand, T. and Bieri, D. "Assessment of cryptocurrencies as an asset class by their characteristics". In: *Investment Management and Financial Innovations* vol. 15, no. 3 (2018), pp. 169–181.

[14] Bachelier, L. "Théorie de la spéculation". In: *Annales scientifiques de l'École Normale Supérieure* vol. 3e série, (1900), pp. 21–86.

[15] Bayer, C., Friz, P., and Gatheral, J. "Pricing under rough volatility". In: *Quantitative Finance* vol. 16, no. 6 (2016), pp. 887–904.

[16] Bolotaeva, O. S., Stepanova, A. A., and Alekseeva, S. S. "The Legal Nature of Cryptocurrency". In: *IOP Conference Series: Earth and Environmental Science* vol. 272, no. 3 (2019), p. 032166.

[17] Bourgey, F. et al. "Local volatility under rough volatility". In: *Mathematical Finance* vol. 33, no. 4 (2023), pp. 1119–1145.

[18] Chatterjee, R. et al. "An efficient and stable method for short maturity Asian options". In: *Journal of Futures Markets* vol. 38, no. 12 (2018), pp. 1470–1486.

[19] Choi, J. et al. "A Black–Scholes user's guide to the Bachelier model". In: *Journal of Futures Markets* vol. 42, no. 5 (2022), pp. 959–980.

[20] Derman, E., Kani, I., and Zou, J. Z. "The Local Volatility Surface: Unlocking the Information in Index Option Prices". In: *Financial Analysts Journal* vol. 52, no. 4 (1996), pp. 25–36.

[21] Dupire, B. "Pricing with a smile". In: *Risk* vol. 7 (1994), pp. 18–20.

[22] Fang, F. et al. “Cryptocurrency trading: a comprehensive survey”. In: *Financial Innovation* vol. 8, no. 1 (2022), p. 13.

[23] Figueroa-López, J. E. and Ólafsson, S. “Short-term asymptotics for the implied volatility skew under a stochastic volatility model with Lévy jumps”. In: *Finance and Stochastics* vol. 20, no. 4 (2016), pp. 973–1020.

[24] Forde, M. and Jacquier, A. “Robust Approximations for Pricing Asian Options and Volatility Swaps Under Stochastic Volatility”. In: *Applied Mathematical Finance* vol. 17, no. 3 (2010), pp. 241–259.

[25] Fouque, J.-P. and Han, C.-H. “Pricing Asian options with stochastic volatility”. In: *Quantitative Finance* vol. 3, no. 5 (2003), pp. 353–362.

[26] Fouque, J.-P., Papanicolaou, G., and Sircar, K. R. “From the implied volatility skew to a robust correction to Black-Scholes American option prices”. In: *International Journal of Theoretical and Applied Finance* vol. 04, no. 04 (2001), pp. 651–675.

[27] Fukasawa, M. “Short-time at-the-money skew and rough fractional volatility”. In: *Quantitative Finance* vol. 17, no. 2 (2017), pp. 189–198.

[28] Fukasawa, M. and Gatheral, J. “A rough SABR formula”. In: (2021). arXiv: 2105.05359.

[29] Galeeva, R. and Ronn, E. “Oil futures volatility smiles in 2020: Why the bachelier smile is flatter”. In: *Review of Derivatives Research* vol. 25, no. 2 (2022), pp. 173–187.

[30] Garman, M. B. and Kohlhagen, S. W. “Foreign currency option values”. In: *Journal of International Money and Finance* vol. 2, no. 3 (1983), pp. 231–237.

[31] Gatheral, J. *The Volatility Surface*. Wiley, 2012.

[32] Goutte, S., Guesmi, K., and Saadi, S. *Cryptofinance*. WORLD SCIENTIFIC, 2021.

[33] Gronwald, M. “Is Bitcoin a Commodity? On price jumps, demand shocks, and certainty of supply”. In: *Journal of International Money and Finance* vol. 97 (2019), pp. 86–92.

[34] Gyöngy, I. “Mimicking the one-dimensional marginal distributions of processes having an ito differential”. In: *Probability Theory and Related Fields* vol. 71, no. 4 (1986), pp. 501–516.

[35] Hagan, P. et al. “Managing Smile Risk”. In: *Wilmott Magazine* vol. 1 (2002), pp. 84–108.

[36] Hazlett, P. K. and Luther, W. J. “Is bitcoin money? And what that means”. In: *The Quarterly Review of Economics and Finance* vol. 77 (2020), pp. 144–149.

[37] Ho Goodman, Laurie S, J. “Interest Rates—Normal or Lognormal?” In: *The Journal of Fixed Income* vol. 13, no. 13 (2003), pp. 33–45.

[38] Hou, A. J. et al. “Pricing Cryptocurrency Options”. In: *Journal of Financial Econometrics* vol. 18, no. 2 (2020), pp. 250–279.

[40] Jäckel, P. “Implied Normal Volatility”. In: *Wilmott* vol. 2017 (2017), pp. 54–57.

[39] Jäckel, P. “Let’s Be Rational”. In: *Wilmott* vol. 2015, no. 75 (2015), pp. 40–53.

[41] Lee, R. “Implied and local volatilities under stochastic volatility”. In: *International Journal of Theoretical and Applied Finance* vol. 4, no. 1 (2001), pp. 45–89.

[42] Lee, R. W. “Implied Volatility: Statics, Dynamics, and Probabilistic Interpretation”. In: *Recent Advances in Applied Probability*. Boston: Kluwer Academic Publishers, 2005, pp. 241–268.

[43] Matic, J. L., Packham, N., and Härdle, W. K. “Hedging cryptocurrency options”. In: *Review of Derivatives Research* vol. 26, no. 1 (2023), pp. 91–133.

[44] Mukhopadhyay, U. et al. “A brief survey of Cryptocurrency systems”. In: *14th Annual Conference on Privacy, Security and Trust (PST)*. IEEE, 2016, pp. 745–752.

[45] Nualart, D. *The Malliavin Calculus and Related Topics*. Probability and Its Applications. Berlin/Heidelberg: Springer-Verlag, 2006.

[46] Nualart, D. and Nualart, E. *Introduction to Malliavin Calculus*. Cambridge University Press, 2018.

[47] Pirjol, D. and Zhu, L. “Short Maturity Asian Options for the CEV Model”. In: *Probability in the Engineering and Informational Sciences* vol. 33, no. 2 (2019), pp. 258–290.

[48] Pirjol, D. and Zhu, L. “Short maturity asian options in local volatility models”. In: *SIAM Journal on Financial Mathematics* vol. 7, no. 1 (2016), pp. 947–992. arXiv: 1609.07559.

[49] Richards, T. “The Future of Payments: Cryptocurrencies, Stablecoins or Central Bank Digital Currencies?” In: *Australian Corporate Treasury Association* (2021).

[50] Schachermayer, W. and Teichmann, J. “How close are the option pricing formulas of Bachelier and Black–Merton–Scholes?” In: *Mathematical Finance* vol. 18, no. 1 (2008), pp. 155–170.

[51] Siu, T. K. and Elliott, R. J. “Bitcoin option pricing with a SETAR-GARCH model”. In: *The European Journal of Finance* vol. 27, no. 6 (2021), pp. 564–595.

[52] Terakado, S. “On the Option Pricing Formula Based on the Bachelier Model”. In: *SSRN Electronic Journal* (2019).

[53] Yang, Z., Ewald, C.-O., and Xiao, Y. “Implied Volatility from Asian Options via Monte Carlo Methods”. In: *International Journal of Theoretical and Applied Finance* vol. 12, no. 02 (2009), pp. 153–178.